

Casetta, F., Coltorti, M., Ickert, R. B. , Bonadiman, C., Giacomoni, P. P. and Ntaflos, T. (2018) Intrusion of shoshonitic magmas at shallow crustal depth: T–P path, H<sub>2</sub>O estimates, and AFC modeling of the Middle Triassic Predazzo Intrusive Complex (Southern Alps, Italy). *Contributions to Mineralogy and Petrology*, 173, 57. (doi:[10.1007/s00410-018-1483-0](https://doi.org/10.1007/s00410-018-1483-0)).

This is the author's final accepted version.

There may be differences between this version and the published version. You are advised to consult the publisher's version if you wish to cite from it.

<http://eprints.gla.ac.uk/166325/>

Deposited on: 09 August 2018

Enlighten – Research publications by members of the University of Glasgow  
<http://eprints.gla.ac.uk>

# Contributions to Mineralogy and Petrology

## Intrusion of shoshonitic magmas at shallow crustal depth: T-P path, H<sub>2</sub>O estimates and AFC modelling of the Middle Triassic Predazzo Intrusive Complex (Southern Alps, Italy)

--Manuscript Draft--

<b>Manuscript Number:</b>	CTMP-D-18-00030R1
<b>Full Title:</b>	Intrusion of shoshonitic magmas at shallow crustal depth: T-P path, H <sub>2</sub> O estimates and AFC modelling of the Middle Triassic Predazzo Intrusive Complex (Southern Alps, Italy)
<b>Article Type:</b>	Original Paper
<b>Keywords:</b>	Predazzo Intrusive Complex; Sr and Nd isotopes; P-T estimates and magma water content; Crustal assimilation; Solidification time; Shoshonitic intrusion.
<b>Corresponding Author:</b>	Federico Casetta Universita degli Studi di Ferrara Ferrara, Italy ITALY
<b>Corresponding Author Secondary Information:</b>	
<b>Corresponding Author's Institution:</b>	Universita degli Studi di Ferrara
<b>Corresponding Author's Secondary Institution:</b>	
<b>First Author:</b>	Federico Casetta
<b>First Author Secondary Information:</b>	
<b>Order of Authors:</b>	Federico Casetta
	Massimo Coltorti
	Ryan B. Ickert
	Costanza Bonadiman
	Pier Paolo Giacomoni
	Theodoros Ntaflos
<b>Order of Authors Secondary Information:</b>	
<b>Funding Information:</b>	
<b>Abstract:</b>	<p>The multi-pulse shoshonitic Predazzo Intrusive Complex represents an ideal igneous laboratory for investigating the chemical and physical conditions of magma emplacement in a crustal context, since numerical models can be constrained by field evidence. It constitutes the most intriguing remnant of the Middle Triassic magmatic systems of the Dolomitic Area (Southern Alps), preserved by the Alpine tectonics. Predazzo Intrusive Complex comprises silica saturated (pyroxenites/gabbros to syenites), silica undersaturated (gabbros to syenites) and silica oversaturated (granites and syenogranites) rock suites. In this paper we modelled its emplacement and evolution with a multiple thermo-/oxy-barometric, hygrometric and EC-AFC approach. At odds with what proposed in literature but according to the field evidence, the emplacement of the Predazzo Intrusive Complex occurred at shallow depth (&lt; 6 km). In this context, the different pulses differed slightly in bulk water content, but shared a common thermal regime, with temperatures between 1000-1100°C and ~600°C at low to moderate oxydizing conditions (-0.1 to +0.7 ΔFMQ). The interaction between the intrusion and the shallow crustal rocks was minimal, with Sr and Nd isotopic compositions indicating an average of 5-6% assimilation of crust. A thermo- and oxy-barometric comparison with the nearby Mt. Monzoni enabled also to speculate about the solidification time of the intrusion, which we infer took place over about 700 ka.</p>
<b>Response to Reviewers:</b>	To the Editor of Contributions to Mineralogy and Petrology

**Intrusion of shoshonitic magmas at shallow crustal depth: T-P path, H<sub>2</sub>O estimates and AFC modelling of the Middle Triassic Predazzo Intrusive Complex (Southern Alps, Italy)**

**Federico Casetta\***

Department of Physics and Earth Sciences, University of Ferrara  
Via Saragat 1, 44121 Ferrara, Italy

**Massimo Coltorti**

Department of Physics and Earth Sciences, University of Ferrara  
Via Saragat 1, 44121 Ferrara, Italy

**Ryan B. Ickert**

Scottish Universities Environmental Research Centre, Scottish Enterprise Technology Park,  
Rankine Avenue, East Kilbride, G75 0QF, UK

**Costanza Bonadiman**

Department of Physics and Earth Sciences, University of Ferrara  
Via Saragat 1, 44121 Ferrara, Italy

**Pier Paolo Giacomoni**

Department of Physics and Earth Sciences, University of Ferrara  
Via Saragat 1, 44121 Ferrara, Italy

**Theodoros Ntaflos**

Department of Lithospheric Research, Universität Wien  
Althanstraße 14 (UZA II), 1090 Wien

\* Corresponding author. Phone +39 0532 974721. E-mail: cstfrc@unife.it

# Intrusion of shoshonitic magmas at shallow crustal depth: T-P path, H<sub>2</sub>O estimates and AFC modelling of the Middle Triassic Predazzo Intrusive Complex (Southern Alps, Italy)

## Abstract

The multi-pulse shoshonitic Predazzo Intrusive Complex represents an ideal igneous laboratory for investigating the chemical and physical conditions of magma emplacement in a crustal context, since numerical models can be constrained by field evidence. It constitutes the most intriguing remnant of the Middle Triassic magmatic systems of the Dolomitic Area (Southern Alps), preserved by the Alpine tectonics. Predazzo Intrusive Complex comprises silica saturated (pyroxenites/gabbros to syenites), silica undersaturated (gabbros to syenites) and silica oversaturated (granites and syenogranites) rock suites. In this paper we modelled its emplacement and evolution with a multiple thermo-/oxy-barometric, hygrometric and EC-AFC approach. At odds with what proposed in literature but according to the field evidence, the emplacement of the Predazzo Intrusive Complex occurred at shallow depth (< 6 km). In this context, the different pulses differed slightly in bulk water content, but shared a common thermal regime, with temperatures between 1000-1100°C and ~600°C at low to moderate oxydizing conditions (-0.1 to +0.7  $\Delta$ FMQ). The interaction between the intrusion and the shallow crustal rocks was minimal, with Sr and Nd isotopic compositions indicating an average of 5-6% assimilation of crust. A thermo- and oxy-barometric comparison with the nearby Mt. Monzoni enabled also to speculate about the solidification time of the intrusion, which we infer took place over about 700 ka.

## Keywords

Predazzo Intrusive Complex; Sr and Nd isotopes; P-T estimates and magma water content; Crustal assimilation; Solidification time; Shoshonitic intrusion.

## 1. Introduction

The Middle Triassic magmatic event in the Southern Alps is expressed in volcano-plutonic sequences outcropping from the Brescian Alps, Alto Vicentino, Dolomites and Carnia areas (Italy) to the Karavanken region (Austria). Most of the igneous products are volcanic and volcanoclastic rocks, with subordinated dyke swarms. Intrusive bodies are instead rare, and mainly located in the Dolomites (Predazzo-Mt. Monzoni-Cima Pape) and Karavanken areas (Gasparotto and Simboli 1991; Gianolla 1992; Bonadiman et al. 1994; Visonà and Zanferrari 2000; Brack et al. 2005; Cassinis et al. 2008; Bellieni et al. 2010; Casetta et al. 2017). These intrusions represent snapshots of magmatic plumbing systems, emplaced during and/or immediately after the eruption of the overlying volcanic products. There are several outstanding geological problems regarding the nature of these complexes, mainly related to their emplacement conditions, and to the relationships between tectonics and magmatism. The Predazzo Intrusive Complex (PIC) represents the ideal “petrologic laboratory” for investigating and reconstructing the features of the Middle Triassic feeding systems, since it offers the possibility to constrain the theoretical and experimental modeling by means of field evidence. As in the case of the nearby Mt. Monzoni, the contact aureole between PIC and the surrounding sedimentary rocks enabled many authors to speculate about the geometry of the intrusive body and its field relationships to the shallow crust (Princivalle et al. 1999; Ferry et al. 2002; Povoden et al. 2002; Gallien et al. 2007). On the basis of petrological and field evidence, Casetta et al. (2017) identified three different magma batches constituting the PIC, interpreted as a multi-pulse body of shoshonitic affinity with variable alkalies and H<sub>2</sub>O-content which led to differentiation from mafic to amphibole and biotite-bearing end-members. However, several issues are still unsolved, such as the (possible) interaction between PIC magmas and crust, and their chemical/physical conditions of emplacement. The latter resulting in a current uncertainty about the depth of the intrusion.

Few thermobarometric and oxybarometric data are reported in literature for the Middle Triassic magmatic systems of the Dolomitic Area. According to Bonadiman et al. (1994), the oxygen fugacity of the nearby Mt. Monzoni system was around the NNO buffer and the crystallization temperature range was between 1044 and 589°C. Despite the clear evidence of a predominant role of water during crystallization, as testified by the wide presence of hydrous phases in the intrusive rocks, no estimates of the H<sub>2</sub>O contents and *P-T* conditions of these Middle Triassic plumbing systems have been performed so far. Taking into account the Al<sup>tot</sup> content of amphiboles, Menegazzo Vitturi et al. (1995) hypothesized a depth of 10-17 km for PIC emplacement, but their values appeared in stark contrast with both the field evidence and the data reported by Visonà and Zanferrari (2000) for the similar and coeval Karawanken pluton (5-9 km).

Therefore, in this paper we made new geochemical and isotopic (<sup>87</sup>Sr/<sup>86</sup>Sr-<sup>143</sup>Nd/<sup>144</sup>Nd) measurements on new samples from PIC that are representative of its main portions. A multiple thermobarometric and hygrometric approach, based on the interaction between distinct single mineral, mineral pairs and mineral-melt equations, corroborated by appropriate simulations by means of Rhyolite-MELTS software (Gualda et al. 2012), enabled us to: (i) provide for the first time *P-T-fO<sub>2</sub>* estimates and H<sub>2</sub>O evaluation of PIC system over its entire evolution; (ii) verify if the depth of the intrusion obtained by the previous petrologic approaches well fit the field evidence. The resulting *P-T-fO<sub>2</sub>* and H<sub>2</sub>O values, together with the isotopic signatures of PIC rocks were then used as input to (iii) quantify the role of assimilation and fractional crystallization processes in the generation of the main PIC magmatic suites.

## 2. Middle Triassic magmatism in the Southern Alps

### 2.1. Geodynamic framework

The Middle Triassic magmatic sequences of the Dolomitic Area are mainly composed of volcanites and volcanoclastites with subordinated and scattered intrusive bodies over an area of

about 2,000 km<sup>2</sup> (Vardabasso 1929, 1930; Castellarin et al. 1980, 1982; Lucchini et al. 1982; Sloman 1989; Bonadiman et al. 1994; Coltorti et al. 1996; Gianolla et al. 2010; Casetta et al. 2017). The Middle Triassic geodynamic framework of Dolomitic Area and the whole Southern Alps domain is still matter of debate, fostered by juxtaposition between the calc-alkaline/shoshonitic orogenic affinity of the magmatic products and evidence for a concomitant extensional-transtensional tectonic regime (Doglioni 1987; Stampfli and Borel 2002, 2004; Doglioni 2007). Several geodynamic models were thus proposed, invoking the presence of: (i) an aborted rift in a passive margin (Bernoulli and Lemoine 1980); (ii) a compression at the NW limb of the Paleo-Tethys (Castellarin et al. 1980); (iii) an “active” mantle upwelling (Stahle et al. 2001); (iv) a transition to back-arc conditions lasting since Carboniferous-Permian, triggered by the northward subduction of the Paleotethys remnants (Ziegler and Stampfli 2001; Stampfli and Borel 2002; 2004; Cassinis et al. 2008; Schmid et al. 2008 Zanetti et al. 2013); (v) an anorogenic rifting concomitant with **arc-like magmatism**, whose signature was inherited by a mantle source previously metasomatised by subduction-related components during the Hercynian orogenic cycle (Bonadiman et al. 1994). This last hypothesis was supported by the similar Sr-Nd isotope signatures of the Middle Triassic magmas in the Southern Alps and the Permian igneous products (260-290 Ma), whose expression were found along the Western and in the Eastern Alps sectors (Barth et al. 1993; Rottura et al. 1998; Monjoie et al. 2007; Schaltegger and Brack 2007; Marocchi et al. 2008; Quick et al. 2009; Willcock et al. 2015; Dal Piaz et al. 2015; Sinigoi et al. 2016; Manzotti et al. 2017). This kind of analogy led to speculate that similar mantle sources, and/or similar melting conditions, could have generated the Middle Triassic and the Permian magmatic episodes. In the Dolomitic Area, thick sequences of **basaltic andesitic to rhyolitic** ignimbrites associated to the Permian Atesina Volcanic District are also the main constituent of the crustal basement of the Dolomitic Area where magmas intruded during Middle Triassic.

## 2.2. The Southern Alps intrusive bodies: geochemical and petrographic overview

In contrast to the large amount of basaltic/latitic volcanic rocks erupted in the Southern Alps during the Ladinian-Carnian, the intrusive bodies are more limited in volume. They are Cima Pape ( $< 3 \text{ km}^2$ ), Mt. Monzoni ( $4.6 \text{ km}^2$ ), Predazzo Intrusive Complex ( $25 \text{ km}^2$ , [see below](#)) in the Dolomitic Area (Italy) and Karawanken (about  $50 \text{ km}^2$ ) in Carinthia (Austria).

The Cima Pape sill and the ca. 230 Ma Mt. Monzoni body (Borsi and Ferrara 1968) are composed of biotite and amphibole-bearing gabbroic to syenitic rocks with shoshonitic affinity, generated mainly by fractional crystallization from parental **basaltic to trachybasaltic magmas** (Gasparotto and Simboli 1991; Bonadiman et al. 1994; Della Lucia 1997). The emplacement of Mt. Monzoni body is thought to be controlled by a syn-genetic ESE-WNW transcurrent tectonics, which created the conditions for a shallow level intrusion and the subsequent magma differentiation. A shallow depth is also suggested for the Cima Pape sill, where a gradual textural transition to the overlying lavas, locally organized in columnar structures (Sarti and Ardizzoni 1984) is observable on field.

The Karawanken pluton (ca. 230 Ma, Lippoldt and Pidgeon 1974) comprises biotite and amphibole-bearing diorites/monzonites to granites/syenites, with rare aplites and pegmatites, showing an overall high-K calc-alkaline to shoshonitic affinity. To explain the production of Karawanken magmas, Visonà and Zanferrari (2000) invoked the occurrence of combined assimilation + **fractional crystallization** processes from a parental **basaltic** melt in a shallow magma chamber (5-9 km). The geochemical differences (i.e. La/Nb and Ba/Nb ratios) between **the** Karawanken pluton and the intrusions of the Dolomitic Area led the authors to suggest the origin of **Karawanken** magmas from an enriched mantle source not previously affected by subductive components, as proposed by Bonadiman et al. (1994) for the Mt. Monzoni body. Irrespective of the volumetric differences, common features of these intrusions are the high-K calc-alkaline to shoshonitic affinity, the modal occurrence of hydrated phases (biotite and amphibole) in the intercumulus assemblages and the shallow depth of emplacement.



### 2.3. The Predazzo Intrusive Complex

The Predazzo Intrusive Complex (PIC, Fig. 1) is a ring-like shaped multi-pulse intrusion with an overall volume of about 4.5 km<sup>3</sup> cropping out in Trentino Alto Adige (NE Italy). Dated at 237.3 ± 1.0 Ma (U/Pb on zircon from granites, Mundil et al., 1996), it intruded the Permian Atesina Volcanic District rhyolitic ignimbrites, the Permo-Triassic sedimentary formations and the overlying volcanic sequences (Brack et al. 1996, 1997, 2005; Mietto et al. 2012), forming well-defined metamorphic aureoles (Princivalle et al. 1999; Ferry et al. 2002; Povoden et al. 2002; Gallien et al. 2007). The intrusion and its related volcanic products were almost completely preserved from the action of the Alpine tectonic event, and kept in their original position with respect to the surrounding rocks. According to Casetta et al. (2017), PIC rocks are grouped in three main units with different geochemical features (Fig. 1), named (in relative order of emplacement) Shoshonitic Silica Saturated (SS, 3.1 km<sup>3</sup>), Granitic Unit (GU, 1.1 km<sup>3</sup>) and Shoshonitic Silica Undersaturated (SU, 0.3 km<sup>3</sup>). The SS and SU suites are composed of pyroxenites/gabbros to syenites (Fig. 2), respectively quartz- and nepheline-bearing, formed as result of fractional crystallization (FC) processes in an almost closed system from two distinct starting monzogabbroic-like magmas (Petersen et al. 1980; Visonà 1997; Marrocchino et al. 2002; Casetta et al. 2017). The Granitic Unit is instead constituted by quartz and biotite-bearing granites/syenogranites (Fig. 2), and apparently seems to represent a different magma batch and/or the result of genetic processes independent from those that generated the SS and SU rocks (Menegazzo Vitturi et al. 1995; Visonà 1997; Casetta et al. 2017). However, the lack of isotopic studies made it impossible to definitively exclude for the three magma bodies a significant involvement of assimilated crustal rocks.

On the other side, the field relationships between the intrusive units, their related dykes and the host rocks suggest a shallow origin of this multi-pulse intrusion, as also testified by the presence of hypabyssal rocks at the hundred-meter-scale transition between the plutonic and the volcanic

sequences (Casetta et al. 2017). Nevertheless, the only thermobarometric studies present in literature, based on the Al<sup>tot</sup> content of amphiboles (Menegazzo Vitturi et al. 1995), proposed a 10-17 km depth for the PIC, giving rise to some uncertainty about its emplacement and crystallization conditions due to the discrepancy between the barometric- and field-based estimates.

### 3. Analytical methods

Whole rock major and trace element analyses were carried out at the Department of Physics and Earth Sciences (University of Ferrara, Italy) using ARL Advant-XP automated X-Ray fluorescence spectrometer. Full matrix correction procedure and intensities were elaborated following Traill and Lachance (1966). Accuracy and precision are better than 2-5% for major elements and 5-10% for trace elements. The detection limits are 0.01 wt% and 1-3 ppm for most of the major and trace element concentrations, respectively.

Rb, Sr, Y, Zr, Nb, Hf, Ta, Th, U, and Rare earth elements (REE) were analyzed by inductively coupled plasma-mass spectrometry (ICP-MS) using a Thermo Series X spectrometer with precision and accuracy better than 10% for all elements, well above the detection limit.

Mineral phases major element compositions were analyzed at the Department of Lithospheric Research, University of Wien (Austria), by using a CAMECA SX100 electron microprobe equipped with four WD and one ED spectrometers. The operating conditions were as follows: 15 kV accelerating voltage, 20 nA beam current, 20 s counting time on peak position. Natural and synthetic standards were used for calibration and PAP corrections were applied to the intensity data (Pouchou and Pichoir 1991).

Whole rock <sup>87</sup>Sr/<sup>86</sup>Sr and <sup>143</sup>Nd/<sup>144</sup>Nd isotopic analyses were performed at the Radiogenic Laboratory of the Scottish Universities Environmental Research Centre (SUERC) of Glasgow by means of a Sector-54 TIMS instrument. Strontium was loaded onto outgassed single Re filaments with a Ta-activator solution; Nd was loaded onto the side of a triple Ta-Re-Ta

filament assembly in H<sub>2</sub>O and ran as Nd<sup>+</sup>. The sample preparation procedures for Sr-Nd isotopic analyses have not been described previously, so we articulate them in full, together with standards and instrumental analytical performance, in the Supplementary Material\_1.

## 4. Whole rock geochemistry

### 4.1. Major and trace element

Shoshonitic Silica Saturated (SS) suite (Fig. 2, Table 1) is mainly constituted by monzogabbros and monzodiorites, with Mg# (calculated as  $Mg/[Mg+Fe^{2+}]$  mol%) of 65-45, and by subordinated monzonites and syenites (Mg# of 53-26 and 45-20 respectively) randomly distributed within the unit (Fig. 1). Volumetrically limited pyroxenitic (Mg# 64-47) and gabbroic (Mg# 65-45) cumulates crop out in the southwestern sector of the intrusion. Shoshonitic Silica Undersaturated (SU) suite (Fig. 2, Table 1) is on average more evolved than the SS one, being dominated by the presence of nepheline-normative monzonites (Mg# 40-39) and syenites (Mg# 36-15), over a minority composed of cumulitic gabbros (Mg# 56-50), monzogabbros (Mg# 59-47) and monzodiorites (Mg# 55-27). Granitic Unit (GU, Fig. 2) is composed of highly evolved granites and syenogranites (69-77 SiO<sub>2</sub> wt%, Table 1) that, according to Chappell and White (2001) discriminating criteria, are ascribable to the I-type granitoids ( $Al/[Na + K + Ca] < 1.1$ ; low P<sub>2</sub>O<sub>5</sub> wt%; decreasing Zr, Sr and Al<sub>2</sub>O<sub>3</sub> wt% with increasing SiO<sub>2</sub> wt%). Few samples show instead intermediate behaviour between I- and S-type rocks.

All SS, SU and GU rocks have K-affinity (Fig. 2), and their K<sub>2</sub>O and SiO<sub>2</sub> contents led to classify them as belonging to shoshonitic (SS and SU) and High-K calc-alkaline (GU) series.

Despite the general similarities, the major and trace element distribution in the SS, SU and GU rocks made it possible to pinpoint their origin from independent magmatic batches. At comparable differentiation degrees, main discriminating features between the SS and SU rocks are the relative enrichment in HFSE (Th, U, Pb), LREE and the higher Na<sub>2</sub>O/K<sub>2</sub>O ratio of the

latters. Such differences are in accordance with the predominant presence of amphibole and other Na and REE-rich phases in the SU rocks (Casetta et al. 2017).

#### 4.2. $^{87}\text{Sr}/^{86}\text{Sr}$ and $^{143}\text{Nd}/^{144}\text{Nd}$ isotopes

Whole rock  $^{87}\text{Sr}/^{86}\text{Sr}$  and  $^{143}\text{Nd}/^{144}\text{Nd}$  isotopic ratios were analysed on representative samples of the SS, SU and GU suites (Table 2). Shoshonitic Silica Saturated samples have initial Sr isotope composition from 0.7039 to 0.7052, whereas their initial Nd isotope compositions range from 0.512191 to 0.512247. Shoshonitic Silica Undersaturated rocks are characterized by a generally higher  $^{143}\text{Nd}/^{144}\text{Nd}_i$  varying from 0.512261 to 0.512289 and by  $^{87}\text{Sr}/^{86}\text{Sr}_i$  comparable with the SS samples (0.7047 to 0.7063).  $^{143}\text{Nd}/^{144}\text{Nd}_i$  range of GU rocks is between 0.512206 and 0.512304, thus comparable to those of both SS and SU suites. High Rb/Sr of the GU rocks resulted in imprecise initial calculated  $^{87}\text{Sr}/^{86}\text{Sr}$  preventing any correlation between the GU and the SS/SU bodies.

### 5. Crystallization sequences and mineral chemistry

To better focus on the  $P$ - $T$ - $f\text{O}_2$  conditions and on the  $\text{H}_2\text{O}$  contents of the PIC system, some remarks on the mineral phase compositions and crystallization sequences of the various units is hereafter summarized. A more detailed description of the petrographic and mineral chemistry features of these rocks was reported by Casetta et al. (2017). The new mineral phases analyses are reported in the [Supplementary Material\\_2](#).

Shoshonitic Silica Saturated rocks are dominated by the presence of clinopyroxene and plagioclase as cumulus phases; minor olivine and orthopyroxene can be found in gabbros and monzogabbros. The intercumulus assemblage is characterized by the ubiquitous presence of plagioclase and biotite, followed by the appearance of amphibole in gabbros to monzodiorites (Fig. 3). Magnetite and Ti-magnetite are often reported in association with biotite, whereas K-feldspar and accessory phases (quartz, apatite, ilmenite, sphene, zircon) modally increase in

more evolved rocks. The main alteration features of the SS rocks consist of sericite formation at the expenses of feldspars, chlorite growth over clinopyroxene, amphibole and biotite, as well as epidote formation at the expenses of clinopyroxene and plagioclase. The following crystallization sequence can be deduced for SS rocks: *olivine* → *clinopyroxene* ( $\pm$ *orthopyroxene*) → *Ti-magnetite/magnetite* → *plagioclase* → *biotite* → *amphibole* → *K-feldspar* → *quartz* ( $\pm$ *accessories*).

The crystallization sequence of the SU magmatic suite mirrors its silica undersaturation and higher Na<sub>2</sub>O content. Orthopyroxene and quartz are in fact absent, and an earlier appearance of amphibole at the expenses of biotite characterises the intercumulus assemblage of the SU rocks (Fig. 3). Other Na-rich minerals like ferrosalitic clinopyroxene, abitic plagioclase and nepheline (Visonà 1997) are variably present. Accessory phases are ugrandite group garnets, epidote, apatite and titanite. As already highlighted by Visonà (1997), many portions of the SU body are hydrothermalized, showing the formation of kaoline, sericite and scapolite. Where this secondary assemblage does not occur, the primary differences between the SU and SS magmatic suites are evident. The likely crystallization sequence of the SU rocks is: *olivine* → *clinopyroxene* → *Ti-magnetite/magnetite* → *plagioclase* → *amphibole* → *biotite* → *K-feldspar* → *nepheline* ( $\pm$ *accessories*).

Syenogranites and granites of the GU are quite homogeneous in composition, being constituted by K-feldspar, plagioclase and quartz, locally associated to several other minerals, among which Fe-rich biotite is the most common. Accessory phases are tourmaline, fluorite, sphene, magnetite, apatite, ilmenite and zircon. Muscovite and chlorite are rare and always grow at the expenses of biotite and amphibole in late hydrothermal stages, whereas the sericitization of feldspars is pervasive. Less common phases are ematite, allanite, scheelite, xenotime, gummite, thorite, uranium micas, molibdenite and other sulphides, irregularly disseminated and generated in the later pneumatolitic and hydrothermal stages (Marzocchi 1987; Visonà 1997). The main

GU paragenesis is composed of: *K-feldspar* + *plagioclase* + *quartz* + *fluorite* + *biotite* (*chlorite* and/or *muscovite*)  $\pm$  *amphibole* + *accessories*.

In the less altered samples, at comparable whole rock differentiation degree, the composition of the most representative minerals clearly discriminate between the SS and SU magmatic suites. For instance, biotites and amphiboles are Al- and Na-enriched in the SU rocks with respect to the SS ones. Amphibole in fact varies from the hornblendic and actinolitic composition in the SS rocks ( $\text{Na}_2\text{O} < 1.5$  wt%;  $\text{Al}_2\text{O}_3 < 8$  wt%) to the hastingsitic/pargasitic composition (rare actinolitic hornblende, Leake et al. 1997) in the SU ones ( $\text{Na}_2\text{O}$  up to  $\sim 2.5$  wt%;  $\text{Al}_2\text{O}_3$  up to  $\sim 18$  wt%). Even the Na content of plagioclase differs between the two magmatic suites: it ranges from  $\text{An}_{84}$  to  $\text{An}_{34}$  in SS samples, and from  $\text{An}_{50}$  to  $\text{An}_{<23}$  in SU rocks. Another discriminating feature is represented by the clinopyroxene composition, augitic/salitic ( $\text{En}_{43-33}$ ) in the SS and salitic/ferrosalitic ( $\text{En}_{37-24}$ ) in the SU rocks (Morimoto, 1988). Furthermore, the manganese content of several phases is quite higher in the SU rocks: Ti-magnetite (0.2-1.9 wt% SU; 0.1-0.4 wt% SS), biotite (0.1- 0.7 wt% SU; 0-0.4 wt% SS), amphibole ( $\sim 0.7$  wt% SU;  $\sim 0.5$  wt% SS) and clinopyroxene (0.5-1.5 wt% SU; 0.2-0.8 wt% SS).

## 6. P, T and H<sub>2</sub>O estimates: thermobarometric evolution of the intrusion

### 6.1. Recover the initial equilibrium conditions

In this section, we apply several methods for estimating the *P*, *T* and H<sub>2</sub>O contents of PIC rocks, taking into account the coexistence of minerals used as thermometers, barometers and/or hygrometers in both the SS and SU crystallization sequences. Apart from the Holland and Blundy (1994), Anderson and Smith (1995), Anderson (1996) and Henry et al. (2005) methods (see below) applied to amphibole-plagioclase pairs and biotite, and specific for intrusive rocks, the other equations used in this study are designed for volcanic samples. As often happens in intrusive contexts, the identification of the parental “melt” from which crystals formed is challenging (e.g. Skaergaard Intrusion; Nielsen 2004; Namur and Humphreys 2018). Intrusive

rocks, in fact, rarely correspond to bulk melt composition, representing a variable mixture of cumulus and intercumulus minerals, removed by the crystallizing melts at various stages of fractionation, thus in equilibrium with different melts in different moments. Casetta et al. (2017) suggested that the cumulitic gabbros and pyroxenites, as well as most of the intermediately evolved rocks of the complex, were generated by various extent of fractional crystallization from a starting trachybasaltic magma in an almost closed system.

It is modelled that the mineral assemblages constituting the PIC rocks (e.g. clinopyroxenes of SS gabbro) showed partial equilibrium with a more evolved melt (e.g. SS trachybasalt), from which then segregated to form the cumulates. The cumulitic nature of a rock itself incorporates the concept that its composition (e.g. Mg# of clinopyroxene) represents an independent physico-chemical system with respect to the deriving melt. Consequently, if we try to consider the intrusive (cumulitic) rock of PIC as a bulk representative of a melt (e.g. in terms of Mg# or CaO/Al<sub>2</sub>O<sub>3</sub>), it is reasonable to find that its mineral constituents (e.g. clinopyroxene or plagioclase), are in evident disequilibrium with the bulk composition (Figg. 4 and 5). They are instead compositionally coherent with a segregation process from a more evolved melt. On the other side, by taking into account more evolved rocks (e.g. monzogabbros to syenites), the amount of crystal disequilibrium progressively decreases (Figg. 4 and 5). This because the ultimate products of the SS/SU fractional crystallization processes, syenitic in composition, progressively approach the eutectic of the system and likely resemble a melt composition: this condition has been also proposed by Morse and Brady (2017) for the syenites of the 1300 Ma old Kiglapait Intrusion (Labrador).

Evidences of the reliability of this genetic model are the observed textural and mineral homogeneities of the SS/SU rocks: any kind of significant zoned texture would result from the introduction of additional magma chamber processes (i.e. mixing) during the formation of the PIC lithotypes, invalidating our assumptions. The unzoned texture, coupled with the crystal size of PIC rocks (e.g. clinopyroxenes up to 6-7 mm in pyroxenites and gabbros) and with the small



volume of the intrusive body ( $4.5 \text{ km}^3$ ), speaks also against a considerable effect of syn- to post-crystallization diffusion processes, which can be a rate-limiting process for thermobarometric estimates. On the other side, thermometers involving clinopyroxene in upper crustal context, commencing cooling from relatively low  $T$ , hold the potential to record the peak temperature conditions, especially in large-sized grains (Müller et al. 2013). If we couple the euhedral unzoned texture of PIC clinopyroxenes with the diffusion rates proposed by several authors (e.g. at about  $1000^\circ\text{C}$   $\log D^{(\text{Ca})} = -21 \text{ m}^2/\text{s}$ ;  $\log D^{(\text{Ti})} = -22 \text{ m}^2/\text{s}$ ;  $\log D^{(\text{Fe})} = -21 \text{ m}^2/\text{s}$ , where  $D$  indicates the diffusion coefficient; see Brady and McCallister 1983; Dimanov et al. 1996; Cherniak and Lyiag 2012; Müller et al. 2013 and references therein), we can argue that the crystal compositions were nearly unmodified by significant diffusion processes. Similar remarks can be made for plagioclase, whose crystallization in plutonic rocks at relatively low  $T$  limit the efficiency of  $\text{CaAl-NaSi}$  diffusion to submicron length scales (Grove et al. 1984). The mineral compositions were therefore considered as representative of the various stages of fractional crystallization of the magmas inside PIC, and were used to constrain the physical parameters of the magma chamber.

On the basis of these assumptions, we matched each mineral (e.g. clinopyroxene of SS cumulates) with an estimated “melt” following the crystal/melt equilibrium partitioning (e.g.  $\text{C}_{\text{px-Liq}} K_{\text{dFe-Mg}}$ , see below), to trace the  $P$ - $T$  path of an hypothetical differentiation trend (e.g. SS suite, see Casetta et al. 2017). This operation enabled us to compute the “melt” composition, to skip the apparent disequilibrium between minerals and cumulitic rocks as a bulk and thus to constrain the  $P$ ,  $T$  and  $\text{H}_2\text{O}$  parameters of the less evolved melts in the PIC feeding system. Afterwards, the application of the “traditional” thermobarometric equations for intrusive contexts (i.e. to amphibole-plagioclase pairs and biotite, see below) enabled us to verify the convergence between the various results as well as to unravel the  $T$ - $P$ - $\text{H}_2\text{O}$  conditions in the later stages of crystallization. A complete list of the applied equations, results, and corresponding errors is reported in Table 4 and discussed in detail in the following sections.



## 6.2. Clinopyroxene-melt thermobarometer and water content of primary magmas

Clinopyroxene is the dominant and ubiquitous phase in the SS and SU rocks, thus clinopyroxene-melt thermobarometry was considered as a valuable starting point to estimate the  $T$ - $P$  intensive variables and  $H_2O$  content of PIC magmatic system since early stage of fractionation. Crystal-melt equilibrium conditions were tested by taking into account the experimentally determine range of  $^{Cpx-Liq}Kd_{Fe-Mg} = 0.24-0.30$  at  $T > 1050^\circ C$  by Putirka et al. (2003). First tests highlighted that all clinopyroxene crystals in the SS and SU units have  $^{Cpx-Liq}Kd_{Fe-Mg} = 0.36-0.68$  (hereinafter the superscript “Liq” indicates the composition of the bulk rock), indicating a disequilibrium towards composition more evolved than their host rock (Fig. 4). The amount of disequilibrium, as said before, decreases with increasing the differentiation degree of the rock (Fig. 4). Such a decrease could be explained by the fact that more evolved lithotypes better approach the eutectic of the system and more likely simulate melt compositions.

Following the FC model of Casetta et al. (2017), clinopyroxenes of each lithotype were thus related to a calculated “melt” composition having the same chemical affinity of their host rock and a more evolved nature (Table 3), by which crystals retrieved their equilibrium conditions.

As shown in the flow chart of Fig. 6a, once chosen the clinopyroxene-melt couple of the SS suite,  $T$ - $P$  pairs were estrapolated by means of the Putirka (2008) equations, assuming variable  $H_2O$  wt% contents of the melt. The water-dependant equations 32b and 33 (Putirka 2008), derived from the  $P$ -independent thermometer and the  $T$ -dependent barometer of Putirka (1996), were firstly applied to constrain the crystallization conditions of clinopyroxene from the melt, obtaining several  $T$ - $P$ - $H_2O$  triplets. Since these triplets are strongly dependant on the chosen melt and on the inferred  $H_2O$  content, they were checked, together with the melt composition, by means of the Rhyolite-MELTS calibration (Gualda et al. 2012). Iterated procedures (Fig. 6a) were developed until a clinopyroxene composition analogous to the starting one was reproduced

by Rhyolite-MELTS. In this way, the two independent approaches reinforce one to another, giving a more robust framework for the thermobarometric and water results. Since the only left starting parameter required by Rhyolite-MELTS was oxygen fugacity, we chose  $f_{O_2} = NNO$  as proposed by Bonadiman et al. (1994) for the Mt. Monzoni intrusion.

However, by increasing the differentiation degree of SS rocks, and/or considering the more alkaline SU magmas, the reliability of Rhyolite-MELTS decreases, as a function of the alkali-enrichment of the system and the related crystallization of amphibole and biotite, for whom thermodynamic parameters are not well constrained (Gualda et al. 2012). Therefore, the use of Masotta et al. (2013) thermobarometer was preferred for the SU suite and for the more evolved SS rocks, and was cross-checked with Putirka (2008) equations (Fig. 6b). As for SS rocks, once assessed the equilibrium between clinopyroxene and melt,  $T$ - $P$  pairs at variable  $H_2O$  contents of the melt were extrapolated by means of the Putirka (2008) method. The resulting  $T$ - $P$ - $H_2O$  triplets were then inputed in Masotta et al. (2013) equation until the resulting  $T$  and  $P$  were comparable to those obtained by Putirka (2008) method at similar water contents.

Some issues for handling this combination of modeling tools should be remarked: (i) since Rhyolite-MELTS is not suitable for amphibole and biotite-dominated rocks, it was only used to simulate the composition of clinopyroxene in equilibrium with the least evolved SS magmas, at the  $P$ ,  $T$  and  $H_2O$  conditions determined by the previous calculations; (ii) the alkaline nature of PIC (especially SU) differentiated rocks implies that clinopyroxene-melt behavior during crystallization and cooling depends not only on Fe and Mg, but also on Ca, Na and Al, so Masotta et al. (2013) equations became progressively more reliable; (iii) iterated and cross-checked calculations using Putirka (2008), Rhyolite-MELTS and Masotta et al. (2013) methods (Fig. 6a-b) were proposed to unravel  $P$ - $T$ - $H_2O$  crystallization conditions avoiding circular relationships between the equations.

The errors proposed for the thermobarometers, oxybarometers and hygrometers are reported in Table 4: while temperatures could be defined within a narrow error range ( $\pm 10$  to  $\pm 20^\circ C$ ) with

both Putirka et al. (2008) and Masotta et al. (2013) equations, the  $P$  estimates were affected by high uncertainties, varying from  $\pm 1.2$  (Masotta et al. 2013) to  $\pm 2.6$  kbar (Putirka et al. 2008).

#### 6.2.1. Clinopyroxene crystallization conditions of Shoshonitic Silica Saturated rocks

The most magnesian clinopyroxene in SS rocks were found within pyroxenites (Mg#<sub>Cpx</sub> 76-78), whereas the less magnesian compositions (Mg#<sub>Cpx</sub> 63-71) were in the monzodiorites and monzonites. The early  $T$ - $P$ -H<sub>2</sub>O crystallization conditions were likely represented by the former, which attained equilibrium with a trachybasaltic melt (Mg# 51; Fig. 4a, Table 3), further confirming the first FC step identified by Casetta et al. (2017). Clinopyroxene-melt thermobarometers indicated a  $P$ - $T$  range of 1.6-2.3 kbar and 1070-1050°C, for water contents of 2.0-2.5 wt% (Table 4). The best fitting data in by Rhyolite-MELTS simulations were obtained at pressure of 1.5 kbar, temperature of 1060°C and 2.5 H<sub>2</sub>O wt%. Consequently, 2.0-2.5 H<sub>2</sub>O wt% could be assumed as the water contents of the first SS magmas intruding the PIC. Clinopyroxenes in the cumulitic gabbros were slightly less homogeneous and less magnesian (Mg#<sub>Cpx</sub> 69-71 cores; 65-66 rims), and resulted in equilibrium with melts varying in Mg# from 43 to 40 (cores) to about Mg# 36 (rims), as shown in Fig. 4a and Table 3. Pressure-temperature paths indicated that cores attained equilibrium in a  $P$  range of 0.5-1.9 kbar and  $T$  of 910-980°C, while rims formed at 0.3-1.2 kbar and 900-920°C, considering H<sub>2</sub>O contents of 3.0-4.0 wt%. Clinopyroxenes in monzogabbros and monzodiorites were nearly unzoned although compositionally comparable to those in gabbros, showing Mg#<sub>Cpx</sub> of 68-72. As for gabbroic rocks, equilibrium was reached with intermediately evolved magmas (Mg# 40, Fig. 4a, Table 3), by which thermobarometric equations indicated a  $T$  range of 940-990°C at  $P$  of 1.4-1.6 kbar, for a H<sub>2</sub>O contents in the melt of 3.0-4.0 wt%. All results are reported in Table 4 and Fig. 7a.

#### 6.2.2. Clinopyroxene crystallization conditions of Shoshonitic Silica Undersaturated rocks

Clinopyroxenes from the SU suite are more alkaline than those of the SS rocks, ranging from salitic-aegirinaugitic to ferrosalitic compositions. The most magnesian compositions in gabbros and monzogabbros ( $\text{Mg\#}_{\text{Cpx}}$  67-63) were in equilibrium with  $\text{Mg\#}$  36 melts (Fig. 4b, Table 3). Pressure-temperature paths indicate a  $P$  range of 0.2-1.6 kbar and  $T$  of 920-940°C at water contents of about 1.0-1.5 wt%. Clinopyroxenes in syenites ( $\text{Mg\#}_{\text{Cpx}}$  60-48) show composition close to the equilibrium with the whole rock (Fig. 4b, Table 3), which represent a theoretical slightly evolved trachytic melt. Thermobarometers yielded a  $P$  of 0.2-1.6 kbar at  $T$  of 810-860°C at water contents between 4.0 and 5.0 wt%. Results are reported in Table 4 and shown in Fig. 7a.

### 6.3. Amphibole and amphibole-plagioclase thermobarometer and hygrometer

Pressure, temperature and  $\text{H}_2\text{O}$  conditions for amphibole crystallization were estimated using amphibole-plagioclase Al-exchange thermobarometers (Holland and Blundy 1994; Anderson and Smith 1995; Anderson 1996) and a single amphibole thermobarometers (Ridolfi et al. 2010; Ridolfi and Renzulli 2012). Amphibole-plagioclase equations were used for mineral pairs in both SS and SU suites, whereas the single amphibole thermobarometers were applied to all amphibole compositions in the SS rocks, but only for amphibole in gabbros in the SU suite. This because of the higher alkali content of SU differentiated magmas, well above the compositional ranges admitted for the calibration of the empirical geothermometers of Ridolfi et al. (2010) and Ridolfi and Renzulli (2012). For the SS and SU amphiboles, the single amphibole equations enabled also the calculation of the water content of the melt from which they crystallized. Contrary to the clinopyroxene-melt equations, the error range for the barometric estimates based on amphibole-plagioclase and single amphibole was lower, ranging between  $\pm 0.03$  and  $\pm 0.6$  kbar, whereas errors on  $T$  estimates were slightly higher ( $\pm 23$  to  $\pm 40^\circ\text{C}$ , Table 4).

### 6.3.1. Amphibole crystallization conditions of Shoshonitic Silica Saturated and Shoshonitic Silica Undersaturated rocks

Pressure-temperature paths obtained from amphibole-plagioclase thermobarometers yielded a  $T$ - $P$  range of 750-845°C and 0.1-1.2 kbar in SS gabbros to monzodiorites (Fig. 7a, Table 4). Single amphibole calculations for the same lithotypes confirmed these values, indicating  $P$  = 0.7-1.4 kbar and  $T$  = 720-810°C. The estimated H<sub>2</sub>O contents of melts in equilibrium with amphiboles of SS gabbros to monzodiorites was between 4.8 and 6.0 wt% (Fig. 7b, Table 4). Amphibole-plagioclase **estimates** for the SU suite yielded similar  $P$  intervals (0.4-1.0 kbar) but at lower  $T$  (620-660°C) for gabbros, and  $P$ - $T$  ranges of 1.6-1.9 kbar and 870-880°C taking into account the mineral pairs in the monzogabbroic rocks (Fig. 7a, Table 4). The single amphibole method, applied only to the actinolitic hornblendes in SU gabbros, provided comparable pressures (0.5-0.6 kbar) and temperatures (700-720°C) with respect to the SS rocks (Fig. 7a, Table 4). The calculated water contents of the melts were similar to **those obtained for the SS** suite (5.1-5.7 wt%, Fig. 7b, Table 4).

As expected, the water contents calculated by these models were higher than those obtained from the clinopyroxene-melt calculations. Amphibole crystallization, in fact, occurred later than clinopyroxene, thus the melt from which amphibole precipitated should have undergone differentiation in some extent, and its water content should have increased. If we consider the water enrichment linked to the fractional crystallization of the SS/SU magmas, together with the concomitant precipitation of volatile-bearing phases, the H<sub>2</sub>O contents resulted from the single amphibole equations appear in line with the calculations proposed by the FC model of Casetta et al. (2017).

### 6.4. Biotite thermometer

Biotite is a ubiquitous phase occurring in the late inter-cumulus mineral assemblages of almost all SS, SU and GU rocks. Its presence enabled us to provide some estimates on the temperatures

of these assemblages, by using of the empirical single-mineral thermometer of Henry et al. (2005), based on the Ti content of biotite.

#### 6.4.1. Biotite crystallization conditions of Shoshonitic Silica Saturated, Shoshonitic Silica Undersaturated and Granitic Unit rocks

Temperature of biotite crystallization in SS pyroxenitic cumulates resulted between 690 and 740°C, whereas a  $T$  interval of 600-660°C was considered representative of SS gabbros to monzodiorites. Biotites from more differentiated SS monzonites yielded a  $T$  of about 540-580°C (Fig. 7a, Table 4). Biotite in SU gabbros and monzogabbros indicated comparable temperatures, ranging between 640 and 660°C (Fig. 7a, Table 4).

The thermometer was also applied to GU syenogranites, resulting in a  $T$  range of 420-570°C: the biotites in GU rocks are however iron-rich, with  $Mg/(Mg+Fe_{tot}) < 0.275$ , just out of the compositional field for which the thermometer was calibrated. Consequently, the resulting temperatures were not used for further modeling purposes.

#### 6.5. Plagioclase-melt thermobarometer and hygrometer

Plagioclase appears in almost all PIC rocks, from the cumulitic pyroxenites, where it is part of the intercumulus assemblages, to the syenitic rocks, where, together with K-feldspar, dominates the paragenesis. Its ubiquitous presence made it an additional tool for investigating the  $T$  and  $H_2O$  content of PIC magmas along the entire SS and SU differentiation trends by means of Putirka (2008) and Lange et al. (2009) equations. Plagioclase from GU granites and syenogranites are compositionally close to the pure albitic end-member, probably because of hydrothermal/alteration processes. This made them unsuitable for the hygrometer application, being its calibration limited to  $An_{37}$  plagioclase (Lange et al. 2009).

As for clinopyroxene, plagioclase equilibrium with its host rock was constrained by means of the experimentally determined values of  $^{Pl-Liq}Kd_{An-Ab} = 0.10 \pm 0.05$  at  $T < 1050$  °C and  $0.27 \pm 0.11$

at  $T \geq 1050$  °C (Putirka 2008). However, Mollo et al. (2011) demonstrated that  $^{Plag-Liq}Kd_{An-Ab}$  is highly sensitive to the cooling rate of the melts, being thus variable between  $0.2 \pm 0.02$  (cooling rate of  $0.5^\circ\text{C}/\text{min}$ ) and  $0.35 \pm 0.03$  (cooling rate of  $15^\circ\text{C}/\text{min}$ ). Thus, all plagioclase-melt equilibria (even at  $T < 1050^\circ\text{C}$ ) were considered following a  $^{Plag-Liq}Kd_{An-Ab}$  in the range of  $0.27 \pm 0.11$  (Putirka 2008), whose interval is also in accordance with the results obtained by Mollo et al. (2011). Cooling rate is in fact an essential factor for the crystallization dynamics of intrusive bodies, as testified by the plagioclase morphological variations in PIC rocks, where it appears as both cumulus and intercumulus phase throughout the entire SS/SU fractionation trends. According to crystallization sequences, plagioclase appeared after clinopyroxene and Fe-Ti oxides, just before or even contemporary to biotite and amphibole in the intercumulus assemblages. Consequently, we considered the thermobarometric values obtained by clinopyroxene, amphibole and biotite calculations for each magmatic suite (see above) to identify the  $P$ - $T$ - $H_2O$  interval in which plagioclase crystallized from the melt. As for clinopyroxene, plagioclase often appeared in disequilibrium with its whole rock composition (Fig. 5), and the amount of disequilibrium gradually decreases with increasing the differentiation degree of the corresponding whole rock. Plagioclase in monzodiorites were in fact closer to the equilibrium with respect to those of pyroxenites and gabbros, whereas most of the plagioclase from monzonites and syenites were in equilibrium with their host rock (Fig. 5). As previously mentioned for clinopyroxene, such a trend could be justified by considering that the more evolved rocks likely resemble melt compositions, being close to the eutectic of the system. Thus, plagioclase compositions were related to estimated melt compositions, according to the differentiation trends proposed by Casetta et al. (2017), to retrieve the equilibrium conditions. Once equilibrated, plagioclase and melt compositions were used as input for the Lange et al. (2009) hygrometer to calculate the amount of  $H_2O$  dissolved in the melt (see flow chart of Fig. 6). For each sample, input  $T$  and  $P$  required in Lange et al. (2009)

equation were chosen in the  $T$ - $P$  interval between those estimated by clinopyroxene-melt calculations and those resulted from amphibole and biotite.

Pressure, temperature and  $H_2O$  were calculated by iterating Lange et al. (2009) method and equation 24a of Putirka (2008) until a matching  $T$  was found. In any case, small variations of  $P$  scarcely affect the results of the hygrometers:  $\pm 1$  kbar corresponds to  $\pm 0.1$  wt%  $H_2O$  calculated in the melt (Giacomoni et al. 2014). Since the  $P$  interval obtained by the previous (clinopyroxene and amphibole) barometers was roughly between 0.2 and 1.9 kbar for all PIC rocks, the  $H_2O$  estimates were almost entirely constrained by temperature changes. As a consequence, the match between  $T$  obtained with Lange et al. (2009) and equation 24a of Putirka (2008) was considered a reliable cross-check and a robust constraint on our geothermal modelling (Fig. 6).

#### 6.5.1. Plagioclase crystallization conditions of Shoshonitic Silica Saturated rocks

Data from clinopyroxene-melt simulations on pyroxenites indicated that SS primary magmas began crystallizing at about 1.5 kbar, 1060°C and 2.5  $H_2O$  wt%. The more anorthitic plagioclase ( $An_{84-73}$ ) were analyzed in the pyroxenites intercumulus assemblage, following clinopyroxene and preceding biotite, thus the  $T$  range of plagioclase crystallization is constrained by the temperatures of crystallization of these two phases. Since pressure does not sensitively affect the calculations, a pressure of 1.5 kbar was used according to the results from clinopyroxene-melt calculations (Fig. 6 and 7). Results indicated that the most anorthitic plagioclase ( $An_{84-73}$ ) crystallized in equilibrium with a trachybasaltic melt (Mg# 51; Fig. 5, Table 3): at  $P = 1.5$  kbar,  $T$  of crystallization resulted of 1060-1081°C for a  $H_2O$  content of 3.0 wt%.

Plagioclase in SS gabbros were in compositional continuity with those of pyroxenites, varying between  $An_{73}$  and  $An_{51}$  in both the cumulus and intercumulus assemblages. As for plagioclase inside pyroxenites, the marked disequilibrium (Fig. 5) was probably related to the cumulitic nature of gabbros and/or a variable cooling rate of the magma. The crystallization sequence and



the comparison with the  $T$  ranges obtained from clinopyroxene, amphibole and biotite suggested that plagioclase crystallized in a temperature interval of 980 to 740°C. Plagioclase with An<sub>73</sub> reached the equilibrium with a Mg# 49 melt (Fig. 5): at  $P$  of 1.5 kbar,  $T$  and H<sub>2</sub>O content resulted of 1016-1053°C and 3.1 wt% respectively. An<sub>63-51</sub> plagioclases were equilibrated with a **basaltic trachyandesitic** melt (Fig. 5, **Table 3**), yielding  $T$  of 920-1021°C and a water content of 3.2-3.4 wt% at pressures of 1.2-1.5 kbar (Fig. 7, Table 4). It is worth noting that for these temperatures, Putirka (2008) proposed a potential partitioning  $^{Plag-Liq} Kd_{An-Ab} = 0.05-0.15$  to attest equilibrium. However, after several iterations, the modelled  $P$ - $T$ -H<sub>2</sub>O terms for PIC magmas were attained only within a  $^{Plag-Liq} Kd_{An-Ab}$  of  $0.27 \pm 0.11$ . Such apparent discrepancies could be explained considering the dependency of An-Ab equilibrium coefficient with the cooling rate (Mollo et al. 2011).

Plagioclase from monzogabbros to monzonites were in a compositional range from An<sub>53</sub> to An<sub>34</sub>, resulting in equilibrium with **basaltic trachyandesitic** to **trachyandesitic** melts (Fig. 5, **Table 3**). At  $P$  of 1.2 kbar,  $T$  resulted between 917 and 989°C, for water contents of 3.9-4.8 wt%, progressively increasing with the differentiation degree of the samples (Fig. 7, Table 4).

#### 6.5.2. Plagioclase crystallization conditions of Shoshonitic Silica Undersaturated rocks

Plagioclase in SU rocks range from An<sub>50-43</sub> in gabbros to An<sub>38-23</sub> in monzogabbros and monzodiorites, and reach the more albitic compositions in syenites, where anorthite content is low (An<sub>23</sub>-An<sub>2</sub>). Plagioclase in gabbros were equilibrated by an intermediately evolved melt, **trachyandesitic** in composition (Fig. 5, **Table 3**). According to the themobarometric data obtained by multiple geothermometers (clinopyroxene, amphibole and biotite), the temperature crystallization interval of plagioclase ranges between 940 and 720°C. Plagioclase-melt thermometers and hygrometers yielded a  $T$  range of 975-990°C at  $P$  of 1.5 kbar, for a water content of 4.1 wt%.

Apart from the nearly pure albitic compositions (likely effects of secondary processes), plagioclase in monzogabbros to syenites vary from An<sub>38</sub> to An<sub>23</sub>. They were equilibrated with an evolved **trachytic** melt (Fig. 5, **Table 3**), thought to be the final product of the SU differentiation trend (Casetta et al. 2017). At  $T-P$  space of 920-936°C and 1.2 kbar, the estimated water contents of melt in equilibrium with An<sub>38</sub> plagioclases was about 4.4 wt%, progressively increasing with the differentiation of the samples (Fig. 7, Table 4).

#### 6.6. K-Feldspar-melt hygrometer

Except for pyroxenites, K-feldspar is present in all PIC rocks, where it occurs as intercumulus (gabbros to monzodiorites) and cumulus (monzonites/syenites) phase. Its composition was used to constrain the amount of H<sub>2</sub>O dissolved in the co-existing melt by means of the equation proposed by Mollo et al. (2015). Such method, based on the Or-Ab exchange between K-feldspar and melt **is calibrated for alkaline differentiated magmas, thus proper for the SS, SU and GU rocks compositions**. Together with the data obtained by the previous equations, such estimates enabled to “track” the H<sub>2</sub>O contents in the progressively differentiating melts. According to Mollo et al. (2015), this method can be applied only to K-feldspar with Or<sub>44-86</sub>, whereas no reliable results were produced for Or<sub>>86</sub> as it extended outside the range of calibrated compositions. K-feldspar and whole rock equilibrium evaluation was attained by minimizing the difference between predicted and measured  $K^{K-Feld-Liq}Kd_{Or-Ab}$ , following equation 2 of the Mollo et al. (2015) model. These conditions were satisfied only by considering K-feldspar compositions in equilibrium with **trachyandesitic to trachytic melts (Table 3)**, further confirming the correspondence between the crystallization sequence and the progressive differentiation model proposed by Casetta et al. (2017).

According to the equilibration temperatures recorded by clinopyroxene, amphibole, biotite and plagioclase, a  $T$  of 900-800°C was used as input for all samples of the SS and SU suites, whereas lower temperatures (800-700°C) were considered for GU syenogranites.

### 6.6.1. K-feldspar crystallization conditions of Shoshonitic Silica Saturated, Shoshonitic Silica Undersaturated and Granitic Unit rocks

Water concentration of melts in equilibrium with K-feldspar in SS gabbros to monzogabbros were in the range of 4.4-5.3 wt% and 5.6-6.5 wt% respectively, whereas higher H<sub>2</sub>O contents (6.1-7.3 wt%) were recorded in monzodiorites. The highest water values were calculated in SS syenites, that in turn show a larger variability of values (H<sub>2</sub>O = 4.6-7.3 wt%; Fig. 7, Table 4). K-feldspar analysed in SU monzogabbros and monzonites indicated H<sub>2</sub>O contents of the crystallizing melts between 5.5-6.3 wt% and 6.7-7.8 wt%, respectively. H<sub>2</sub>O estimates for GU syenogranites range between 8 and 11 wt%, being however meaningless in the physical system compatible with the body emplacement. The solubility of water at  $P < 2.5$  kbar for rhyolitic-trachytic melts in fact do not exceed 7 wt%, as experimentally and theoretically determined in the  $T$  range of 500-1000°C (Di Matteo et al. 2004; Liu et al. 2005). These values were therefore discharged in the discussion.

## 7. Oxygen fugacity

The two main magmatic suites (SS and SU) are formed by the differentiation of melts which began crystallizing at pressures lower than 2.0 kbar and at similar  $T$  ranges (1050-1000°C). Main differences between the SS and SU suites could be found by taking into account the total amount of water of the crystallizing melts: SS primitive melts in fact were characterized by an higher water contents with respect to that of SU ones (2.0-2.5 wt% vs. 1.0-1.5 wt%, respectively). Classically, it is considered that dissolved molecular H<sub>2</sub>O reacts with oxygens of the silicate network producing two OH<sup>-</sup> groups (e.g. Stolper 1982; Silver and Stolper 1985; Kohn 2000). The overall reaction reading as  $H_2O + O^{2-} = 2OH^-$  may thus be considered as the counterpart of the water solubility in evaluating the redox conditions.

To effectively quantify such differences, we estimated the  $f\text{O}_2$  conditions of each portion of PIC by means of the  $T$ - $f\text{O}_2$  model of Burkhard (1991), based on the biotite/K-feldspar/magnetite equilibrium in biotite-bearing intrusive rocks. Burkhard's (1991) empirical equation complements that of Kress and Carmichael (1988), enabling to calculate oxygen fugacity and temperature by two independent formulas. Water fugacity required in Burkhard's (1991) equation was calculated at a fixed  $P$  of 1.5 kbar following Burnham et al. (1969). Sanidine activity was considered according to Waldbaum and Thompson (1969), whereas magnetite activity was approximated at unity (Burkhard 1991). Since this equation required as input the amount of  $\text{Fe}^{2+}$  in biotite,  $\text{Fe}^{2+}/\text{Fe}^{3+}$  ratios of SS, SU and GU biotites were calculated following Dymek (1983). Because the compositional spectrum of biotite and sanidine in each rock is slightly variable, we calculated two  $T$ - $f\text{O}_2$  pairs for each lithotype (Fig. 8, Table 4), to account for the possible oxygen fugacity ranges. According to Burkhard (1991), the error on each calculation was of  $\pm 0.3$  log units.

As shown in Fig. 8, oxygen fugacity in SS rocks resulted in a range from -14.1 to -10.7  $\log f\text{O}_2$ , at temperatures comprised between 790 and 1000°C (Table 4). Such values plot between the FMQ and NNO buffers (+0.2 to +0.7  $\Delta\text{FMQ}$ , Fig. 8), and are well comparable to the values chosen as input for the Rhyolite-MELTS model above developed (-9.34  $\log f\text{O}_2$  at 1060°C), further confirming the validity of the calculated parameters. Rocks from the SU and GU suites were characterized by values of -11.9 to -10.2  $\log f\text{O}_2$  at  $T$  of 920-1050°C (-0.1 to +0.3  $\Delta\text{FMQ}$ , Fig. 8), and -12.9 to -11.8  $\log f\text{O}_2$  at  $T$  of 850-920°C (around +0.4  $\Delta\text{FMQ}$ , Fig. 8), respectively (Table 4). Syenogranites of the GU suite were characterized by a behavior comparable to that of SS rocks, whereas SU rocks record slightly more reduced conditions.

## 8. EC-AFC processes

As shown by the thermobarometric and hygrometric models, the two main magmatic suites (SS and SU) emplaced and crystallized at comparable pressures and temperatures conditions. The

only differences can be identified when water content and oxygen fugacity are considered, being the SU system characterized by lower H<sub>2</sub>O content and by more reduced conditions. Anyway, such slight divergences are not able to justify the marked geochemical variations between SS and SU magmas (see also Casetta et al. 2017). To account for the geochemical features of the SS and SU batches, we developed several Energy-Constrained Assimilation and Fractional Crystallization (EC-AFC) models (Bohrson and Spera 2001; Spera and Bohrson 2001), based on <sup>87</sup>Sr/<sup>86</sup>Sr and <sup>143</sup>Nd/<sup>144</sup>Nd. The purpose of this calculation was to discriminate between the original (i.e. mantle-derived) signature of SS/SU magmas and the effects of assimilation (and/or contamination) during the emplacement and differentiation of PIC magmas. Specifically, the main target of the models were: (i) verifying if the isotopic signature of SU rocks was generated an interaction between SS magmas and crust; (ii) quantify the eventual (if any) crustal assimilation during the differentiation of the SS/SU magmatic suites; (iii) discriminate between assimilation and contamination processes.

A wide spectrum of Permo-Triassic crustal rock isotopic signatures from the literature were considered in the EC-AFC model as potential assimilants. These are Triassic carbonates (Martin and Macdougall 1995; Blendiger et al. 2015), Permian intrusives of Mt. Croce (central-eastern Southern Alps; Rottura et al. 1997) and Serie dei Laghi (southwestern Alps; Sinigoi et al. 2016, and references therein), Permian rhyolitic ignimbrites of the Atesina Volcanic District (Barth et al. 1993), and the Kinzigite formation (southwestern Alps; Voshage et al. 1990).

Geothermobarometric and hygrometric results (Table 4) were used to to calculate assimilants and starting magmas' specific heat [J/(KgK)], heat of crystallization (J/Kg) and heat of fusion (J/Kg) according to Spera (2000), Bohrson and Spera (2001) and Spera and Bohrson (2001, Table 5). Specific heat [J/(KgK)] and liquidus T (°C) of carbonate assimilant (Table 5) were considered accordingly to Dallai et al. (2011) and Eppelbaum et al. (2014).

The absence of <sup>87</sup>Sr/<sup>86</sup>Sr and <sup>143</sup>Nd/<sup>144</sup>Nd variations with increasing silica content for both SS and SU suites and the lack of overlap between SS and SU compositional fields suggested that

the two suites have a different origin. A slight  $^{87}\text{Sr}/^{86}\text{Sr}$  increase was however noted for both SS and SU samples while approaching the intrusion borders (Table 2). On the other side, the  $^{143}\text{Nd}/^{144}\text{Nd}$  of both SS and SU rocks were not sensitive to the distance from intrusion edges, ruling out the occurrence of contamination processes during magma emplacement. Therefore, the Nd isotopic enrichment of the SU suite can be considered as a primary feature, directly function of its mantle source or alternatively derived from assimilation of crustal components. In this view, the EC-AFC equations were applied to the less contaminated compositions to better constrain the Sr and (especially) Nd isotopic variations among the magmatic suites.

The EC-AFC model from a starting SS composition (Fig. 9) showed that none of the chosen crustal components was able to drive the initial SS  $^{87}\text{Sr}/^{86}\text{Sr}$  and  $^{143}\text{Nd}/^{144}\text{Nd}$  ratios towards the SU field. This simulation reinforced the primary nature of the Nd isotopes enrichment of the SU body, ruling out the genesis of the SU rocks via crustal assimilation by an SS starting magma. The model was instead able to explain the isotopic variability of the SS samples. Almost all assimilation models well fitted the isotopic trend of SS rocks, suggesting that small amounts of crustal components were assimilated during magma storage. As shown in Fig. 9, the less depleted  $^{143}\text{Nd}/^{144}\text{Nd}$  end-members were achieved by an interaction between magma and 2-10% of crust, represented by kinzigites (Voshage et al. 1990), Mt. Croce granodiorites (Rottura et al. 1997) and/or Atesina Volcanic District rhyolitic ignimbrites (Barth et al. 1993). A 5% assimilation of carbonates (Martin and Macdougall 1995; Blendiger et al. 2015) and/or Serie dei Laghi-like granites (Sinigoi et al. 2016) instead reproduced the more depleted  $^{143}\text{Nd}/^{144}\text{Nd}$  ratios.

A second EC-AFC model was attempted to explain the isotopic variations of SU samples, but their scattered distribution prevented to retrace the assimilation path. Nevertheless, this model was used just to quantify the crustal contribution in the Nd isotopic variations of the SU samples. As a result, the  $^{143}\text{Nd}/^{144}\text{Nd}$  range of the SU suite was achieved by a 2-7% assimilation

of the crustal components (carbonates, Atesina Volcanic District rhyolitic ignimbrites, Mt. Croce granodiorites, Serie dei Laghi granites and amphibolitic kinzigites).

On the whole, the Nd isotopic ranges of both SS and SU suites could be explained by low amounts of assimilation, whereas Sr isotopic variability is more likely derived from contamination processes at the intrusion borders during magma emplacement, where fluid mobilization and local metamorphic reactions occurred (Ferry et al. 2002; Gallien et al. 2007).

As reported in Table 2, the Sr isotopic signature of PIC rocks appears to be more sensitive to their distance to the intrusion edges rather than to their degree of differentiation, being thus the  $^{143}\text{Nd}/^{144}\text{Nd}$  ratio the best proxy to discriminate the two magmatic suites. Given this, the Sr variations of the SU suite at near constant  $^{143}\text{Nd}/^{144}\text{Nd}$  could be also affected by i) slight alteration effects, unavoidable for such a small body and/or ii) the contact halo between PIC and the wall rocks.

## 9. Discussion

### 9.1. Emplacement of the Shoshonitic Silica Saturated and Shoshonitic Silica Undersaturated magmas

The SS and SU intrusive bodies formed as result of fractional crystallization of two distinct trachybasaltic melts, which differentiated along two independent trends over a short time span.

The result of this process was the generation of a large spectrum of intrusive rocks whose cumulus+intercumulus assemblages progressively vary in composition, reaching the most evolved nature in the syenitic rocks. The textural/compositional homogeneity of the main cumulus phases of PIC rocks, together with the scarce efficiency of syn- to post-crystallization diffusion processes on such large-sized crystals, led us to hypothesize that their composition is directly function of the physical conditions at which they formed and segregated from the melt.

In this scenario, clinopyroxene and plagioclase were considered as “snapshots” of the fractional



crystallization processes, able to provide informations on the *T-P* conditions of the melts from which they generated.

If we compare the clinopyroxene and plagioclase compositions to that of their host rock, in fact, the disequilibrium is evident (Figg. 4 and 5). Clinopyroxene of SS gabbros (Mg# 55), for example, are characterized by Mg# of 65-71, ideally in equilibrium with melt with Mg# < 43, quite far from the bulk rock composition of the gabbro. The most magnesian ones (Mg#<sub>Cpx</sub> 76-78), in pyroxenites, are theoretically in equilibrium with a trachybasaltic melt (Mg# 51), further confirming that the mafic rocks of the complex are cumulates formed during the initial stages of fractionation of the trachybasaltic melt. On the other hand, the less magnesian clinopyroxene crystals tracked in syenites were almost in equilibrium with their host rocks, corroborating the assumption that the more differentiated rocks of the complex resemble the composition of melts and approach the eutectic of the system. On the basis of the results obtained by the proposed “equilibration model”, in turn supporting the differentiation model of Casetta et al. (2017), PIC rocks were formed during progressive stages of fractional crystallization from starting trachybasaltic melts.

Once evaluated the disequilibrium conditions and reconduted the clinopyroxene/plagioclase compositions to their ideal equilibrium conditions, thermobarometric and hygrometric calculations enabled us to retrieve the *T-P-H<sub>2</sub>O* parameters of the less evolved melts in the feeding system. The “classical” thermobarometric approach for intrusive rocks (amphibole-plagioclase and biotite equations) was then used to verify the previous results. These thermobarometers and hygrometers provided *T-P-H<sub>2</sub>O* informations for the later crystallization stages.

According to our estimates, some differences between the emplacement conditions of SS and SU magmas can be highlighted. Oxygen fugacities of the PIC plumbing system are between -0.1 and +0.7  $\Delta$ FMQ (Fig. 8), confirming the oxidation conditions proposed by Bonadiman et al. (1994) for Mt. Monzoni intrusion at comparable temperature intervals, further highlighting



the low to moderate oxydizing components that characterized the magmatic systems of the Dolomitic Area during Triassic.

On the basis of clinopyroxene-melt thermometric and hygrometric calculations, SS magmas result slightly water-enriched ( $H_2O = 2.0-2.5$  wt%) with respect to SU ones ( $H_2O = 1.0- 1.5$  wt%), during the first crystallization stages ( $T \sim 1000-1100^\circ C$ , Fig. 7, Table 4). With increasing differentiation, the water content of PIC rocks increased up to 5-8 wt%, value compatible with the amount of fractionation (79-94%) proposed by Casetta et al. (2017), by taking into account the role of amphibole and biotite during differentiation.

The  $T$ - $P$  estimates (Fig. 7, Table 4) indicated that both magma batches cooled from a starting  $T$  of  $\sim 1000-1100^\circ C$  (cumulus assemblage) down to  $\sim 600^\circ C$  (intercumulus assemblage), sharing a common thermal regime. The pressure obtained by applying various mineral-mineral and mineral-melt equilibria were subsequently used to estimate the emplacement depth of the PIC plumbing system, and all the pressures were filtered to extrapolate the best-fit from all models, taking into account the errors of the different methods (Table 4). The resulting pressure values were between 0.4 and 1.7 kbar for both SS and SU intrusive bodies, yielding a depth of about 1.4-5.6 km considering a  $\Delta P/\Delta z$  of 0.29 kbar/km. With respect to the depth (10-17 km) proposed by Menegazzo Vitturi et al. (1995), our estimates suggested that PIC represents an intrusion in the shallow crust, with SS and SU magma batches emplaced within the same thermal regime.

Despite the common geothermobarometric evolution and slightly different water contents, SS and SU bodies can be distinguished in terms of  $^{87}Sr/^{86}Sr$  and  $^{143}Nd/^{144}Nd$ , reinforcing the preliminary PIC model that, on the basis of mineral and bulk rock elemental geochemistry (Casetta et al. 2017) suggested that SS and SU series represent two independent magma pulses. EC-AFC models (Bohrson and Spera 2001; Spera and Bohrson 2001) show that assimilation of various types of Permo-Triassic crustal components by a starting SS magma could not account for the higher  $^{143}Nd/^{144}Nd$  of the SU batch, ruling out any possible derivation of the SU suite from the SS one. Therefore, the Nd isotopic enrichment of the SU suite could be interpreted as

an original mantle signature or, alternatively, could be ascribed to assimilation processes occurring within the crust. We prefer the first hypothesis, since the second one would imply the existence of a common mantle-segregated magma with a  $^{143}\text{Nd}/^{144}\text{Nd}$  ratio high enough to be able to “split” in the SS and SU trends by varying the nature of the assimilant, and such a magma has never been documented in the Dolomitic Area.

The same EC-AFC models demonstrated that both suites assimilated a small proportion of crustal components (5-6% on average, Fig. 9). That amount of assimilation is, however, able to explain the  $^{143}\text{Nd}/^{144}\text{Nd}$  variation throughout SS/SU samples, being that the  $^{87}\text{Sr}/^{86}\text{Sr}$  was affected by late contamination that occurred at the intrusion edges. The fit between PIC isotopic data and the crustal end-members of the Triassic carbonates, the Permian magmatic rocks and the metamorphic basement of the Ivrea Zone is consistent with a geochemical influence on the PIC of a basement that could be attributed to the Ivrea Zone. This hypothesis was also suggested by Barth et al. (1993) to explain the Atesina Volcanic District-Cima d’Asta magma genesis.

In summary, both SS and SU batches are characterized by a strong contribution of an enriched mantle component, even if the lack of primitive products cannot directly quantify its role in the original source. Anyway, if examined in the light of their temporal relationships, the major, trace element and Sr-Nd isotopic signature of the SS and SU bodies enable to define the progressive evolution of the PIC magmatic suites. In turn, this geochemical evolution could be linked to a time-related (slight) variation of the mantle source, even if an accurate dating of the two single bodies would help in better deciphering the time scale of such process. On the other side, the magmatic evolution in the shallow crust for both the SS and SU batches was confined in the same thermal regime.

## 9.2. Origin of the Granitic Unit

The GU rocks (granites and syenogranites) differ from the other PIC magmatic suites (SS and SU), mainly in terms of silica saturation, FeO, MgO, K<sub>2</sub>O and Rb contents (Casetta et al. 2017).

Moreover the estimated volume of the GU portion of the complex ( $1.1 \text{ km}^3$ ) is unrealistically larger than that of the SS/SU syenites ( $\leq 0.25 \text{ km}^3$ ) if we consider the already high ( $> 90\%$ ) fractionation degrees from which these latters generated. This means that, if the GU portion was the result of  $\sim 95\%$  fractionation of a SS/SU magma,  $\sim 20 \text{ km}^3$  of SS/SU rocks should be intruded somewhere. This fact is in stark contrast to what is observable on field.

The GU magmas evolved at redox states comparable to SS/SU ones (about  $+0.4 \Delta\text{FMQ}$ ) and record temperatures down to  $800\text{-}850^\circ\text{C}$  (Fig. 8). Put this all together, it is reasonable to hypothesize that the GU granites/syenogranites were generated by magmatic differentiation from a calc-alkaline parental melt, the primitive/intermediate products of which are not exposed in the PIC area. It should be emphasized that GU rocks are similar to the Middle Triassic calc-alkaline/high-K calc-alkaline rhyolites found in Carnia (Tarvisio area, Julian Alps; Gianolla 1992) and Alto Vicentino regions (Recoaro-Schio area, Southern Alps; De Vecchi et al. 1974; Barbieri et al. 1982). In these latters, the entire high-K calc-alkaline trend is documented, further highlighting the existence of a similar differentiation suite during the Triassic magmatic event. In such a context, GU rocks could represent the corresponding intrusives of the rhyolites of these areas, even if further studies are needed to better investigate this comparison.

### 9.3 Solidification time of PIC

According to Bonadiman et al. (1994) the solidification time of Mt. Monzoni intrusion, emplaced at  $P$ - $T$ - $z$  conditions similar to those of PIC, was about 300 ka. The thermobarometric results obtained for PIC magmas and their subsequent application to the Spera (2000), Bohrsen and Spera (2001) and Spera and Bohrsen (2001) equations, enabled to model the cooling time of PIC, expected to be slightly higher than that of Mt. Monzoni, due to its larger volume ( $4.5 \text{ km}^3$  vs.  $1.0\text{-}1.5 \text{ km}^3$ ).

In order to make an accurate comparison with Bonadiman et al. (1994), Spera (1980) equation was applied to PIC by assuming the thermal estimates already used for the EC-AFC calculations

and/or derived from Ryolite-MELTS modelling (see Table 5). By taking into account the whole volume of PIC, the solidification time resulted about 700 ka. Even if this time value was obtained without discriminating the single volumes of the SS, SU and GU bodies, it was considered reliable taking into account the similar thermal regimes calculated for the SS, SU and GU suites and the limited re-heating effects provided by the subsequent magma pulses.

## 10. Conclusions

A coupled thermobarometric and isotopic study of the main magmatic suites of the Predazzo Intrusive Complex enabled us to set out some remarkable points on the emplacement conditions of the Middle Triassic magmas in the Dolomitic Area. They can be summarized as:

1. Predazzo Intrusive Complex emplacement occurred at a depth of 1.4-5.6 km (0.40-1.65 kbar), consistent with the field relationships suggesting consanguinity with the overlying effusive rocks. Its solidification time was about 700 ka, slightly higher but comparable to that proposed by Bonadiman et al. (1994) for the near Mt. Monzoni intrusion.

2. Despite similar  $T$ - $P$  of magma emplacement of the three unites,  $H_2O$  and  $fO_2$  data indicated that SU primary magmas were characterized by lower water contents and oxidizing conditions than the SS ones (1.0-1.5 vs. 2.0-2.5  $H_2O$  wt%; -0.1/+0.33 vs. +0.2/+0.7  $\Delta FMQ$ , respectively). Plagioclase-melt, amphibole and K-feldspar-melt hygrometers indicated highly hydrated conditions of magmas and progressive  $H_2O$  enrichment during differentiation.

3. The  $^{87}Sr/^{86}Sr$  and  $^{143}Nd/^{144}Nd$  of PIC magmas plot in the enriched mantle source field. This feature speaks in favour of the presence of a subduction-signature in the mantle beneath Southern Alps during Triassic, as already proposed by Bonadiman et al. (1994) and Zanetti et al. (2013). Even if the absence of primary products in the Dolomitic Area prevents to exactly quantify the role of the enriched mantle component in the magma genesis, its contribution was undoubtedly high.

4. The EC-AFC models cannot account for the genesis of SU rocks via crustal assimilation starting from a SS magma, thus indicating two distinct geochemical signatures for SS and SU magmas. In turn, this difference could be ascribed to a time-related change in the mantle source, slightly moving towards a more  $^{143}\text{Nd}/^{144}\text{Nd}$  enriched component.

5. A low degree of crustal assimilation (5-6%) was able to explain the Nd isotopic variability of both SS and SU magmas, whereas the Sr isotopic variations were more likely the results of contamination processes at PIC edges. Fractional crystallization was the major (and almost only) process acting during the differentiation of SS and SU magmas, confirming what hypothesized by Petersen et al. (1980) and Casetta et al. (2017). The signature of the Triassic magmas is consistent with an Ivrea-like basement beneath the Dolomitic Area.

6. Despite petrography, whole-rock and mineral chemistry suggested an I-type affinity for GU granites/syenogranites, the wide range and the uncertainty on their isotopic signature leaves the question on the origin of GU suite still unsolved. However, the geochemical and petrographic similarities with the coheval calc-alkaline/high-K calc-alkaline rhyolites found in Carnia (Gianolla 1992) and Alto Vicentino (De Vecchi et al. 1974; Barbieri et al. 1982; Bellieni et al. 2010) suggest the presence of a high-K calc-alkaline series also in the Dolomitic Area.

## Acknowledgments

We are grateful to Andrea Marzoli and Matteo Masotta for their careful and constructive reviews that significantly improved the quality of the paper, and we would also acknowledge Timothy L. Grove for his editorial guidance. The IUSS Mobility Research Programme of the University of Ferrara, grant n. 570 for Long Period, 2016 (FC) and The Italian National Research Program PRIN\_2015/prot. 20158A9 (CB) supported this research. Anne Kelly and Vincent Gallagher are also thanked for making the Sr and Nd isotopic analyses at SUERC.

## References

- Anderson JL (1996) Status of thermobarometry in granitic batholiths. *Geol Soc Am Spec Pap* 315: 125-138. <https://doi.org/10.1017/S0263593300006544>
- Anderson JL, Smith DR (1995) The effects of temperature and  $fO_2$  on the Al-in-hornblende barometer. *Am Min* 80(5-6): 549-559.
- Barbieri G, De Vecchi GP, De Zanche V, Mietto P, Sedeà R (1982) Stratigrafia e petrologia del magmatismo triassico nell'area di Recoaro. Guida alla geologia del Sudalpino centro-orientale. *Soc Geol It Guide Geologiche Regionali*: 179-187.
- Barth S, Oberli F, Meier M, Blattner P, Bargossi GM, Di Battistini G (1993) The evolution of a calc-alkaline basic to silicic magma system: geochemical and Rb–Sr, Sm–Nd, and  $^{18}O/^{16}O$  isotopic evidence from the Late Hercynian Atesina-Cima d'Asta volcanoplutonic complex, northern Italy. *Geochim Cosmochim Acta* 57: 4285-4300. [https://doi.org/10.1016/0016-7037\(93\)90323-O](https://doi.org/10.1016/0016-7037(93)90323-O)
- Bellieni G, Fioretti AM, Marzoli A, Visonà D (2010) Permo–Paleogene magmatism in the eastern Alps. *Rend Lincei* 21: S51-S71. <https://doi.org/10.1007/s12210-010-0095-z>
- Bernoulli D, Lemoine M (1980) Birth and Early Evolution of the Tethys: the Overall Situation. *Mem Bur Rech Géol Minières* 115: 168-179.
- Blendinger W, Lohmeier S, Bertini A, Meißner E, Sattler CD (2015) A new model for the formation of Dolomite in the Triassic dolomites, Northern Italy. *J Pet Geo* 38(1): 5-36. [10.1111/jpg.12596](https://doi.org/10.1111/jpg.12596)
- Bohrson WA, Spera FJ (2001) Energy-constrained open-system magmatic processes II: application of energy-constrained assimilation–fractional crystallization (EC-AFC) model to magmatic systems. *J Petrol* 42(5): 1019-1041. <https://doi.org/10.1093/petrology/42.5.1019>
- Bonadiman C, Coltorti M, Siena F (1994) Petrogenesis and T- $fO_2$  estimates of Mt. Monzoni complex (Central Dolomites, Southern Alps): a Triassic shoshonitic intrusion in a transcurent geodynamic setting. *Eur J Mineral* 6: 943-966. [10.1127/ejm/6/6/0943](https://doi.org/10.1127/ejm/6/6/0943)

- Borsi S, Ferrara G (1968) Isotopic age measurements of the M. Monzoni intrusive complex. *Miner Petrogr Acta* 14: 171-183.
- Brack P, Mundil R, Oberli F, Meier M, Rieber H (1996) Biostratigraphic and radiometric age data question the Milankovitch characteristics of the Latemar cycles (Southern Alps, Italy). *Geology* 24(4): 371-375. [https://doi.org/10.1130/0091-7613\(1996\)024<0371:BARADQ>2.3.CO;2](https://doi.org/10.1130/0091-7613(1996)024<0371:BARADQ>2.3.CO;2)
- Brack P, Mundil R, Oberli F, Meier M, Rieber H (1997) Biostratigraphic and radiometric age data question the Milankovitch characteristics of the Latemar cycles (Southern Alps, Italy). Reply: *Geology* 25(5): 471-472.
- Brack P, Rieber H, Nicora A, Mundil R (2005) The Global boundary Stratotype Section and Point (GSSP) of the Ladinian Stage (Middle Triassic) at Bagolino (Southern Alps, Northern Italy) and its implications for the Triassic time scale. *Episodes* 28 (4): 233-244.
- Brady JB, McCallister RH (1983) Diffusion data for clinopyroxenes from homogenization and self-diffusion experiments. *Am Min* 68: 95-105
- Burkhard DJM (1991) Temperature and redox path of biotite-bearing intrusives: a method of estimation applied to S- and I-type granites from Australia. *Earth Planet Sci Lett* 104: 89-98. [https://doi.org/10.1016/0012-821X\(91\)90240-I](https://doi.org/10.1016/0012-821X(91)90240-I)
- Burnham DJM, Holloway JR, Davis NF (1969) Thermodynamic properties of water to 1000°C and 10,000 bars. *Geol Soc Am Spec Pap* 132: 96.
- Casetta F, Coltorti M, Marrocchino E (2017) Petrological evolution of the Middle Triassic Predazzo Intrusive Complex, Italian Alps. *Int Geol Rev* 60(8): 977-997. <https://doi.org/10.1080/00206814.2017.1363676>
- Cassinis G, Cortesogno L, Gaggero L, Perotti CR, Buzzi L (2008) Permian to Triassic geodynamic and magmatic evolution of the Brescian Prealps (eastern Lombardy, Italy). *B Soc Geol Ital* 127(3): 501-518.

- Castellarin A, Lucchini F, Rossi PL, Sartori L, Simboli G, Sommavilla E (1982) Note geologiche sulle intrusioni di Predazzo e dei M. Monzoni. Guida alla geologia del Sudalpino centro-orientale: Guide geologiche regionali SGI: 211-219.
- Castellarin A, Lucchini F, Rossi PL, Simboli G, Bosellini A, Sommavilla E (1980) Middle Triassic magmatism in Southern Alps II: A geodynamic model. Riv Ital Paleontol S 85(3-4): 1111-1124.
- Chappell BW, White AJR (2001) Two contrasting granite types: 25 years later. Aust J Earth Sci 48(4): 489-499. 10.1046/j.1440-0952.2001.00882.x
- Cherniak DJ, Liang Y (2012) Ti diffusion in natural pyroxene. Geochim Cosmochim Acta 98: 31-47. <https://doi.org/10.1016/j.gca.2012.09.021>
- Coltorti M, Siena F, Visonà D (1996) Aspetti petrologici del magmatismo Triassico dell'area di Predazzo. 78° Riunione estiva Soc. Geol. It: Geologia delle Dolomiti. San Cassiano (1996), Conference Abstract.
- Dallai L, Cioni R, Boschi C, D'Oriano C (2011) Carbonate-derived CO<sub>2</sub> purging magma at depth: influence on the eruptive activity of Somma-Vesuvius, Italy. Earth Planet Sci Lett 310(1): 84-95. <https://doi.org/10.1016/j.epsl.2011.07.013>
- Dal Piaz G, Bistacchi A, Gianotti F et al. (2015) Carta Geologica d'Italia-Foglio 070 Monte Cervino. Carta Geologica d'Italia, 1:50.000 scale: 70.
- De Vecchi G, De Zanche V, Sedeà R (1974) Osservazioni preliminari sulle manifestazioni magmatiche triassiche nelle Prealpi Vicentine (area di Recoaro-Schio-Posina). B Soc Geol Ital 93(2): 397-409.
- Della Lucia A (1997) Aspetti vulcanologici e petrologici del complesso vulcano-plutonico Triassico di Cima Pape (Pale di San Lucano, BL). Unpublished master thesis, University of Ferrara.



- Dimanov A, Jaoul O, Sautter V. (1996) Calcium self-diffusion in natural diopside single crystals. *Geochim Cosmochim Acta* 60(21): 4095-4106. [https://doi.org/10.1016/S0016-7037\(96\)00250-5](https://doi.org/10.1016/S0016-7037(96)00250-5)
- Di Matteo V, Carroll MR, Behrens H, Vetere F, Brooker RA (2004) Water solubility in trachytic melts. *Chem Geol* 213(1-3): 187-196. <https://doi.org/10.1016/j.chemgeo.2004.08.042>
- Doglioni C (1987) Tectonics of the Dolomites (Southern Alps, Northern Italy). *J Struct Geol* 9: 181-193. [https://doi.org/10.1016/0191-8141\(87\)90024-1](https://doi.org/10.1016/0191-8141(87)90024-1)
- Doglioni C (2007) Tectonics of the Dolomites. *Bull Angew Geol* 12(2): 11-15.
- Dymek FR (1983) Titanium, aluminium and interlayer cation substitution in biotite from high-grade gneisses, West Greenland. *Am Mineral* 68: 880-899.
- Eppelbaum L, Kutasov I, Pilchin A (2014) Thermal properties of rocks and density of fluids. In: *Applied geothermics*. Springer Berlin Heidelberg, pp. 99-149.
- Ferry JM, Wing BA, Penniston-Dorland SC, Rumble D (2002) The direction of fluid flow during contact metamorphism of siliceous carbonate rocks: new data for the Monzoni and Predazzo aureoles, northern Italy, and a global review. *Contrib Mineral Petrol* 142(6): 679-699. <https://doi.org/10.1007/s00410-001-0316-7>
- Gallien F, Abart R, Wyhlidal S (2007) Contact metamorphism and selective metasomatism of the layered Bellerophon Formation in the eastern Monzoni contact aureole, northern Italy. *Mineral Petrol* 91(1): 25-53. <https://doi.org/10.1007/s00710-007-0184-6>
- Gasparotto G, Simboli G (1991) Mineralogia, petrografia e schemi evolutivi delle magmatiti triassiche del complesso di Cima Pape (Dolomiti Orientali). *Mineral Petrogr Acta* 34: 205-234.
- Giacomoni PP, Ferlito C, Coltorti M, Bonadiman C, Lanzafame G (2014) Plagioclase as archive of magma ascent dynamics on “open conduit” volcanoes: The 2001–2006 eruptive period at Mt. Etna. *Earth Sci Rev* 138: 371-393. <https://doi.org/10.1016/j.earscirev.2014.06.009>

- Gianolla P (1992) Evoluzione mediotriassica del vulcanismo di Rio Freddo (Api Giulie, Italia). Mem Sci Geol 44: 193-209.
- Gianolla P, Avanzini M, Breda A et al. (2010) Dolomites, 7th International Triassic Field Workshop, Field trip to the World Heritage Site of the Tethyan Triassic. September 5-10 2010, Dolomites, Southern Alps, Italy. With the adesion of Fondazione Dolomiti-Dolomiten-Dolomites-Dolomitis Unesco.
- Grove TL, Baker MB, Kinzler RJ (1984) Coupled CaAl-NaSi diffusion in plagioclase feldspar: Experiments and applications to cooling rate speedometry. *Geochim Cosmochim Acta* 48: 2113-2121.
- Gualda GAR, Ghiorso MS, Lemons RV, Carley TL (2012) Rhyolite-MELTS: a Modified Calibration of MELTS Optimized for Silica-rich, Fluid-bearing Magmatic Systems. *J Petrol* 53: 875-890. <https://doi.org/10.1093/petrology/egr080>
- Henry DJ, Guidotti CV, Thomson JA (2005) The Ti-saturation surface for low-to-medium pressure metapelitic biotites: Implications for geothermometry and Ti-substitution mechanisms. *Am Mineral* 90(2-3): 316-328. <https://doi.org/10.2138/am.2005.1498>
- Holland T, Blundy J (1994) Non-ideal interactions in calcic amphiboles and their bearing on amphibole-plagioclase thermometry. *Contrib Mineral Petrol* 116(4): 433-447. <https://doi.org/10.1007/BF00310910>
- Huebner JS, Sato M (1970) The oxygen fugacity-temperature relationships of manganese oxide and nickel oxide buffers. *Am Mineral* 55: 934-952.
- Ickert RB (2013) Algorithms for estimating uncertainties in initial radiogenic isotope ratios and model ages. *Chem Geol* 340: 131-138. <https://doi.org/10.1016/j.chemgeo.2013.01.001>
- Kohn SC (2000) The dissolution mechanisms of water in silicate melts; a synthesis of recent data. *Mineral Mag* 64(3): 389-408. <https://doi.org/10.1180/002646100549463>
- Kress VC, Carmichael IS (1988) Stoichiometry of the iron oxidation reactions in silicate melts. *Am Mineral* 73: 1267-1274.

- Kress VC, Carmichael IS (1991) The compressibility of silicate liquids containing  $\text{Fe}_2\text{O}_3$  and the effect of composition, temperature, oxygen fugacity and pressure on their redox states. *Contrib Mineral Petrol* 108(1-2): 82-92. [10.1007/BF00307328](https://doi.org/10.1007/BF00307328)
- Lange RA, Frey HM, Hektor J (2009) A thermodynamic model for the plagioclase-liquid hygrometer/thermometer. *Am Mineral* 94(4): 494-506. <https://doi.org/10.2138/am.2009.3011>
- Laurenzi MA, Visonà D, (1996)  $^{40}\text{Ar}/^{39}\text{Ar}$  Chronology of Predazzo magmatic complex (Southern Alps, Italy). 78° Riunione estiva Soc. Geol. It: Geologia delle Dolomiti. San Cassiano (1996): 16-18.
- Le Maitre RW (2002) A classification of igneous rocks and glossary of terms. Cambridge University Press.
- Leake BE, Arps CES, Birch WD (1997) Nomenclature of amphiboles: Report of the Subcommittee on Amphiboles of the International Mineralogical Association, Commission on New Minerals and Mineral Names. *Am Mineral* 82: 1019-1037. <https://doi.org/10.1180/minmag.1997.061.405.13>
- Lippolt H, Pidgeon R (1974) Isotopic mineral ages of a diorite from the Eisenkappel intrusion, Austria. *Zeitschrift für Naturforschung* 29a.
- Liu Y, Zhang Y, Behrens H (2005) Solubility of  $\text{H}_2\text{O}$  in rhyolitic melts at low pressures and a new empirical model for mixed  $\text{H}_2\text{O}$ - $\text{CO}_2$  solubility in rhyolitic melts. *J Volcanol Geotherm Res* 143(1-3): 219-235. <https://doi.org/10.1016/j.jvolgeores.2004.09.019>
- Lucchini F, Rossi PL, Simboli G (1982) Il magmatismo triassico dell'area di Predazzo (Alpi Meridionali, Italia). In Castellarin A, Vai GB (eds) Guida alla Geologia del Sudalpino centro-orientale: Guide Geologiche Regionali Società Geologica Italiana: pp. 221-230.
- Lugmair GW, Marti K (1978) Lunar initial  $^{143}\text{Nd}/^{144}\text{Nd}$ : differential evolution of Lunar crust and mantle. *Earth Planet Sci Lett* 39: 349-357. [https://doi.org/10.1016/0012-821X\(78\)90021-3](https://doi.org/10.1016/0012-821X(78)90021-3)

- Manzotti P, Ballèvre M, Dal Piaz GV (2017) Continental gabbros in the Dent Blanche Tectonic System (Western Alps): from the pre-Alpine crustal structure of the Adriatic palaeo-margin to the geometry of an alleged subduction interface. *J Geol Soc* 174(3): 541-556.
- Marocchi M, Morelli C, Mair V, Klötzli U, Bargossi GM (2008) Evolution of large silicic magma systems: new U–Pb zircon data on the NW Permian Athesian Volcanic Group (Southern Alps, Italy). *J Geol* 116: 480-498.
- Marrocchino E, Coltorti M, Visonà D, Thirwall, MF (2002) Petrology of Predazzo magmatic complex (Trento, Italy). *Geochim Cosmochim Acta* 66(15°): A486-A486.
- Martin EE, Macdougall JD (1995) Sr and Nd isotopes at the permian/triassic boundary: A record of climate change. *Chem Geol* 125(1-2): 73-99. [https://doi.org/10.1016/0009-2541\(95\)00081-V](https://doi.org/10.1016/0009-2541(95)00081-V)
- Marzocchi C (1987) Petrologia e metallogenesi del complesso eruttivo di Predazzo (TN): con particolare riguardo al settore meridionale. University of Ferrara, unpublished master thesis.
- Masotta M, Mollo S, Freda C, Gaeta M, Moore G (2013) Clinopyroxene–liquid thermometers and barometers specific to alkaline differentiated magmas. *Contrib Mineral Petrol* 166(6): 1545-1561. <https://doi.org/10.1007/s00410-013-0927-9>
- Menegazzo Vitturi L, Visonà D, Zantedeschi C (1995) Amphibole composition in rocks from Predazzo volcano-plutonic complex (Southern Alps, Italy). *Mem Sci Geol* 47: 87-94.
- Mietto P, Manfrin S, Preto N et al. (2012) The Global Boundary Stratotype Section and Point (GSSP) of the Carnian Stage (Late Triassic) at Prati di Stuores/ Stuores Wiesen Section (Southern Alps, NE Italy). *Episodes* 35(3): 414-430.
- Mollo S, Masotta M, Forni F, Bachmann O, De Astis G, Moore G, Scarlato P (2015) A K-feldspar–liquid hygrometer specific to alkaline differentiated magmas. *Chem Geol* 392: 1-8. <https://doi.org/10.1016/j.chemgeo.2014.11.010>

- Mollo S, Putirka K, Iezzi G, Del Gaudio P, Scarlato P (2011) Plagioclase–melt (dis) equilibrium due to cooling dynamics: implications for thermometry, barometry and hygrometry. *Lithos* 125(1): 221-235. <https://doi.org/10.1016/j.lithos.2011.02.008>
- Monjoie P, Bussy F, Schaltegger U, Mulch A, Lapierre H, Pfeifer HR (2007) Contrasting magma types and timing of intrusion in the Permian layered mafic complex of Mont Collon (Western Alps, Valais, Switzerland): evidence from U/Pb zircon and  $^{40}\text{Ar}/^{39}\text{Ar}$  amphibole dating. *Swiss J Geosci* 100(1): 125-135. <https://doi.org/10.1007/s00015-007-1210-8>
- Morimoto N (1988) Nomenclature of pyroxenes. *Mineral Petrol* 39(1): 55-76. <https://doi.org/10.1007/BF01226262>
- Morse SA, Brady JB (2017) Thermal History of the Upper Zone of the Kiglapait Intrusion. *J Petrol* 58(7): 1319-1332. [10.1093/petrology/egx055](https://doi.org/10.1093/petrology/egx055)
- Müller T, Dohmen R, Becker HW, Ter Heege JH, Chakraborty S (2013) Fe-Mg interdiffusion rates in clinopyroxene: experimental data and implications for Fe–Mg exchange geothermometers. *Contrib Mineral Petrol* 166(6): 1563-1576. [10.1007/s00410-013-0941-y](https://doi.org/10.1007/s00410-013-0941-y)
- Mundil R, Brack P, Laurenzi MA (1996) High resolution U/Pb single zircon age determinations: new constraints on the timing of Middle Triassic magmatism in the Southern Alps. 78° Riunione estiva Soc. Geol. It: Geologia delle Dolomiti. San Cassiano (1996), Conference Abstract.
- Myers JT, Eugster HP (1983) The system Fe-Si-O: Oxygen buffer calibrations to 1500 K. *Contrib Mineral Petrol* 82(1): 75-90. <https://doi.org/10.1007/BF00371177>
- Namur O, Humphreys MCS (2018) Trace Element Constraints on the Differentiation and Crystal Mush Solidification in the Skaergaard Intrusion, Greenland. *J Petrol* 1-31. doi: [10.1093/petrology/egy032](https://doi.org/10.1093/petrology/egy032)
- Nielsen TFD (2004) The Shape and Volume of the Skaergaard Intrusion, Greenland: Implications for Mass Balance and Bulk Composition. *J Petrol* 45(3): 507-530. [10.1093/petrology/egg092](https://doi.org/10.1093/petrology/egg092)

- Petersen JS, Morten L, Simboli G, Lucchini F (1980) REE abundances in the Predazzo-Monzoni intrusive complex, Dolomites, North Italy. *Riv Ital Paleontol* 85: 1065-1080.
- Pin C, Sills JD (1986) Petrogenesis of layered gabbros and ultramafic rocks from Val Sesia, the Ivrea Zone, NW Italy: trace element and isotope geochemistry. *Geol Soc Spec Publ* 24: 231-249. <https://doi.org/10.1144/GSL.SP.1986.024.01.21>
- Pouchou JL, Pichoir F (1991) Quantitative analysis of homogeneous or stratified microvolumes applying the model "PAP". In *Electron probe quantitation*. Springer US, pp. 31-75. [https://doi.org/10.1007/978-1-4899-2617-3\\_4](https://doi.org/10.1007/978-1-4899-2617-3_4)
- Povoden E, Horacek M, Abart R (2002) Contact metamorphism of siliceous dolomite and impure limestones from the Werfen formation in the eastern Monzoni contact aureole. *Mineral Petrol* 76(1): 99-120. <https://doi.org/10.1007/s007100200034>
- Princivalle F, Della Giusta A, De Min A, Piccirillo EM (1999) Crystal chemistry and significance of cation ordering in Mg-Al rich spinels from high-grade hornfels (Predazzo-Monzoni, NE Italy). *Mineral Mag* 63(2): 257-257. <https://doi.org/10.1180/002646199548367>
- Putirka KD (2008) Thermometers and barometers for volcanic systems. *Rev Mineral Geochem* 69(1): 61-120. <https://doi.org/10.2138/rmg.2008.69.3>
- Putirka K, Johnson M, Kinzler R, Longhi J, Walker D (1996) Thermobarometry of mafic igneous rocks based on clinopyroxene-liquid equilibria, 0–30 kbar. *Contrib Mineral Petrol* 123(1): 92-108. <https://doi.org/10.1007/s004100050145>
- Putirka K, Mikaelian H, Ryerson F, Shaw H (2003) New clinopyroxene-liquid thermobarometers for mafic, evolved, and volatile-bearing lava compositions, with applications to lavas from Tibet and the Snake River Plain, Idaho. *Am Mineral* 88: 1542-1554. <https://doi.org/10.2138/am-2003-1017>

- Quick JE, Sinigoi S, Peressini G, Demarchi G, Wooden JL, Sbisà A (2009) Magmatic plumbing of a large Permian caldera exposed to a depth of 25 km. *Geology* 37: 603-606. <https://doi.org/10.1130/G30003A.1>
- Ridolfi F, Renzulli A (2012) Calcic amphiboles in calc-alkaline and alkaline magmas: thermobarometric and chemometric empirical equations valid up to 1,130° C and 2.2 GPa. *Contrib Mineral Petrol* 163(5): 877-895. <https://doi.org/10.1007/s00410-011-0704-6>
- Ridolfi F, Renzulli A, Puerini M (2010) Stability and chemical equilibrium of amphibole in calc-alkaline magmas: an overview, new thermobarometric formulations and application to subduction-related volcanoes. *Contrib Mineral Petrol* 160(1): 45-66. <https://doi.org/10.1007/s00410-009-0465-7>
- Rotenberg E, Davis DW, Amelin Y, Ghosh S, Bergquist BA (2012) Determination of the decay-constant of  $^{87}\text{Rb}$  by laboratory accumulation of  $^{87}\text{Sr}$ . *Geochim Cosmochim Acta* 85: 41-57. <https://doi.org/10.1016/j.gca.2012.01.016>
- Rottura A, Bargossi GM, Caggianelli A, Del Moro A, Visonà D, Tranne CA (1998) Origin and significance of the Permian high-K calc-alkaline magmatism in the central-eastern Southern Alps, Italy. *Lithos* 45: 329-348. [https://doi.org/10.1016/S0024-4937\(98\)00038-3](https://doi.org/10.1016/S0024-4937(98)00038-3)
- Rottura A, Del Moro A, Caggianelli A, Bargossi GM, Gasparotto G (1997) Petrogenesis of the Monte Croce granitoids in the context of Permian magmatism in the Southern Alps, Italy. *Eur J Mineral* 9(6): 1293-1310. [10.1127/ejm/9/6/1293](https://doi.org/10.1127/ejm/9/6/1293)
- Sarti M, Ardizzoni F (1984) Tettonica Triassica nel gruppo di Cima Pape-Pale di Sanson (Dolomiti Bellunesi). *Mem Sci Geol* 36: 353-370.
- Schaltegger U, Brack P (2007) Crustal-scale magmatic systems during intracontinental strike-slip tectonics: U, Pb and Hf isotopic constraints from Permian magmatic rocks of the Southern Alps. *Int J Earth Sci* 96(6): 1131-1151. <https://doi.org/10.1007/s00531-006-0165-8>

- Schmid SM, Bernoulli D, Fügenschuh B et al. (2008) The Alpine-Carpathian-Dinaridic orogenic system: correlation and evolution of tectonic units. *Swiss J Geosci* 101(1): 139-183. <https://doi.org/10.1007/s00015-008-1247-3>
- Silver L, Stolper E (1985) A thermodynamic model for hydrous silicate melts. *J Geol* 93(2): 161-177.
- Sinigoi S, Quick JE, Demarchi G, Klotzli U (2016) Production of hybrid granitic magma at the advancing front of basaltic underplating: Inferences from the Sesia Magmatic System (south - western Alps, Italy). *Lithos* 252-253: 109-122. <https://doi.org/10.1016/j.lithos.2016.02.018>
- Sloman LE (1989) Triassic shoshonites from the dolomites, northern Italy: Alkaline arc rocks in a strike-slip setting. *J Geophys Res: Solid Earth* 94(B4): 4655-4666. [10.1029/JB094iB04p04655](https://doi.org/10.1029/JB094iB04p04655)
- Spera FJ (1980) Thermal evolution of plutons: a parameterized approach. *Science* 207: 299-301. [10.1126/science.207.4428.299](https://doi.org/10.1126/science.207.4428.299)
- Spera FJ (2000) Physical properties of magmas. In Sigurdsson H (ed.) *Encyclopedia of Volcanoes*. New York: Academic Press, pp. 171-190.
- Spera FJ, Bohron WA (2001) Energy-constrained open-system magmatic processes I: General model and energy-constrained assimilation and fractional crystallization (EC-AFC) formulation. *J Petrol* 42(5): 999-1018. <https://doi.org/10.1093/petrology/42.5.999>
- Stahle V, Frenzel G, Hess JC, Saupé F, Schmidt ST, Schneider W (2001) Permian metabasalt and Triassic alkaline dykes in the northern Ivrea zone: clues to the post-Variscan geodynamic evolution of the Southern Alps. *Schweiz Mineral Petrogr Mitt* 81(1): 1-21.
- Stampfli GM, Borel GD (2002) A plate tectonic model for the Paleozoic and Mesozoic constrained by dynamic plate boundaries and restored synthetic oceanic isochrones. *Earth Planet Sci Lett* 196(1): 17-33. [https://doi.org/10.1016/S0012-821X\(01\)00588-X](https://doi.org/10.1016/S0012-821X(01)00588-X)
- Stampfli GM, Borel GD (2004) The TRANSMED transects in space and time: constraints on the paleotectonic evolution of the Mediterranean domain. In *The TRANSMED Atlas: The*



- Mediterranean region from crust to mantle, pp. 53-80. [https://doi.org/10.1007/978-3-642-18919-7\\_3](https://doi.org/10.1007/978-3-642-18919-7_3)
- Stolper E (1982) The speciation of water in silicate melts. *Geochim Cosmochim Acta* 46(12): 2609-2620. [https://doi.org/10.1016/0016-7037\(82\)90381-7](https://doi.org/10.1016/0016-7037(82)90381-7)
- Trall RJ, Lachance GR (1966) A practical solution to the matrix problem in X-ray analysis. II. Application to a multicomponent alloy system. *Can Spectrosc* 11(3): 63-71.
- Vardabasso S (1929) Rapporti tra attività magmatica e vicende tettoniche nella provincia petrografica di Predazzo: Studi Trentini di Scienze Naturali 11.
- Vardabasso S (1930) Carta geologica del territorio eruttivo di Predazzo e Monzoni. Ufficio Idrografico del Magistrato alle Acque di Venezia, 1:25000 scale.
- Visonà D (1997) The Predazzo multipulse intrusive body (Western Dolomites, Italy). Field and mineralogical studies. *Mem Sci Geol* 49: 117-125.
- Visonà D, Zanferrari A (2000) Some constraints on geochemical features in the Triassic mantle of the easternmost Austroalpine–Southalpine domain: evidence from the Karawanken pluton (Carinthia, Austria). *Int J Earth Sci* 89(1): 40-51. <https://doi.org/10.1007/s005310050316>
- Voshage H, Hofmann AW, Mazzucchelli M, Rivalenti G, Sinigoi S, Raczek I, Demarchi G (1990) Isotopic evidence from the Ivrea Zone for a hybrid lower crust formed by magmatic underplating. *Nature* 347(6295): 731-736. [10.1038/347731a0](https://doi.org/10.1038/347731a0)
- Waldbaum DR, Thompson JB (1969) Mixing properties of sanidine crystalline solutions: IV. Phase diagrams from equations of state. *Am Mineral* 54: 1274-1298.
- Willcock MAW, Bargossi GM, Weinberg RF, Gasparotto G, Cas RAF, Giordano G, Marocchi M (2015) A complex magma reservoir system for a large volume intra-to extra-caldera ignimbrite: Mineralogical and chemical architecture of the VEI8, Permian Ora ignimbrite (Italy). *J Volcanol Geotherm Res* 306: 17-40. <https://doi.org/10.1016/j.jvolgeores.2015.09.015>

Zanetti A, Mazzucchelli M, Sinigoi S, Giovanardi T, Peressini G, Fanning M (2013) SHRIMP U–Pb Zircon Triassic intrusion age of the Finero mafic complex (Ivrea–Verbano zone, Western Alps) and its geodynamic implications. *J Petrol* 54(11): 2235-2265. <https://doi.org/10.1093/petrology/egt046>

Ziegler PA, Stampfli GM (2001) Late Palaeozoic-Early Mesozoic plate boundary reorganization: collapse of the Variscan orogen and opening of Neotethys. *Nat Brescia* 25: 17-34.

Zindler A, Hart SR (1986) Chemical geodynamics. *Annu Rev Earth Planet Sci* 14: 493-571.

## Figure Captions

### Fig. 1 (colour online)

Simplified geological map of the Predazzo Intrusive Complex (PIC). On the left bottom corner, the study area location with respect to the NE sector of Italy is shown

### Fig. 2 (colour online)

(a) Total Alkali vs. Silica and (b) K<sub>2</sub>O vs. Na<sub>2</sub>O diagrams for Predazzo Intrusive Complex rocks (Le Maitre 2002). SS = Shoshonitic Silica Saturated; SU = Shoshonitic Silica Undersaturated; GU = Granitic Unit

### Fig. 3 (colour online)

Textural sketches of Predazzo Intrusive Complex rocks and corresponding photomicrographs showing the crystallization relationships between biotite and amphibole in the intercumulus assemblage of (a, b) Shoshonitic Silica Saturated monzodiorites and (c, d) Shoshonitic Silica Undersaturated monzogabbros. Each labelled mineral phase in the right photomicrographs is contraddistinct by a different colour in the left sketches. Amph = amphibole; Ap = apatite; Bt

= biotite; Cpx = clinopyroxene; K-Feld = K-feldspar; Ox = Fe-Ti oxide; Plag = plagioclase; Qz = quartz; Ser = sericite

#### Fig. 4 (colour online)

Mg# vs.  $K_{Fe-Mg}^{Cpx-Liq}$  of clinopyroxene from the (a) Shoshonitic Silica Saturated and (b) Shoshonitic Silica Undersaturated rocks. The white symbols represent the disequilibrium between crystals and their host rock composition, whose whole rock Mg# (wr Mg#) is also reported. The filled symbols represent the attained equilibrium conditions after the calculation of melt composition in equilibrium. “Liq” indicates both the composition of the crystals host rocks (white symbols, prior to equilibration process) and that of the calculated “melt” (filled symbols, after equilibration process). The length of the dashed arrows is directly function of the amount of disequilibrium between the crystals and their host rock. The equilibrium range of  $K_{Fe-Mg}^{Cpx-Liq} = 0.24-0.30$  (black lines) is from Putirka et al. (2003)

#### Fig. 5 (colour online)

Anorthite ( $X_{An}$ ) vs.  $K_{An-Ab}^{Plag-Liq}$  of plagioclase from the (a) Shoshonitic Silica Saturated and (b) Shoshonitic Silica Undersaturated rocks. As in Fig. 4, white symbols represent the disequilibrium between crystals and their host rock composition (whose Mg# is reported as “wr Mg#”), whereas filled symbols represent the attained equilibrium conditions after the equilibration processes. “Liq” indicates both the composition of the crystals host rocks (white symbols, prior to equilibration process) and that of the calculated “melt” (filled symbols, after equilibration process). The length of the dashed arrows is directly function of the amount of disequilibrium between the crystals and their host rock. The chosen equilibrium range of  $K_{An-Ab}^{Plag-Liq} = 0.27 \pm 0.11$  (black lines) is from Putirka (2008)

#### Fig. 6 (colour online)

Flow chart representing the rationality of our models for clinopyroxene (Cpx) and plagioclase (Plag) thermobarometry and hygrometry, from the starting mineral compositions (black squares) to the final  $P$ - $T$ - $H_2O$  triplets. (a) Model for clinopyroxenes in the less differentiated Shoshonitic Silica Saturated rocks; (b) Model for clinopyroxenes in the evolved Shoshonitic Silica Saturated and in the Shoshonitic Silica Undersaturated rocks; (c) Model for plagioclases in both Shoshonitic Silica Saturated and Shoshonitic Silica Undersaturated rocks

**Fig. 7 (colour online)**

(a) Temperature vs. pressure and (b) temperature vs. water content diagrams for Predazzo Intrusive Complex rocks. SS = Shoshonitic Silica Saturated; SU = Shoshonitic Silica Undersaturated. The reported values were obtained from the several thermobarometric approaches explained in text. Cpx = clinopyroxene; Amph = amphibole; Plag = plagioclase; K-Feld = K-feldspar. Dashed interval in (a) represent the best-fit pressure range between the various estimates, whereas the shaded field represents the temperature interval resulted from biotite thermometry. Depth was calculated by considering a  $\Delta P/\Delta z$  of 0.29 kbar/km

**Fig. 8 (colour online)**

Temperature vs. oxygen fugacity (expressed in  $\log fO_2$ ) diagram for Predazzo Intrusive Complex rocks. SS = Shoshonitic Silica Saturated; SU = Shoshonitic Silica Undersaturated. FMQ and NNO buffers are from Myers and Eugster (1983) and Huebner and Sato (1970), respectively. Up on the right, insert with the same oxygen fugacity data expressed in terms of  $\Delta FMQ$  to facilitate the comparison between the various magmatic suites

**Fig. 9 (Colour online)**

Diagrams showing the  $^{87}Sr/^{86}Sr$  vs.  $^{143}Nd/^{144}Nd$  isotopic ratios of Predazzo Intrusive Complex rocks compared to those of Permo-Triassic crustal components (all values corrected to 234 Ma).

SS = Shoshonitic Silica Saturated; SU = Shoshonitic Silica Undersaturated. Triassic carbonates field from Martin and Macdougall (1995) and Blendiger et al. (2015); Permian intrusives (Mt. Croce and Serie dei Laghi) field from Rottura et al. (1997) and Sinigoi et al. (2016, and references therein); Athesina Volcanic District (AVD) Permian ignimbrites field from Barth et al. (1993); **Val Sesia Permian mafic rocks field from Voshage et al. (1990), Pin and Sills (1996) and Sinigoi et al. (2016)**; Kinzigite formation field from Voshage et al. (1990). (a) Sr-Nd isotopic ratios of Predazzo Intrusive Complex rocks plotted against those of the Permo-Triassic crustal components, the enriched 1 (EMI), high- $\mu$  (HIMU, where  $\mu = {}^{238}\text{U}/{}^{204}\text{Pb}$ ) and depleted (DMM) mantle end-members (Zindler and Hart 1986); **the insert corresponds to the area reported in diagram (b)**. (b) EC-AFC trends (Bohrson and Spera 2001; Spera and Bohrson 2001) for the Shoshonitic Silica Saturated suite by considering variable crustal assimilants. 1 = assimilation of Triassic carbonates; 2 = assimilation of AVD ignimbrites; 3 = assimilation of Mt. Croce granodiorites; 4 = assimilation of Serie dei Laghi granites; 5 = assimilation of Kinzigite formation amphibolites

**Intrusion of shoshonitic magmas at shallow crustal depth: T-P path, H<sub>2</sub>O estimates and  
AFC modelling of the Middle Triassic Predazzo Intrusive Complex (Southern Alps,  
Italy)**

**Federico Casetta\***

Department of Physics and Earth Sciences, University of Ferrara  
Via Saragat 1, 44121 Ferrara, Italy

**Massimo Coltorti**

Department of Physics and Earth Sciences, University of Ferrara  
Via Saragat 1, 44121 Ferrara, Italy

**Ryan B. Ickert**

Scottish Universities Environmental Research Centre, Scottish Enterprise Technology Park,  
Rankine Avenue, East Kilbride, G75 0QF, UK

**Costanza Bonadiman**

Department of Physics and Earth Sciences, University of Ferrara  
Via Saragat 1, 44121 Ferrara, Italy

**Pier Paolo Giacomoni**

Department of Physics and Earth Sciences, University of Ferrara  
Via Saragat 1, 44121 Ferrara, Italy

**Theodoros Ntaflos**

Department of Lithospheric Research, Universität Wien  
Althanstraße 14 (UZA II), 1090 Wien

\* Corresponding author. Phone +39 0532 974721. E-mail: cstfrc@unife.it

**Intrusion of shoshonitic magmas at shallow crustal depth: T-P path, H<sub>2</sub>O estimates and AFC modelling of the Middle Triassic Predazzo Intrusive Complex (Southern Alps, Italy)**

**Abstract**

The multi-pulse shoshonitic Predazzo Intrusive Complex represents an ideal igneous laboratory for investigating the chemical and physical conditions of magma emplacement in a crustal context, since numerical models can be constrained by field evidence. It constitutes the most intriguing remnant of the Middle Triassic magmatic systems of the Dolomitic Area (Southern Alps), preserved by the Alpine tectonics. Predazzo Intrusive Complex comprises silica saturated (pyroxenites/gabbros to syenites), silica undersaturated (gabbros to syenites) and silica oversaturated (granites and syenogranites) rock suites. In this paper we modelled its emplacement and evolution with a multiple thermo-/oxy-barometric, hygrometric and EC-AFC approach. At odds with what proposed in literature but according to the field evidence, the emplacement of the Predazzo Intrusive Complex occurred at shallow depth (< 6 km). In this context, the different pulses differed slightly in bulk water content, but shared a common thermal regime, with temperatures between 1000-1100°C and ~600°C at low to moderate oxydizing conditions (-0.1 to +0.7 ΔFMQ). The interaction between the intrusion and the shallow crustal rocks was minimal, with Sr and Nd isotopic compositions indicating an average of 5-6% assimilation of crust. A thermo- and oxy-barometric comparison with the nearby Mt. Monzoni enabled also to speculate about the solidification time of the intrusion, which we infer took place over about 700 ka.

**Keywords**

Predazzo Intrusive Complex; Sr and Nd isotopes; P-T estimates and magma water content; Crustal assimilation; Solidification time; Shoshonitic intrusion.

## 1. Introduction

The Middle Triassic magmatic event in the Southern Alps is expressed in volcano-plutonic sequences outcropping from the Brescian Alps, Alto Vicentino, Dolomites and Carnia areas (Italy) to the Karavanken region (Austria). Most of the igneous products are volcanic and volcanoclastic rocks, with subordinated dyke swarms. Intrusive bodies are instead rare, and mainly located in the Dolomites (Predazzo-Mt. Monzoni-Cima Pape) and Karavanken areas (Gasparotto and Simboli 1991; Gianolla 1992; Bonadiman et al. 1994; Visonà and Zanferrari 2000; Brack et al. 2005; Cassinis et al. 2008; Bellieni et al. 2010; Casetta et al. 2017). These intrusions represent snapshots of magmatic plumbing systems, emplaced during and/or immediately after the eruption of the overlying volcanic products. There are several outstanding geological problems regarding the nature of these complexes, mainly related to their emplacement conditions, and to the relationships between tectonics and magmatism. The Predazzo Intrusive Complex (PIC) represents the ideal “petrologic laboratory” for investigating and reconstructing the features of the Middle Triassic feeding systems, since it offers the possibility to constrain the theoretical and experimental modeling by means of field evidence. As in the case of the nearby Mt. Monzoni, the contact aureole between PIC and the surrounding sedimentary rocks enabled many authors to speculate about the geometry of the intrusive body and its field relationships to the shallow crust (Princivalle et al. 1999; Ferry et al. 2002; Povoden et al. 2002; Gallien et al. 2007). On the basis of petrological and field evidence, Casetta et al. (2017) identified three different magma batches constituting the PIC, interpreted as a multi-pulse body of shoshonitic affinity with variable alkalies and H<sub>2</sub>O-content which led to differentiation from mafic to amphibole and biotite-bearing end-members. However, several issues are still unsolved, such as the (possible) interaction between PIC magmas and crust, and their chemical/physical conditions of emplacement. The latter resulting in a current uncertainty about the depth of the intrusion.



Few thermobarometric and oxybarometric data are reported in literature for the Middle Triassic magmatic systems of the Dolomitic Area. According to Bonadiman et al. (1994), the oxygen fugacity of the nearby Mt. Monzoni system was around the NNO buffer and the crystallization temperature range was between 1044 and 589°C. Despite the clear evidence of a predominant role of water during crystallization, as testified by the wide presence of hydrous phases in the intrusive rocks, no estimates of the H<sub>2</sub>O contents and *P-T* conditions of these Middle Triassic plumbing systems have been performed so far. Taking into account the Al<sup>tot</sup> content of amphiboles, Menegazzo Vitturi et al. (1995) hypothesized a depth of 10-17 km for PIC emplacement, but their values appeared in stark contrast with both the field evidence and the data reported by Visonà and Zanferrari (2000) for the similar and coeval Karawanken pluton (5-9 km).

Therefore, in this paper we made new geochemical and isotopic (<sup>87</sup>Sr/<sup>86</sup>Sr-<sup>143</sup>Nd/<sup>144</sup>Nd) measurements on new samples from PIC that are representative of its main portions. A multiple thermobarometric and hygrometric approach, based on the interaction between distinct single mineral, mineral pairs and mineral-melt equations, corroborated by appropriate simulations by means of Rhyolite-MELTS software (Gualda et al. 2012), enabled us to: (i) provide for the first time *P-T-fO<sub>2</sub>* estimates and H<sub>2</sub>O evaluation of PIC system over its entire evolution; (ii) verify if the depth of the intrusion obtained by the previous petrologic approaches well fit the field evidence. The resulting *P-T-fO<sub>2</sub>* and H<sub>2</sub>O values, together with the isotopic signatures of PIC rocks were then used as input to (iii) quantify the role of assimilation and fractional crystallization processes in the generation of the main PIC magmatic suites.

## 2. Middle Triassic magmatism in the Southern Alps

### 2.1. Geodynamic framework

The Middle Triassic magmatic sequences of the Dolomitic Area are mainly composed of volcanites and volcanoclastites with subordinated and scattered intrusive bodies over an area of

about 2,000 km<sup>2</sup> (Vardabasso 1929, 1930; Castellarin et al. 1980, 1982; Lucchini et al. 1982; Sloman 1989; Bonadiman et al. 1994; Coltorti et al. 1996; Gianolla et al. 2010; Casetta et al. 2017). The Middle Triassic geodynamic framework of Dolomitic Area and the whole Southern Alps domain is still matter of debate, fostered by juxtaposition between the calc-alkaline/shoshonitic orogenic affinity of the magmatic products and evidence for a concomitant extensional-transensional tectonic regime (Doglioni 1987; Stampfli and Borel 2002, 2004; Doglioni 2007). Several geodynamic models were thus proposed, invoking the presence of: (i) an aborted rift in a passive margin (Bernoulli and Lemoine 1980); (ii) a compression at the NW limb of the Paleo-Tethys (Castellarin et al. 1980); (iii) an “active” mantle upwelling (Stahle et al. 2001); (iv) a transition to back-arc conditions lasting since Carboniferous-Permian, triggered by the northward subduction of the Paleotethys remnants (Ziegler and Stampfli 2001; Stampfli and Borel 2002; 2004; Cassinis et al. 2008; Schmid et al. 2008 Zanetti et al. 2013); (v) an anorogenic rifting concomitant with arc-like magmatism, whose signature was inherited by a mantle source previously metasomatised by subduction-related components during the Hercynian orogenic cycle (Bonadiman et al. 1994). This last hypothesis was supported by the similar Sr-Nd isotope signatures of the Middle Triassic magmas in the Southern Alps and the Permian igneous products (260-290 Ma), whose expression were found along the Western and in the Eastern Alps sectors (Barth et al. 1993; Rottura et al. 1998; Monjoie et al. 2007; Schaltegger and Brack 2007; Marocchi et al. 2008; Quick et al. 2009; Willcock et al. 2015; Dal Piaz et al. 2015; Sinigoi et al. 2016; Manzotti et al. 2017). This kind of analogy led to speculate that similar mantle sources, and/or similar melting conditions, could have generated the Middle Triassic and the Permian magmatic episodes. In the Dolomitic Area, thick sequences of basaltic andesitic to rhyolitic ignimbrites associated to the Permian Atesina Volcanic District are also the main constituent of the crustal basement of the Dolomitic Area where magmas intruded during Middle Triassic.

## 2.2. The Southern Alps intrusive bodies: geochemical and petrographic overview

In contrast to the large amount of basaltic/latitic volcanic rocks erupted in the Southern Alps during the Ladinian-Carnian, the intrusive bodies are more limited in volume. They are Cima Pape ( $< 3 \text{ km}^2$ ), Mt. Monzoni ( $4.6 \text{ km}^2$ ), Predazzo Intrusive Complex ( $25 \text{ km}^2$ , see below) in the Dolomitic Area (Italy) and Karawanken (about  $50 \text{ km}^2$ ) in Carinthia (Austria).

The Cima Pape sill and the ca. 230 Ma Mt. Monzoni body (Borsi and Ferrara 1968) are composed of biotite and amphibole-bearing gabbroic to syenitic rocks with shoshonitic affinity, generated mainly by fractional crystallization from parental basaltic to trachybasaltic magmas (Gasparotto and Simboli 1991; Bonadiman et al. 1994; Della Lucia 1997). The emplacement of Mt. Monzoni body is thought to be controlled by a syn-genetic ESE-WNW transcurrent tectonics, which created the conditions for a shallow level intrusion and the subsequent magma differentiation. A shallow depth is also suggested for the Cima Pape sill, where a gradual textural transition to the overlying lavas, locally organized in columnar structures (Sarti and Ardizzoni 1984) is observable on field.

The Karawanken pluton (ca. 230 Ma, Lippoldt and Pidgeon 1974) comprises biotite and amphibole-bearing diorites/monzonites to granites/syenites, with rare aplites and pegmatites, showing an overall high-K calc-alkaline to shoshonitic affinity. To explain the production of Karawanken magmas, Visonà and Zanferrari (2000) invoked the occurrence of combined assimilation + fractional crystallization processes from a parental basaltic melt in a shallow magma chamber (5-9 km). The geochemical differences (i.e. La/Nb and Ba/Nb ratios) between the Karawanken pluton and the intrusions of the Dolomitic Area led the authors to suggest the origin of Karawanken magmas from an enriched mantle source not previously affected by subductive components, as proposed by Bonadiman et al. (1994) for the Mt. Monzoni body.

Irrespective of the volumetric differences, common features of these intrusions are the high-K calc-alkaline to shoshonitic affinity, the modal occurrence of hydrated phases (biotite and amphibole) in the intercumulus assemblages and the shallow depth of emplacement.

### 2.3. The Predazzo Intrusive Complex

The Predazzo Intrusive Complex (PIC, Fig. 1) is a ring-like shaped multi-pulse intrusion with an overall volume of about 4.5 km<sup>3</sup> cropping out in Trentino Alto Adige (NE Italy). Dated at 237.3 ± 1.0 Ma (U/Pb on zircon from granites, Mundil et al., 1996), it intruded the Permian Atesina Volcanic District rhyolitic ignimbrites, the Permo-Triassic sedimentary formations and the overlying volcanic sequences (Brack et al. 1996, 1997, 2005; Mietto et al. 2012), forming well-defined metamorphic aureoles (Princivalle et al. 1999; Ferry et al. 2002; Povoden et al. 2002; Gallien et al. 2007). The intrusion and its related volcanic products were almost completely preserved from the action of the Alpine tectonic event, and kept in their original position with respect to the surrounding rocks. According to Casetta et al. (2017), PIC rocks are grouped in three main units with different geochemical features (Fig. 1), named (in relative order of emplacement) Shoshonitic Silica Saturated (SS, 3.1 km<sup>3</sup>), Granitic Unit (GU, 1.1 km<sup>3</sup>) and Shoshonitic Silica Undersaturated (SU, 0.3 km<sup>3</sup>). The SS and SU suites are composed of pyroxenites/gabbros to syenites (Fig. 2), respectively quartz- and nepheline-bearing, formed as result of fractional crystallization (FC) processes in an almost closed system from two distinct starting monzogabbroic-like magmas (Petersen et al. 1980; Visonà 1997; Marrocchino et al. 2002; Casetta et al. 2017). The Granitic Unit is instead constituted by quartz and biotite-bearing granites/syenogranites (Fig. 2), and apparently seems to represent a different magma batch and/or the result of genetic processes independent from those that generated the SS and SU rocks (Menegazzo Vitturi et al. 1995; Visonà 1997; Casetta et al. 2017). However, the lack of isotopic studies made it impossible to definitively exclude for the three magma bodies a significant involvement of assimilated crustal rocks.

On the other side, the field relationships between the intrusive units, their related dykes and the host rocks suggest a shallow origin of this multi-pulse intrusion, as also testified by the presence of hypabyssal rocks at the hundred-meter-scale transition between the plutonic and the volcanic

sequences (Casetta et al. 2017). Nevertheless, the only thermobarometric studies present in literature, based on the  $Al^{tot}$  content of amphiboles (Menegazzo Vitturi et al. 1995), proposed a 10-17 km depth for the PIC, giving rise to some uncertainty about its emplacement and crystallization conditions due to the discrepancy between the barometric- and field-based estimates.

### 3. Analytical methods

Whole rock major and trace element analyses were carried out at the Department of Physics and Earth Sciences (University of Ferrara, Italy) using ARL Advant-XP automated X-Ray fluorescence spectrometer. Full matrix correction procedure and intensities were elaborated following Traill and Lachance (1966). Accuracy and precision are better than 2-5% for major elements and 5-10% for trace elements. The detection limits are 0.01 wt% and 1-3 ppm for most of the major and trace element concentrations, respectively.

Rb, Sr, Y, Zr, Nb, Hf, Ta, Th, U, and Rare earth elements (REE) were analyzed by inductively coupled plasma-mass spectrometry (ICP-MS) using a Thermo Series X spectrometer with precision and accuracy better than 10% for all elements, well above the detection limit.

Mineral phases major element compositions were analyzed at the Department of Lithospheric Research, University of Wien (Austria), by using a CAMECA SX100 electron microprobe equipped with four WD and one ED spectrometers. The operating conditions were as follows: 15 kV accelerating voltage, 20 nA beam current, 20 s counting time on peak position. Natural and synthetic standards were used for calibration and PAP corrections were applied to the intensity data (Pouchou and Pichoir 1991).

Whole rock  $^{87}Sr/^{86}Sr$  and  $^{143}Nd/^{144}Nd$  isotopic analyses were performed at the Radiogenic Laboratory of the Scottish Universities Environmental Research Centre (SUERC) of Glasgow by means of a Sector-54 TIMS instrument. Strontium was loaded onto outgassed single Re filaments with a Ta-activator solution; Nd was loaded onto the side of a triple Ta-Re-Ta

filament assembly in H<sub>2</sub>O and ran as Nd<sup>+</sup>. The sample preparation procedures for Sr-Nd isotopic analyses have not been described previously, so we articulate them in full, together with standards and instrumental analytical performance, in the Supplementary Material\_1.

## 4. Whole rock geochemistry

### 4.1. Major and trace element

Shoshonitic Silica Saturated (SS) suite (Fig. 2, Table 1) is mainly constituted by monzogabbros and monzodiorites, with Mg# (calculated as  $\text{Mg}/[\text{Mg}+\text{Fe}^{2+}]$  mol%) of 65-45, and by subordinated monzonites and syenites (Mg# of 53-26 and 45-20 respectively) randomly distributed within the unit (Fig. 1). Volumetrically limited pyroxenitic (Mg# 64-47) and gabbroic (Mg# 65-45) cumulates crop out in the southwestern sector of the intrusion. Shoshonitic Silica Undersaturated (SU) suite (Fig. 2, Table 1) is on average more evolved than the SS one, being dominated by the presence of nepheline-normative monzonites (Mg# 40-39) and syenites (Mg# 36-15), over a minority composed of cumulitic gabbros (Mg# 56-50), monzogabbros (Mg# 59-47) and monzodiorites (Mg# 55-27). Granitic Unit (GU, Fig. 2) is composed of highly evolved granites and syenogranites (69-77 SiO<sub>2</sub> wt%, Table 1) that, according to Chappell and White (2001) discriminating criteria, are ascribable to the I-type granitoids ( $\text{Al}/[\text{Na} + \text{K} + \text{Ca}] < 1.1$ ; low P<sub>2</sub>O<sub>5</sub> wt%; decreasing Zr, Sr and Al<sub>2</sub>O<sub>3</sub> wt% with increasing SiO<sub>2</sub> wt%). Few samples show instead intermediate behaviour between I- and S-type rocks.

All SS, SU and GU rocks have K-affinity (Fig. 2), and their K<sub>2</sub>O and SiO<sub>2</sub> contents led to classify them as belonging to shoshonitic (SS and SU) and High-K calc-alkaline (GU) series.

Despite the general similarities, the major and trace element distribution in the SS, SU and GU rocks made it possible to pinpoint their origin from independent magmatic batches. At comparable differentiation degrees, main discriminating features between the SS and SU rocks are the relative enrichment in HFSE (Th, U, Pb), LREE and the higher Na<sub>2</sub>O/K<sub>2</sub>O ratio of the

latters. Such differences are in accordance with the predominant presence of amphibole and other Na and REE-rich phases in the SU rocks (Casetta et al. 2017).

#### 4.2. $^{87}\text{Sr}/^{86}\text{Sr}$ and $^{143}\text{Nd}/^{144}\text{Nd}$ isotopes

Whole rock  $^{87}\text{Sr}/^{86}\text{Sr}$  and  $^{143}\text{Nd}/^{144}\text{Nd}$  isotopic ratios were analysed on representative samples of the SS, SU and GU suites (Table 2). Shoshonitic Silica Saturated samples have initial Sr isotope composition from 0.7039 to 0.7052, whereas their initial Nd isotope compositions range from 0.512191 to 0.512247. Shoshonitic Silica Undersaturated rocks are characterized by a generally higher  $^{143}\text{Nd}/^{144}\text{Nd}_i$  varying from 0.512261 to 0.512289 and by  $^{87}\text{Sr}/^{86}\text{Sr}_i$  comparable with the SS samples (0.7047 to 0.7063).  $^{143}\text{Nd}/^{144}\text{Nd}_i$  range of GU rocks is between 0.512206 and 0.512304, thus comparable to those of both SS and SU suites. High Rb/Sr of the GU rocks resulted in imprecise initial calculated  $^{87}\text{Sr}/^{86}\text{Sr}$  preventing any correlation between the GU and the SS/SU bodies.

### 5. Crystallization sequences and mineral chemistry

To better focus on the  $P$ - $T$ - $f\text{O}_2$  conditions and on the  $\text{H}_2\text{O}$  contents of the PIC system, some remarks on the mineral phase compositions and crystallization sequences of the various units is hereafter summarized. A more detailed description of the petrographic and mineral chemistry features of these rocks was reported by Casetta et al. (2017). The new mineral phases analyses are reported in the Supplementary Material\_2.

Shoshonitic Silica Saturated rocks are dominated by the presence of clinopyroxene and plagioclase as cumulus phases; minor olivine and orthopyroxene can be found in gabbros and monzogabbros. The intercumulus assemblage is characterized by the ubiquitous presence of plagioclase and biotite, followed by the appearance of amphibole in gabbros to monzodiorites (Fig. 3). Magnetite and Ti-magnetite are often reported in association with biotite, whereas K-feldspar and accessory phases (quartz, apatite, ilmenite, sphene, zircon) modally increase in

more evolved rocks. The main alteration features of the SS rocks consist of sericite formation at the expenses of feldspars, chlorite growth over clinopyroxene, amphibole and biotite, as well as epidote formation at the expenses of clinopyroxene and plagioclase. The following crystallization sequence can be deduced for SS rocks: *olivine* → *clinopyroxene* ( $\pm$ *orthopyroxene*) → *Ti-magnetite/magnetite* → *plagioclase* → *biotite* → *amphibole* → *K-feldspar* → *quartz* ( $\pm$ *accessories*).

The crystallization sequence of the SU magmatic suite mirrors its silica undersaturation and higher Na<sub>2</sub>O content. Orthopyroxene and quartz are in fact absent, and an earlier appearance of amphibole at the expenses of biotite characterises the intercumulus assemblage of the SU rocks (Fig. 3). Other Na-rich minerals like ferrosalitic clinopyroxene, abitic plagioclase and nepheline (Visonà 1997) are variably present. Accessory phases are ugrandite group garnets, epidote, apatite and titanite. As already highlighted by Visonà (1997), many portions of the SU body are hydrothermalized, showing the formation of kaoline, sericite and scapolite. Where this secondary assemblage does not occur, the primary differences between the SU and SS magmatic suites are evident. The likely crystallization sequence of the SU rocks is: *olivine* → *clinopyroxene* → *Ti-magnetite/magnetite* → *plagioclase* → *amphibole* → *biotite* → *K-feldspar* → *nepheline* ( $\pm$ *accessories*).

Syenogranites and granites of the GU are quite homogeneous in composition, being constituted by K-feldspar, plagioclase and quartz, locally associated to several other minerals, among which Fe-rich biotite is the most common. Accessory phases are tourmaline, fluorite, sphene, magnetite, apatite, ilmenite and zircon. Muscovite and chlorite are rare and always grow at the expenses of biotite and amphibole in late hydrothermal stages, whereas the sericitization of feldspars is pervasive. Less common phases are ematite, allanite, scheelite, xenotime, gummite, thorite, uranium micas, molibdenite and other sulphides, irregularly disseminated and generated in the later pneumatolitic and hydrothermal stages (Marzocchi 1987; Visonà 1997). The main



GU paragenesis is composed of: *K-feldspar + plagioclase + quartz + fluorite + biotite (chlorite and/or muscovite) ± amphibole + accessories.*

In the less altered samples, at comparable whole rock differentiation degree, the composition of the most representative minerals clearly discriminate between the SS and SU magmatic suites. For instance, biotites and amphiboles are Al- and Na-enriched in the SU rocks with respect to the SS ones. Amphibole in fact varies from the hornblendic and actinolitic composition in the SS rocks ( $\text{Na}_2\text{O} < 1.5 \text{ wt\%}$ ;  $\text{Al}_2\text{O}_3 < 8 \text{ wt\%}$ ) to the hastingsitic/pargasitic composition (rare actinolitic hornblende, Leake et al. 1997) in the SU ones ( $\text{Na}_2\text{O}$  up to  $\sim 2.5 \text{ wt\%}$ ;  $\text{Al}_2\text{O}_3$  up to  $\sim 18 \text{ wt\%}$ ). Even the Na content of plagioclase differs between the two magmatic suites: it ranges from  $\text{An}_{84}$  to  $\text{An}_{34}$  in SS samples, and from  $\text{An}_{50}$  to  $\text{An}_{<23}$  in SU rocks. Another discriminating feature is represented by the clinopyroxene composition, augitic/salitic ( $\text{En}_{43-33}$ ) in the SS and salitic/ferrosalitic ( $\text{En}_{37-24}$ ) in the SU rocks (Morimoto, 1988). Furthermore, the manganese content of several phases is quite higher in the SU rocks: Ti-magnetite (0.2-1.9 wt% SU; 0.1-0.4 wt% SS), biotite (0.1- 0.7 wt% SU; 0-0.4 wt% SS), amphibole ( $\sim 0.7 \text{ wt\%}$  SU;  $\sim 0.5 \text{ wt\%}$  SS) and clinopyroxene (0.5-1.5 wt% SU; 0.2-0.8 wt% SS).

## 6. P, T and H<sub>2</sub>O estimates: thermobarometric evolution of the intrusion

### 6.1. Recover the initial equilibrium conditions

In this section, we apply several methods for estimating the *P*, *T* and H<sub>2</sub>O contents of PIC rocks, taking into account the coexistence of minerals used as thermometers, barometers and/or hygrometers in both the SS and SU crystallization sequences. Apart from the Holland and Blundy (1994), Anderson and Smith (1995), Anderson (1996) and Henry et al. (2005) methods (see below) applied to amphibole-plagioclase pairs and biotite, and specific for intrusive rocks, the other equations used in this study are designed for volcanic samples. As often happens in intrusive contexts, the identification of the parental “melt” from which crystals formed is challenging (e.g. Skaergaard Intrusion; Nielsen 2004; Namur and Humphreys 2018). Intrusive

rocks, in fact, rarely correspond to bulk melt composition, representing a variable mixture of cumulus and intercumulus minerals, removed by the crystallizing melts at various stages of fractionation, thus in equilibrium with different melts in different moments. Casetta et al. (2017) suggested that the cumulitic gabbros and pyroxenites, as well as most of the intermediately evolved rocks of the complex, were generated by various extent of fractional crystallization from a starting trachybasaltic magma in an almost closed system.

It is modelled that the mineral assemblages constituting the PIC rocks (e.g. clinopyroxenes of SS gabbro) showed partial equilibrium with a more evolved melt (e.g. SS trachybasalt), from which then segregated to form the cumulates. The cumulitic nature of a rock itself incorporates the concept that its composition (e.g. Mg# of clinopyroxene) represents an independent physico-chemical system with respect to the deriving melt. Consequently, if we try to consider the intrusive (cumulitic) rock of PIC as a bulk representative of a melt (e.g. in terms of Mg# or CaO/Al<sub>2</sub>O<sub>3</sub>), it is reasonable to find that its mineral constituents (e.g. clinopyroxene or plagioclase), are in evident disequilibrium with the bulk composition (Figg. 4 and 5). They are instead compositionally coherent with a segregation process from a more evolved melt. On the other side, by taking into account more evolved rocks (e.g. monzogabbros to syenites), the amount of crystal disequilibrium progressively decreases (Figg. 4 and 5). This because the ultimate products of the SS/SU fractional crystallization processes, syenitic in composition, progressively approach the eutectic of the system and likely resemble a melt composition: this condition has been also proposed by Morse and Brady (2017) for the syenites of the 1300 Ma old Kiglapait Intrusion (Labrador).

Evidences of the reliability of this genetic model are the observed textural and mineral homogeneities of the SS/SU rocks: any kind of significant zoned texture would result from the introduction of additional magma chamber processes (i.e. mixing) during the formation of the PIC lithotypes, invalidating our assumptions. The unzoned texture, coupled with the crystal size of PIC rocks (e.g. clinopyroxenes up to 6-7 mm in pyroxenites and gabbros) and with the small

volume of the intrusive body ( $4.5 \text{ km}^3$ ), speaks also against a considerable effect of syn- to post-  
 crystallization diffusion processes, which can be a rate-limiting process for thermobarometric  
 estimates. On the other side, thermometers involving clinopyroxene in upper crustal context,  
 commencing cooling from relatively low  $T$ , hold the potential to record the peak temperature  
 conditions, especially in large-sized grains (Müller et al. 2013). If we couple the euhedral  
 unzoned texture of PIC clinopyroxenes with the diffusion rates proposed by several authors  
 (e.g. at about  $1000^\circ\text{C}$   $\log D^{(\text{Ca})} = -21 \text{ m}^2/\text{s}$ ;  $\log D^{(\text{Ti})} = -22 \text{ m}^2/\text{s}$ ;  $\log D^{(\text{Fe})} = -21 \text{ m}^2/\text{s}$ , where  $D$   
 indicates the diffusion coefficient; see Brady and McCallister 1983; Dimanov et al. 1996;  
 Cherniak and Lyiag 2012; Müller et al. 2013 and references therein), we can argue that the  
 crystal compositions were nearly unmodified by significant diffusion processes. Similar  
 remarks can be made for plagioclase, whose crystallization in plutonic rocks at relatively low  
 $T$  limit the efficiency of  $\text{CaAl-NaSi}$  diffusion to submicron length scales (Grove et al. 1984).  
 The mineral compositions were therefore considered as representative of the various stages of  
 fractional crystallization of the magmas inside PIC, and were used to constrain the physical  
 parameters of the magma chamber.

On the basis of these assumptions, we matched each mineral (e.g. clinopyroxene of SS  
 cumulates) with an estimated “melt” following the crystal/melt equilibrium partitioning (e.g.  
 $\text{C}_{\text{px-Liq}} \text{Kd}_{\text{Fe-Mg}}$ , see below), to trace the  $P$ - $T$  path of an hypothetical differentiation trend (e.g. SS  
 suite, see Casetta et al. 2017). This operation enabled us to compute the “melt” composition, to  
 skip the apparent disequilibrium between minerals and cumulitic rocks as a bulk and thus to  
 constrain the  $P$ ,  $T$  and  $\text{H}_2\text{O}$  parameters of the less evolved melts in the PIC feeding system.  
 Afterwards, the application of the “traditional” thermobarometric equations for intrusive  
 contexts (i.e. to amphibole-plagioclase pairs and biotite, see below) enabled us to verify the  
 convergence between the various results as well as to unravel the  $T$ - $P$ - $\text{H}_2\text{O}$  conditions in the  
 later stages of crystallization. A complete list of the applied equations, results, and  
 corresponding errors is reported in Table 4 and discussed in detail in the following sections.

## 6.2. Clinopyroxene-melt thermobarometer and water content of primary magmas

Clinopyroxene is the dominant and ubiquitous phase in the SS and SU rocks, thus clinopyroxene-melt thermobarometry was considered as a valuable starting point to estimate the  $T$ - $P$  intensive variables and  $H_2O$  content of PIC magmatic system since early stage of fractionation. Crystal-melt equilibrium conditions were tested by taking into account the experimentally determine range of  $^{Cpx-Liq}Kd_{Fe-Mg} = 0.24-0.30$  at  $T > 1050^\circ C$  by Putirka et al. (2003). First tests highlighted that all clinopyroxene crystals in the SS and SU units have  $^{Cpx-Liq}Kd_{Fe-Mg} = 0.36-0.68$  (hereinafter the superscript “Liq” indicates the composition of the bulk rock), indicating a disequilibrium towards composition more evolved than their host rock (Fig. 4). The amount of disequilibrium, as said before, decreases with increasing the differentiation degree of the rock (Fig. 4). Such a decrease could be explained by the fact that more evolved lithotypes better approach the eutectic of the system and more likely simulate melt compositions.

Following the FC model of Casetta et al. (2017), clinopyroxenes of each lithotype were thus related to a calculated “melt” composition having the same chemical affinity of their host rock and a more evolved nature (Table 3), by which crystals retrieved their equilibrium conditions. As shown in the flow chart of Fig. 6a, once chosen the clinopyroxene-melt couple of the SS suite,  $T$ - $P$  pairs were estrapolated by means of the Putirka (2008) equations, assuming variable  $H_2O$  wt% contents of the melt. The water-dependant equations 32b and 33 (Putirka 2008), derived from the  $P$ -independent thermometer and the  $T$ -dependent barometer of Putirka (1996), were firstly applied to constrain the crystallization conditions of clinopyroxene from the melt, obtaining several  $T$ - $P$ - $H_2O$  triplets. Since these triplets are strongly dependant on the chosen melt and on the inferred  $H_2O$  content, they were checked, together with the melt composition, by means of the Rhyolite-MELTS calibration (Gualda et al. 2012). Iterated procedures (Fig. 6a) were developed until a clinopyroxene composition analogous to the starting one was reproduced

by Rhyolite-MELTS. In this way, the two independent approaches reinforce one to another, giving a more robust framework for the thermobarometric and water results. Since the only left starting parameter required by Rhyolite-MELTS was oxygen fugacity, we chose  $f_{O_2} = NNO$  as proposed by Bonadiman et al. (1994) for the Mt. Monzoni intrusion.

However, by increasing the differentiation degree of SS rocks, and/or considering the more alkaline SU magmas, the reliability of Rhyolite-MELTS decreases, as a function of the alkali-enrichment of the system and the related crystallization of amphibole and biotite, for whom thermodynamic parameters are not well constrained (Gualda et al. 2012). Therefore, the use of Masotta et al. (2013) thermobarometer was preferred for the SU suite and for the more evolved SS rocks, and was cross-checked with Putirka (2008) equations (Fig. 6b). As for SS rocks, once assessed the equilibrium between clinopyroxene and melt,  $T$ - $P$  pairs at variable  $H_2O$  contents of the melt were extrapolated by means of the Putirka (2008) method. The resulting  $T$ - $P$ - $H_2O$  triplets were then inputed in Masotta et al. (2013) equation until the resulting  $T$  and  $P$  were comparable to those obtained by Putirka (2008) method at similar water contents.

Some issues for handling this combination of modeling tools should be remarked: (i) since Rhyolite-MELTS is not suitable for amphibole and biotite-dominated rocks, it was only used to simulate the composition of clinopyroxene in equilibrium with the least evolved SS magmas, at the  $P$ ,  $T$  and  $H_2O$  conditions determined by the previous calculations; (ii) the alkaline nature of PIC (especially SU) differentiated rocks implies that clinopyroxene-melt behavior during crystallization and cooling depends not only on Fe and Mg, but also on Ca, Na and Al, so Masotta et al. (2013) equations became progressively more reliable; (iii) iterated and cross-checked calculations using Putirka (2008), Rhyolite-MELTS and Masotta et al. (2013) methods (Fig. 6a-b) were proposed to unravel  $P$ - $T$ - $H_2O$  crystallization conditions avoiding circular relationships between the equations.

The errors proposed for the thermobarometers, oxybarometers and hygrometers are reported in Table 4: while temperatures could be defined within a narrow error range ( $\pm 10$  to  $\pm 20^\circ C$ ) with

both Putirka et al. (2008) and Masotta et al. (2013) equations, the  $P$  estimates were affected by high uncertainties, varying from  $\pm 1.2$  (Masotta et al. 2013) to  $\pm 2.6$  kbar (Putirka et al. 2008).

#### 6.2.1. Clinopyroxene crystallization conditions of Shoshonitic Silica Saturated rocks

The most magnesian clinopyroxene in SS rocks were found within pyroxenites (Mg#<sub>Cpx</sub> 76-78), whereas the less magnesian compositions (Mg#<sub>Cpx</sub> 63-71) were in the monzodiorites and monzonites. The early  $T$ - $P$ -H<sub>2</sub>O crystallization conditions were likely represented by the former, which attained equilibrium with a trachybasaltic melt (Mg# 51; Fig. 4a, Table 3), further confirming the first FC step identified by Casetta et al. (2017). Clinopyroxene-melt thermobarometers indicated a  $P$ - $T$  range of 1.6-2.3 kbar and 1070-1050°C, for water contents of 2.0-2.5 wt% (Table 4). The best fitting data in by Rhyolite-MELTS simulations were obtained at pressure of 1.5 kbar, temperature of 1060°C and 2.5 H<sub>2</sub>O wt%. Consequently, 2.0-2.5 H<sub>2</sub>O wt% could be assumed as the water contents of the first SS magmas intruding the PIC. Clinopyroxenes in the cumulitic gabbros were slightly less homogeneous and less magnesian (Mg#<sub>Cpx</sub> 69-71 cores; 65-66 rims), and resulted in equilibrium with melts varying in Mg# from 43 to 40 (cores) to about Mg# 36 (rims), as shown in Fig. 4a and Table 3. Pressure-temperature paths indicated that cores attained equilibrium in a  $P$  range of 0.5-1.9 kbar and  $T$  of 910-980°C, while rims formed at 0.3-1.2 kbar and 900-920°C, considering H<sub>2</sub>O contents of 3.0-4.0 wt%. Clinopyroxenes in monzogabbros and monzodiorites were nearly unzoned although compositionally comparable to those in gabbros, showing Mg#<sub>Cpx</sub> of 68-72. As for gabbroic rocks, equilibrium was reached with intermediately evolved magmas (Mg# 40, Fig. 4a, Table 3), by which thermobarometric equations indicated a  $T$  range of 940-990°C at  $P$  of 1.4-1.6 kbar, for a H<sub>2</sub>O contents in the melt of 3.0-4.0 wt%. All results are reported in Table 4 and Fig. 7a.

#### 6.2.2. Clinopyroxene crystallization conditions of Shoshonitic Silica Undersaturated rocks

Clinopyroxenes from the SU suite are more alkaline than those of the SS rocks, ranging from salitic-aegirinaugitic to ferrosalitic compositions. The most magnesian compositions in gabbros and monzogabbros ( $Mg\#_{Cpx}$  67-63) were in equilibrium with  $Mg\#$  36 melts (Fig. 4b, Table 3). Pressure-temperature paths indicate a  $P$  range of 0.2-1.6 kbar and  $T$  of 920-940°C at water contents of about 1.0-1.5 wt%. Clinopyroxenes in syenites ( $Mg\#_{Cpx}$  60-48) show composition close to the equilibrium with the whole rock (Fig. 4b, Table 3), which represent a theoretical slightly evolved trachytic melt. Thermobarometers yielded a  $P$  of 0.2-1.6 kbar at  $T$  of 810-860°C at water contents between 4.0 and 5.0 wt%. Results are reported in Table 4 and shown in Fig. 7a.

### 6.3. Amphibole and amphibole-plagioclase thermobarometer and hygrometer

Pressure, temperature and  $H_2O$  conditions for amphibole crystallization were estimated using amphibole-plagioclase Al-exchange thermobarometers (Holland and Blundy 1994; Anderson and Smith 1995; Anderson 1996) and a single amphibole thermobarometers (Ridolfi et al. 2010; Ridolfi and Renzulli 2012). Amphibole-plagioclase equations were used for mineral pairs in both SS and SU suites, whereas the single amphibole thermobarometers were applied to all amphibole compositions in the SS rocks, but only for amphibole in gabbros in the SU suite. This because of the higher alkali content of SU differentiated magmas, well above the compositional ranges admitted for the calibration of the empirical geothermometers of Ridolfi et al. (2010) and Ridolfi and Renzulli (2012). For the SS and SU amphiboles, the single amphibole equations enabled also the calculation of the water content of the melt from which they crystallized. Contrary to the clinopyroxene-melt equations, the error range for the barometric estimates based on amphibole-plagioclase and single amphibole was lower, ranging between  $\pm 0.03$  and  $\pm 0.6$  kbar, whereas errors on  $T$  estimates were slightly higher ( $\pm 23$  to  $\pm 40^\circ C$ , Table 4).

### 6.3.1. Amphibole crystallization conditions of Shoshonitic Silica Saturated and Shoshonitic Silica Undersaturated rocks

Pressure-temperature paths obtained from amphibole-plagioclase thermobarometers yielded a  $T$ - $P$  range of 750-845°C and 0.1-1.2 kbar in SS gabbros to monzodiorites (Fig. 7a, Table 4). Single amphibole calculations for the same lithotypes confirmed these values, indicating  $P$  = 0.7-1.4 kbar and  $T$  = 720-810°C. The estimated H<sub>2</sub>O contents of melts in equilibrium with amphiboles of SS gabbros to monzodiorites was between 4.8 and 6.0 wt% (Fig. 7b, Table 4). Amphibole-plagioclase estimates for the SU suite yielded similar  $P$  intervals (0.4-1.0 kbar) but at lower  $T$  (620-660°C) for gabbros, and  $P$ - $T$  ranges of 1.6-1.9 kbar and 870-880°C taking into account the mineral pairs in the monzogabbroic rocks (Fig. 7a, Table 4). The single amphibole method, applied only to the actinolitic hornblendes in SU gabbros, provided comparable pressures (0.5-0.6 kbar) and temperatures (700-720°C) with respect to the SS rocks (Fig. 7a, Table 4). The calculated water contents of the melts were similar to those obtained for the SS suite (5.1-5.7 wt%, Fig. 7b, Table 4).

As expected, the water contents calculated by these models were higher than those obtained from the clinopyroxene-melt calculations. Amphibole crystallization, in fact, occurred later than clinopyroxene, thus the melt from which amphibole precipitated should have undergone differentiation in some extent, and its water content should have increased. If we consider the water enrichment linked to the fractional crystallization of the SS/SU magmas, together with the concomitant precipitation of volatile-bearing phases, the H<sub>2</sub>O contents resulted from the single amphibole equations appear in line with the calculations proposed by the FC model of Casetta et al. (2017).

### 6.4. Biotite thermometer

Biotite is a ubiquitous phase occurring in the late inter-cumulus mineral assemblages of almost all SS, SU and GU rocks. Its presence enabled us to provide some estimates on the temperatures



of these assemblages, by using of the empirical single-mineral thermometer of Henry et al. (2005), based on the Ti content of biotite.

#### 6.4.1. Biotite crystallization conditions of Shoshonitic Silica Saturated, Shoshonitic Silica Undersaturated and Granitic Unit rocks

Temperature of biotite crystallization in SS pyroxenitic cumulates resulted between 690 and 740°C, whereas a  $T$  interval of 600-660°C was considered representative of SS gabbros to monzodiorites. Biotites from more differentiated SS monzonites yielded a  $T$  of about 540-580°C (Fig. 7a, Table 4). Biotite in SU gabbros and monzogabbros indicated comparable temperatures, ranging between 640 and 660°C (Fig. 7a, Table 4).

The thermometer was also applied to GU syenogranites, resulting in a  $T$  range of 420-570°C: the biotites in GU rocks are however iron-rich, with  $Mg/(Mg+Fe_{tot}) < 0.275$ , just out of the compositional field for which the thermometer was calibrated. Consequently, the resulting temperatures were not used for further modeling purposes.

#### 6.5. Plagioclase-melt thermobarometer and hygrometer

Plagioclase appears in almost all PIC rocks, from the cumulitic pyroxenites, where it is part of the intercumulus assemblages, to the syenitic rocks, where, together with K-feldspar, dominates the paragenesis. Its ubiquitous presence made it an additional tool for investigating the  $T$  and  $H_2O$  content of PIC magmas along the entire SS and SU differentiation trends by means of Putirka (2008) and Lange et al. (2009) equations. Plagioclase from GU granites and syenogranites are compositionally close to the pure albitic end-member, probably because of hydrothermal/alteration processes. This made them unsuitable for the hygrometer application, being its calibration limited to  $An_{37}$  plagioclase (Lange et al. 2009).

As for clinopyroxene, plagioclase equilibrium with its host rock was constrained by means of the experimentally determined values of  $^{Pl-Liq}Kd_{An-Ab} = 0.10 \pm 0.05$  at  $T < 1050$  °C and  $0.27 \pm 0.11$

at  $T \geq 1050$  °C (Putirka 2008). However, Mollo et al. (2011) demonstrated that  $^{Plag-Liq}Kd_{An-Ab}$  is highly sensitive to the cooling rate of the melts, being thus variable between  $0.2 \pm 0.02$  (cooling rate of  $0.5^\circ\text{C}/\text{min}$ ) and  $0.35 \pm 0.03$  (cooling rate of  $15^\circ\text{C}/\text{min}$ ). Thus, all plagioclase-melt equilibria (even at  $T < 1050^\circ\text{C}$ ) were considered following a  $^{Plag-Liq}Kd_{An-Ab}$  in the range of  $0.27 \pm 0.11$  (Putirka 2008), whose interval is also in accordance with the results obtained by Mollo et al. (2011). Cooling rate is in fact an essential factor for the crystallization dynamics of intrusive bodies, as testified by the plagioclase morphological variations in PIC rocks, where it appears as both cumulus and intercumulus phase throughout the entire SS/SU fractionation trends. According to crystallization sequences, plagioclase appeared after clinopyroxene and Fe-Ti oxides, just before or even contemporary to biotite and amphibole in the intercumulus assemblages. Consequently, we considered the thermobarometric values obtained by clinopyroxene, amphibole and biotite calculations for each magmatic suite (see above) to identify the  $P$ - $T$ - $H_2O$  interval in which plagioclase crystallized from the melt. As for clinopyroxene, plagioclase often appeared in disequilibrium with its whole rock composition (Fig. 5), and the amount of disequilibrium gradually decreases with increasing the differentiation degree of the corresponding whole rock. Plagioclase in monzodiorites were in fact closer to the equilibrium with respect to those of pyroxenites and gabbros, whereas most of the plagioclase from monzonites and syenites were in equilibrium with their host rock (Fig. 5). As previously mentioned for clinopyroxene, such a trend could be justified by considering that the more evolved rocks likely resemble melt compositions, being close to the eutectic of the system. Thus, plagioclase compositions were related to estimated melt compositions, according to the differentiation trends proposed by Casetta et al. (2017), to retrieve the equilibrium conditions. Once equilibrated, plagioclase and melt compositions were used as input for the Lange et al. (2009) hygrometer to calculate the amount of  $H_2O$  dissolved in the melt (see flow chart of Fig. 6). For each sample, input  $T$  and  $P$  required in Lange et al. (2009)

equation were chosen in the  $T$ - $P$  interval between those estimated by clinopyroxene-melt calculations and those resulted from amphibole and biotite.

Pressure, temperature and  $H_2O$  were calculated by iterating Lange et al. (2009) method and equation 24a of Putirka (2008) until a matching  $T$  was found. In any case, small variations of  $P$  scarcely affect the results of the hygrometers:  $\pm 1$  kbar corresponds to  $\pm 0.1$  wt%  $H_2O$  calculated in the melt (Giacomoni et al. 2014). Since the  $P$  interval obtained by the previous (clinopyroxene and amphibole) barometers was roughly between 0.2 and 1.9 kbar for all PIC rocks, the  $H_2O$  estimates were almost entirely constrained by temperature changes. As a consequence, the match between  $T$  obtained with Lange et al. (2009) and equation 24a of Putirka (2008) was considered a reliable cross-check and a robust constraint on our geothermal modelling (Fig. 6).

#### 6.5.1. Plagioclase crystallization conditions of Shoshonitic Silica Saturated rocks

Data from clinopyroxene-melt simulations on pyroxenites indicated that SS primary magmas began crystallizing at about 1.5 kbar, 1060°C and 2.5  $H_2O$  wt%. The more anorthitic plagioclase ( $An_{84-73}$ ) were analyzed in the pyroxenites intercumulus assemblage, following clinopyroxene and preceding biotite, thus the  $T$  range of plagioclase crystallization is constrained by the temperatures of crystallization of these two phases. Since pressure does not sensitively affect the calculations, a pressure of 1.5 kbar was used according to the results from clinopyroxene-melt calculations (Fig. 6 and 7). Results indicated that the most anorthitic plagioclase ( $An_{84-73}$ ) crystallized in equilibrium with a trachybasaltic melt (Mg# 51; Fig. 5, Table 3): at  $P = 1.5$  kbar,  $T$  of crystallization resulted of 1060-1081°C for a  $H_2O$  content of 3.0 wt%.

Plagioclase in SS gabbros were in compositional continuity with those of pyroxenites, varying between  $An_{73}$  and  $An_{51}$  in both the cumulus and intercumulus assemblages. As for plagioclase inside pyroxenites, the marked disequilibrium (Fig. 5) was probably related to the cumulitic nature of gabbros and/or a variable cooling rate of the magma. The crystallization sequence and

the comparison with the  $T$  ranges obtained from clinopyroxene, amphibole and biotite suggested that plagioclase crystallized in a temperature interval of 980 to 740°C. Plagioclase with An<sub>73</sub> reached the equilibrium with a Mg# 49 melt (Fig. 5): at  $P$  of 1.5 kbar,  $T$  and H<sub>2</sub>O content resulted of 1016-1053°C and 3.1 wt% respectively. An<sub>63-51</sub> plagioclases were equilibrated with a basaltic trachyandesitic melt (Fig. 5, Table 3), yielding  $T$  of 920-1021°C and a water content of 3.2-3.4 wt% at pressures of 1.2-1.5 kbar (Fig. 7, Table 4). It is worth noting that for these temperatures, Putirka (2008) proposed a potential partitioning  $^{Plag-Liq} Kd_{An-Ab} = 0.05-0.15$  to attest equilibrium. However, after several iterations, the modelled  $P$ - $T$ -H<sub>2</sub>O terms for PIC magmas were attained only within a  $^{Plag-Liq} Kd_{An-Ab}$  of  $0.27 \pm 0.11$ . Such apparent discrepancies could be explained considering the dependency of An-Ab equilibrium coefficient with the cooling rate (Mollo et al. 2011).

Plagioclase from monzogabbros to monzonites were in a compositional range from An<sub>53</sub> to An<sub>34</sub>, resulting in equilibrium with basaltic trachyandesitic to trachyandesitic melts (Fig. 5, Table 3). At  $P$  of 1.2 kbar,  $T$  resulted between 917 and 989°C, for water contents of 3.9-4.8 wt%, progressively increasing with the differentiation degree of the samples (Fig. 7, Table 4).

#### 6.5.2. Plagioclase crystallization conditions of Shoshonitic Silica Undersaturated rocks

Plagioclase in SU rocks range from An<sub>50-43</sub> in gabbros to An<sub>38-23</sub> in monzogabbros and monzodiorites, and reach the more albitic compositions in syenites, where anorthite content is low (An<sub>23</sub>-An<sub>2</sub>). Plagioclase in gabbros were equilibrated by an intermediately evolved melt, trachyandesitic in composition (Fig. 5, Table 3). According to the themobarometric data obtained by multiple geothermometers (clinopyroxene, amphibole and biotite), the temperature crystallization interval of plagioclase ranges between 940 and 720°C. Plagioclase-melt thermometers and hygrometers yielded a  $T$  range of 975-990°C at  $P$  of 1.5 kbar, for a water content of 4.1 wt%.

Apart from the nearly pure albitic compositions (likely effects of secondary processes), plagioclase in monzogabbros to syenites vary from An<sub>38</sub> to An<sub>23</sub>. They were equilibrated with an evolved trachytic melt (Fig. 5, Table 3), thought to be the final product of the SU differentiation trend (Casetta et al. 2017). At  $T-P$  space of 920-936°C and 1.2 kbar, the estimated water contents of melt in equilibrium with An<sub>38</sub> plagioclases was about 4.4 wt%, progressively increasing with the differentiation of the samples (Fig. 7, Table 4).

#### 6.6. K-Feldspar-melt hygrometer

Except for pyroxenites, K-feldspar is present in all PIC rocks, where it occurs as intercumulus (gabbros to monzodiorites) and cumulus (monzonites/syenites) phase. Its composition was used to constrain the amount of H<sub>2</sub>O dissolved in the co-existing melt by means of the equation proposed by Mollo et al. (2015). Such method, based on the Or-Ab exchange between K-feldspar and melt is calibrated for alkaline differentiated magmas, thus proper for the SS, SU and GU rocks compositions. Together with the data obtained by the previous equations, such estimates enabled to “track” the H<sub>2</sub>O contents in the progressively differentiating melts. According to Mollo et al. (2015), this method can be applied only to K-feldspar with Or<sub>44-86</sub>, whereas no reliable results were produced for Or<sub>>86</sub> as it extended outside the range of calibrated compositions. K-feldspar and whole rock equilibrium evaluation was attained by minimizing the difference between predicted and measured  $K^{K-Feld-Liq}Kd_{Or-Ab}$ , following equation 2 of the Mollo et al. (2015) model. These conditions were satisfied only by considering K-feldspar compositions in equilibrium with trachyandesitic to trachytic melts (Table 3), further confirming the correspondence between the crystallization sequence and the progressive differentiation model proposed by Casetta et al. (2017).

According to the equilibration temperatures recorded by clinopyroxene, amphibole, biotite and plagioclase, a  $T$  of 900-800°C was used as input for all samples of the SS and SU suites, whereas lower temperatures (800-700°C) were considered for GU syenogranites.

### 6.6.1. *K-feldspar crystallization conditions of Shoshonitic Silica Saturated, Shoshonitic Silica Undersaturated and Granitic Unit rocks*

Water concentration of melts in equilibrium with K-feldspar in SS gabbros to monzogabbros were in the range of 4.4-5.3 wt% and 5.6-6.5 wt% respectively, whereas higher H<sub>2</sub>O contents (6.1-7.3 wt%) were recorded in monzodiorites. The highest water values were calculated in SS syenites, that in turn show a larger variability of values (H<sub>2</sub>O = 4.6-7.3 wt%; Fig. 7, Table 4). K-feldspar analysed in SU monzogabbros and monzonites indicated H<sub>2</sub>O contents of the crystallizing melts between 5.5-6.3 wt% and 6.7-7.8 wt%, respectively. H<sub>2</sub>O estimates for GU syenogranites range between 8 and 11 wt%, being however meaningless in the physical system compatible with the body emplacement. The solubility of water at  $P < 2.5$  kbar for rhyolitic-trachytic melts in fact do not exceed 7 wt%, as experimentally and theoretically determined in the  $T$  range of 500-1000°C (Di Matteo et al. 2004; Liu et al. 2005). These values were therefore discharged in the discussion.

## 7. Oxygen fugacity

The two main magmatic suites (SS and SU) are formed by the differentiation of melts which began crystallizing at pressures lower than 2.0 kbar and at similar  $T$  ranges (1050-1000°C). Main differences between the SS and SU suites could be found by taking into account the total amount of water of the crystallizing melts: SS primitive melts in fact were characterized by an higher water contents with respect to that of SU ones (2.0-2.5 wt% vs. 1.0-1.5 wt%, respectively). Classically, it is considered that dissolved molecular H<sub>2</sub>O reacts with oxygens of the silicate network producing two OH<sup>-</sup> groups (e.g. Stolper 1982; Silver and Stolper 1985; Kohn 2000). The overall reaction reading as  $\text{H}_2\text{O} + \text{O}^{2-} = 2\text{OH}^-$  may thus be considered as the counterpart of the water solubility in evaluating the redox conditions.

To effectively quantify such differences, we estimated the  $f\text{O}_2$  conditions of each portion of PIC by means of the  $T$ - $f\text{O}_2$  model of Burkhard (1991), based on the biotite/K-feldspar/magnetite equilibrium in biotite-bearing intrusive rocks. Burkhard's (1991) empirical equation complements that of Kress and Carmichael (1988), enabling to calculate oxygen fugacity and temperature by two independent formulas. Water fugacity required in Burkhard's (1991) equation was calculated at a fixed  $P$  of 1.5 kbar following Burnham et al. (1969). Sanidine activity was considered according to Waldbaum and Thompson (1969), whereas magnetite activity was approximated at unity (Burkhard 1991). Since this equation required as input the amount of  $\text{Fe}^{2+}$  in biotite,  $\text{Fe}^{2+}/\text{Fe}^{3+}$  ratios of SS, SU and GU biotites were calculated following Dymek (1983). Because the compositional spectrum of biotite and sanidine in each rock is slightly variable, we calculated two  $T$ - $f\text{O}_2$  pairs for each lithotype (Fig. 8, Table 4), to account for the possible oxygen fugacity ranges. According to Burkhard (1991), the error on each calculation was of  $\pm 0.3$  log units.

As shown in Fig. 8, oxygen fugacity in SS rocks resulted in a range from -14.1 to -10.7  $\log f\text{O}_2$ , at temperatures comprised between 790 and 1000°C (Table 4). Such values plot between the FMQ and NNO buffers (+0.2 to +0.7  $\Delta\text{FMQ}$ , Fig. 8), and are well comparable to the values chosen as input for the Rhyolite-MELTS model above developed (-9.34  $\log f\text{O}_2$  at 1060°C), further confirming the validity of the calculated parameters. Rocks from the SU and GU suites were characterized by values of -11.9 to -10.2  $\log f\text{O}_2$  at  $T$  of 920-1050°C (-0.1 to +0.3  $\Delta\text{FMQ}$ , Fig. 8), and -12.9 to -11.8  $\log f\text{O}_2$  at  $T$  of 850-920°C (around +0.4  $\Delta\text{FMQ}$ , Fig. 8), respectively (Table 4). Syenogranites of the GU suite were characterized by a behavior comparable to that of SS rocks, whereas SU rocks record slightly more reduced conditions.

## 8. EC-AFC processes

As shown by the thermobarometric and hygrometric models, the two main magmatic suites (SS and SU) emplaced and crystallized at comparable pressures and temperatures conditions. The

only differences can be identified when water content and oxygen fugacity are considered, being the SU system characterized by lower H<sub>2</sub>O content and by more reduced conditions. Anyway, such slight divergences are not able to justify the marked geochemical variations between SS and SU magmas (see also Casetta et al. 2017). To account for the geochemical features of the SS and SU batches, we developed several Energy-Constrained Assimilation and Fractional Crystallization (EC-AFC) models (Bohrson and Spera 2001; Spera and Bohrson 2001), based on <sup>87</sup>Sr/<sup>86</sup>Sr and <sup>143</sup>Nd/<sup>144</sup>Nd. The purpose of this calculation was to discriminate between the original (i.e. mantle-derived) signature of SS/SU magmas and the effects of assimilation (and/or contamination) during the emplacement and differentiation of PIC magmas. Specifically, the main target of the models were: (i) verifying if the isotopic signature of SU rocks was generated an interaction between SS magmas and crust; (ii) quantify the eventual (if any) crustal assimilation during the differentiation of the SS/SU magmatic suites; (iii) discriminate between assimilation and contamination processes.

A wide spectrum of Permo-Triassic crustal rock isotopic signatures from the literature were considered in the EC-AFC model as potential assimilants. These are Triassic carbonates (Martin and Macdougall 1995; Blendiger et al. 2015), Permian intrusives of Mt. Croce (central-eastern Southern Alps; Rottura et al. 1997) and Serie dei Laghi (southwestern Alps; Sinigoi et al. 2016, and references therein), Permian rhyolitic ignimbrites of the Atesina Volcanic District (Barth et al. 1993), and the Kinzigite formation (southwestern Alps; Voshage et al. 1990). Geothermobarometric and hygrometric results (Table 4) were used to to calculate assimilants and starting magmas' specific heat [J/(KgK)], heat of crystallization (J/Kg) and heat of fusion (J/Kg) according to Spera (2000), Bohrson and Spera (2001) and Spera and Bohrson (2001, Table 5). Specific heat [J/(KgK)] and liquidus T (°C) of carbonate assimilant (Table 5) were considered accordingly to Dallai et al. (2011) and Eppelbaum et al. (2014).

The absence of <sup>87</sup>Sr/<sup>86</sup>Sr and <sup>143</sup>Nd/<sup>144</sup>Nd variations with increasing silica content for both SS and SU suites and the lack of overlap between SS and SU compositional fields suggested that



the two suites have a different origin. A slight  $^{87}\text{Sr}/^{86}\text{Sr}$  increase was however noted for both SS and SU samples while approaching the intrusion borders (Table 2). On the other side, the  $^{143}\text{Nd}/^{144}\text{Nd}$  of both SS and SU rocks were not sensitive to the distance from intrusion edges, ruling out the occurrence of contamination processes during magma emplacement. Therefore, the Nd isotopic enrichment of the SU suite can be considered as a primary feature, directly function of its mantle source or alternatively derived from assimilation of crustal components. In this view, the EC-AFC equations were applied to the less contaminated compositions to better constrain the Sr and (especially) Nd isotopic variations among the magmatic suites.

The EC-AFC model from a starting SS composition (Fig. 9) showed that none of the chosen crustal components was able to drive the initial SS  $^{87}\text{Sr}/^{86}\text{Sr}$  and  $^{143}\text{Nd}/^{144}\text{Nd}$  ratios towards the SU field. This simulation reinforced the primary nature of the Nd isotopes enrichment of the SU body, ruling out the genesis of the SU rocks via crustal assimilation by an SS starting magma. The model was instead able to explain the isotopic variability of the SS samples. Almost all assimilation models well fitted the isotopic trend of SS rocks, suggesting that small amounts of crustal components were assimilated during magma storage. As shown in Fig. 9, the less depleted  $^{143}\text{Nd}/^{144}\text{Nd}$  end-members were achieved by an interaction between magma and 2-10% of crust, represented by kinzigites (Voshage et al. 1990), Mt. Croce granodiorites (Rottura et al. 1997) and/or Atesina Volcanic District rhyolitic ignimbrites (Barth et al. 1993). A 5% assimilation of carbonates (Martin and Macdougall 1995; Blendiger et al. 2015) and/or Serie dei Laghi-like granites (Sinigoi et al. 2016) instead reproduced the more depleted  $^{143}\text{Nd}/^{144}\text{Nd}$  ratios.

A second EC-AFC model was attempted to explain the isotopic variations of SU samples, but their scattered distribution prevented to retrace the assimilation path. Nevertheless, this model was used just to quantify the crustal contribution in the Nd isotopic variations of the SU samples. As a result, the  $^{143}\text{Nd}/^{144}\text{Nd}$  range of the SU suite was achieved by a 2-7% assimilation

of the crustal components (carbonates, Atesina Volcanic District rhyolitic ignimbrites, Mt. Croce granodiorites, Serie dei Laghi granites and amphibolitic kinzigites).

On the whole, the Nd isotopic ranges of both SS and SU suites could be explained by low amounts of assimilation, whereas Sr isotopic variability is more likely derived from contamination processes at the intrusion borders during magma emplacement, where fluid mobilization and local metamorphic reactions occurred (Ferry et al. 2002; Gallien et al. 2007). As reported in Table 2, the Sr isotopic signature of PIC rocks appears to be more sensitive to their distance to the intrusion edges rather than to their degree of differentiation, being thus the  $^{143}\text{Nd}/^{144}\text{Nd}$  ratio the best proxy to discriminate the two magmatic suites. Given this, the Sr variations of the SU suite at near constant  $^{143}\text{Nd}/^{144}\text{Nd}$  could be also affected by i) slight alteration effects, unavoidable for such a small body and/or ii) the contact halo between PIC and the wall rocks.

## 9. Discussion

### 9.1. Emplacement of the Shoshonitic Silica Saturated and Shoshonitic Silica Undersaturated magmas

The SS and SU intrusive bodies formed as result of fractional crystallization of two distinct trachybasaltic melts, which differentiated along two independent trends over a short time span. The result of this process was the generation of a large spectrum of intrusive rocks whose cumulus+intercumulus assemblages progressively vary in composition, reaching the most evolved nature in the syenitic rocks. The textural/compositional homogeneity of the main cumulus phases of PIC rocks, together with the scarce efficiency of syn- to post-crystallization diffusion processes on such large-sized crystals, led us to hypothesize that their composition is directly function of the physical conditions at which they formed and segregated from the melt. In this scenario, clinopyroxene and plagioclase were considered as “snapshots” of the fractional

crystallization processes, able to provide informations on the  $T$ - $P$  conditions of the melts from which they generated.

If we compare the clinopyroxene and plagioclase compositions to that of their host rock, in fact, the disequilibrium is evident (Figg. 4 and 5). Clinopyroxene of SS gabbros (Mg# 55), for example, are characterized by Mg# of 65-71, ideally in equilibrium with melt with Mg# < 43, quite far from the bulk rock composition of the gabbro. The most magnesian ones (Mg#<sub>Cpx</sub> 76-78), in pyroxenites, are theoretically in equilibrium with a trachybasaltic melt (Mg# 51), further confirming that the mafic rocks of the complex are cumulates formed during the initial stages of fractionation of the trachybasaltic melt. On the other hand, the less magnesian clinopyroxene crystals tracked in syenites were almost in equilibrium with their host rocks, corroborating the assumption that the more differentiated rocks of the complex resemble the composition of melts and approach the eutectic of the system. On the basis of the results obtained by the proposed “equilibration model”, in turn supporting the differentiation model of Casetta et al. (2017), PIC rocks were formed during progressive stages of fractional crystallization from starting trachybasaltic melts.

Once evaluated the disequilibrium conditions and reconduted the clinopyroxene/plagioclase compositions to their ideal equilibrium conditions, thermobarometric and hygrometric calculations enabled us to retrieve the  $T$ - $P$ -H<sub>2</sub>O parameters of the less evolved melts in the feeding system. The “classical” thermobarometric approach for intrusive rocks (amphibole-plagioclase and biotite equations) was then used to verify the previous results. These thermobarometers and hygrometers provided  $T$ - $P$ -H<sub>2</sub>O informations for the later crystallization stages.

According to our estimates, some differences between the emplacement conditions of SS and SU magmas can be highlighted. Oxygen fugacities of the PIC plumbing system are between -0.1 and +0.7  $\Delta$ FMQ (Fig. 8), confirming the oxidation conditions proposed by Bonadiman et al. (1994) for Mt. Monzoni intrusion at comparable temperature intervals, further highlighting

the low to moderate oxydizing components that characterized the magmatic systems of the Dolomitic Area during Triassic.

On the basis of clinopyroxene-melt thermometric and hygrometric calculations, SS magmas result slightly water-enriched ( $H_2O = 2.0-2.5$  wt%) with respect to SU ones ( $H_2O = 1.0- 1.5$  wt%), during the first crystallization stages ( $T \sim 1000-1100^\circ C$ , Fig. 7, Table 4). With increasing differentiation, the water content of PIC rocks increased up to 5-8 wt%, value compatible with the amount of fractionation (79-94%) proposed by Casetta et al. (2017), by taking into account the role of amphibole and biotite during differentiation.

The  $T$ - $P$  estimates (Fig. 7, Table 4) indicated that both magma batches cooled from a starting  $T$  of  $\sim 1000-1100^\circ C$  (cumulus assemblage) down to  $\sim 600^\circ C$  (intercumulus assemblage), sharing a common thermal regime. The pressure obtained by applying various mineral-mineral and mineral-melt equilibria were subsequently used to estimate the emplacement depth of the PIC plumbing system, and all the pressures were filtered to extrapolate the best-fit from all models, taking into account the errors of the different methods (Table 4). The resulting pressure values were between 0.4 and 1.7 kbar for both SS and SU intrusive bodies, yielding a depth of about 1.4-5.6 km considering a  $\Delta P/\Delta z$  of 0.29 kbar/km. With respect to the depth (10-17 km) proposed by Menegazzo Vitturi et al. (1995), our estimates suggested that PIC represents an intrusion in the shallow crust, with SS and SU magma batches emplaced within the same thermal regime.

Despite the common geothermobarometric evolution and slightly different water contents, SS and SU bodies can be distinguished in terms of  $^{87}Sr/^{86}Sr$  and  $^{143}Nd/^{144}Nd$ , reinforcing the preliminary PIC model that, on the basis of mineral and bulk rock elemental geochemistry (Casetta et al. 2017) suggested that SS and SU series represent two independent magma pulses. EC-AFC models (Bohrson and Spera 2001; Spera and Bohrson 2001) show that assimilation of various types of Permo-Triassic crustal components by a starting SS magma could not account for the higher  $^{143}Nd/^{144}Nd$  of the SU batch, ruling out any possible derivation of the SU suite from the SS one. Therefore, the Nd isotopic enrichment of the SU suite could be interpreted as

an original mantle signature or, alternatively, could be ascribed to assimilation processes occurring within the crust. We prefer the first hypothesis, since the second one would imply the existence of a common mantle-segregated magma with a  $^{143}\text{Nd}/^{144}\text{Nd}$  ratio high enough to be able to “split” in the SS and SU trends by varying the nature of the assimilant, and such a magma has never been documented in the Dolomitic Area.

The same EC-AFC models demonstrated that both suites assimilated a small proportion of crustal components (5-6% on average, Fig. 9). That amount of assimilation is, however, able to explain the  $^{143}\text{Nd}/^{144}\text{Nd}$  variation throughout SS/SU samples, being that the  $^{87}\text{Sr}/^{86}\text{Sr}$  was affected by late contamination that occurred at the intrusion edges. The fit between PIC isotopic data and the crustal end-members of the Triassic carbonates, the Permian magmatic rocks and the metamorphic basement of the Ivrea Zone is consistent with a geochemical influence on the PIC of a basement that could be attributed to the Ivrea Zone. This hypothesis was also suggested by Barth et al. (1993) to explain the Atesina Volcanic District-Cima d’Asta magma genesis.

In summary, both SS and SU batches are characterized by a strong contribution of an enriched mantle component, even if the lack of primitive products cannot directly quantify its role in the original source. Anyway, if examined in the light of their temporal relationships, the major, trace element and Sr-Nd isotopic signature of the SS and SU bodies enable to define the progressive evolution of the PIC magmatic suites. In turn, this geochemical evolution could be linked to a time-related (slight) variation of the mantle source, even if an accurate dating of the two single bodies would help in better deciphering the time scale of such process. On the other side, the magmatic evolution in the shallow crust for both the SS and SU batches was confined in the same thermal regime.

## 9.2. Origin of the Granitic Unit

The GU rocks (granites and syenogranites) differ from the other PIC magmatic suites (SS and SU), mainly in terms of silica saturation, FeO, MgO, K<sub>2</sub>O and Rb contents (Casetta et al. 2017).

Moreover the estimated volume of the GU portion of the complex ( $1.1 \text{ km}^3$ ) is unrealistically larger than that of the SS/SU syenites ( $\leq 0.25 \text{ km}^3$ ) if we consider the already high ( $> 90\%$ ) fractionation degrees from which these latters generated. This means that, if the GU portion was the result of  $\sim 95\%$  fractionation of a SS/SU magma,  $\sim 20 \text{ km}^3$  of SS/SU rocks should be intruded somewhere. This fact is in stark contrast to what is observable on field.

The GU magmas evolved at redox states comparable to SS/SU ones (about  $+0.4 \Delta\text{FMQ}$ ) and record temperatures down to  $800\text{-}850^\circ\text{C}$  (Fig. 8). Put this all together, it is reasonable to hypothesize that the GU granites/syenogranites were generated by magmatic differentiation from a calc-alkaline parental melt, the primitive/intermediate products of which are not exposed in the PIC area. It should be emphasized that GU rocks are similar to the Middle Triassic calc-alkaline/high-K calc-alkaline rhyolites found in Carnia (Tarvisio area, Julian Alps; Gianolla 1992) and Alto Vicentino regions (Recoaro-Schio area, Southern Alps; De Vecchi et al. 1974; Barbieri et al. 1982). In these latters, the entire high-K calc-alkaline trend is documented, further highlighting the existence of a similar differentiation suite during the Triassic magmatic event. In such a context, GU rocks could represent the corresponding intrusives of the rhyolites of these areas, even if further studies are needed to better investigate this comparison.

### 9.3 Solidification time of PIC

According to Bonadiman et al. (1994) the solidification time of Mt. Monzoni intrusion, emplaced at  $P$ - $T$ - $z$  conditions similar to those of PIC, was about 300 ka. The thermobarometric results obtained for PIC magmas and their subsequent application to the Spera (2000), Bohrsen and Spera (2001) and Spera and Bohrsen (2001) equations, enabled to model the cooling time of PIC, expected to be slightly higher than that of Mt. Monzoni, due to its larger volume ( $4.5 \text{ km}^3$  vs.  $1.0\text{-}1.5 \text{ km}^3$ ).

In order to make an accurate comparison with Bonadiman et al. (1994), Spera (1980) equation was applied to PIC by assuming the thermal estimates already used for the EC-AFC calculations

and/or derived from Ryolite-MELTS modelling (see Table 5). By taking into account the whole volume of PIC, the solidification time resulted about 700 ka. Even if this time value was obtained without discriminating the single volumes of the SS, SU and GU bodies, it was considered reliable taking into account the similar thermal regimes calculated for the SS, SU and GU suites and the limited re-heating effects provided by the subsequent magma pulses.

## 10. Conclusions

A coupled thermobarometric and isotopic study of the main magmatic suites of the Predazzo Intrusive Complex enabled us to set out some remarkable points on the emplacement conditions of the Middle Triassic magmas in the Dolomitic Area. They can be summarized as:

1. Predazzo Intrusive Complex emplacement occurred at a depth of 1.4-5.6 km (0.40-1.65 kbar), consistent with the field relationships suggesting consanguinity with the overlying effusive rocks. Its solidification time was about 700 ka, slightly higher but comparable to that proposed by Bonadiman et al. (1994) for the near Mt. Monzoni intrusion.

2. Despite similar  $T$ - $P$  of magma emplacement of the three unites,  $H_2O$  and  $fO_2$  data indicated that SU primary magmas were characterized by lower water contents and oxidizing conditions than the SS ones (1.0-1.5 vs. 2.0-2.5  $H_2O$  wt%; -0.1/+0.33 vs. +0.2/+0.7  $\Delta FMQ$ , respectively). Plagioclase-melt, amphibole and K-feldspar-melt hygrometers indicated highly hydrated conditions of magmas and progressive  $H_2O$  enrichment during differentiation.

3. The  $^{87}Sr/^{86}Sr$  and  $^{143}Nd/^{144}Nd$  of PIC magmas plot in the enriched mantle source field. This feature speaks in favour of the presence of a subduction-signature in the mantle beneath Southern Alps during Triassic, as already proposed by Bonadiman et al. (1994) and Zanetti et al. (2013). Even if the absence of primary products in the Dolomitic Area prevents to exactly quantify the role of the enriched mantle component in the magma genesis, its contribution was undoubtedly high.

4. The EC-AFC models cannot account for the genesis of SU rocks via crustal assimilation starting from a SS magma, thus indicating two distinct geochemical signatures for SS and SU magmas. In turn, this difference could be ascribed to a time-related change in the mantle source, slightly moving towards a more  $^{143}\text{Nd}/^{144}\text{Nd}$  enriched component.

5. A low degree of crustal assimilation (5-6%) was able to explain the Nd isotopic variability of both SS and SU magmas, whereas the Sr isotopic variations were more likely the results of contamination processes at PIC edges. Fractional crystallization was the major (and almost only) process acting during the differentiation of SS and SU magmas, confirming what hypothesized by Petersen et al. (1980) and Casetta et al. (2017). The signature of the Triassic magmas is consistent with an Ivrea-like basement beneath the Dolomitic Area.

6. Despite petrography, whole-rock and mineral chemistry suggested an I-type affinity for GU granites/syenogranites, the wide range and the uncertainty on their isotopic signature leaves the question on the origin of GU suite still unsolved. However, the geochemical and petrographic similarities with the coheval calc-alkaline/high-K calc-alkaline rhyolites found in Carnia (Gianolla 1992) and Alto Vicentino (De Vecchi et al. 1974; Barbieri et al. 1982; Bellieni et al. 2010) suggest the presence of a high-K calc-alkaline series also in the Dolomitic Area.

## Acknowledgments

We are grateful to Andrea Marzoli and Matteo Masotta for their careful and constructive reviews that significantly improved the quality of the paper, and we would also acknowledge Timothy L. Grove for his editorial guidance. The IUSS Mobility Research Programme of the University of Ferrara, grant n. 570 for Long Period, 2016 (FC) and The Italian National Research Program PRIN\_2015/prot. 20158A9 (CB) supported this research. Anne Kelly and Vincent Gallagher are also thanked for making the Sr and Nd isotopic analyses at SUERC.

## References



- Anderson JL (1996) Status of thermobarometry in granitic batholiths. *Geol Soc Am Spec Pap* 315: 125-138. <https://doi.org/10.1017/S0263593300006544>
- Anderson JL, Smith DR (1995) The effects of temperature and  $fO_2$  on the Al-in-hornblende barometer. *Am Min* 80(5-6): 549-559.
- Barbieri G, De Vecchi GP, De Zanche V, Mietto P, Sedeà R (1982) Stratigrafia e petrologia del magmatismo triassico nell'area di Recoaro. Guida alla geologia del Sudalpino centro-orientale. *Soc Geol It Guide Geologiche Regionali*: 179-187.
- Barth S, Oberli F, Meier M, Blattner P, Bargossi GM, Di Battistini G (1993) The evolution of a calc-alkaline basic to silicic magma system: geochemical and Rb–Sr, Sm–Nd, and  $^{18}O/^{16}O$  isotopic evidence from the Late Hercynian Atesina-Cima d'Asta volcanoplutonic complex, northern Italy. *Geochim Cosmochim Acta* 57: 4285-4300. [https://doi.org/10.1016/0016-7037\(93\)90323-O](https://doi.org/10.1016/0016-7037(93)90323-O)
- Bellieni G, Fioretti AM, Marzoli A, Visonà D (2010) Permo–Paleogene magmatism in the eastern Alps. *Rend Lincei* 21: S51-S71. <https://doi.org/10.1007/s12210-010-0095-z>
- Bernoulli D, Lemoine M (1980) Birth and Early Evolution of the Tethys: the Overall Situation. *Mem Bur Rech Géol Minières* 115: 168-179.
- Blendinger W, Lohmeier S, Bertini A, Meißner E, Sattler CD (2015) A new model for the formation of Dolomite in the Triassic dolomites, Northern Italy. *J Pet Geo* 38(1): 5-36. [10.1111/jpg.12596](https://doi.org/10.1111/jpg.12596)
- Bohrson WA, Spera FJ (2001) Energy-constrained open-system magmatic processes II: application of energy-constrained assimilation–fractional crystallization (EC-AFC) model to magmatic systems. *J Petrol* 42(5): 1019-1041. <https://doi.org/10.1093/petrology/42.5.1019>
- Bonadiman C, Coltorti M, Siena F (1994) Petrogenesis and T- $fO_2$  estimates of Mt. Monzoni complex (Central Dolomites, Southern Alps): a Triassic shoshonitic intrusion in a transcurent geodynamic setting. *Eur J Mineral* 6: 943-966. [10.1127/ejm/6/6/0943](https://doi.org/10.1127/ejm/6/6/0943)

- Borsi S, Ferrara G (1968) Isotopic age measurements of the M. Monzoni intrusive complex. *Miner Petrogr Acta* 14: 171-183.
- Brack P, Mundil R, Oberli F, Meier M, Rieber H (1996) Biostratigraphic and radiometric age data question the Milankovitch characteristics of the Latemar cycles (Southern Alps, Italy). *Geology* 24(4): 371-375. [https://doi.org/10.1130/0091-7613\(1996\)024<0371:BARADQ>2.3.CO;2](https://doi.org/10.1130/0091-7613(1996)024<0371:BARADQ>2.3.CO;2)
- Brack P, Mundil R, Oberli F, Meier M, Rieber H (1997) Biostratigraphic and radiometric age data question the Milankovitch characteristics of the Latemar cycles (Southern Alps, Italy). Reply: *Geology* 25(5): 471-472.
- Brack P, Rieber H, Nicora A, Mundil R (2005) The Global boundary Stratotype Section and Point (GSSP) of the Ladinian Stage (Middle Triassic) at Bagolino (Southern Alps, Northern Italy) and its implications for the Triassic time scale. *Episodes* 28 (4): 233-244.
- Brady JB, McCallister RH (1983) Diffusion data for clinopyroxenes from homogenization and self-diffusion experiments. *Am Min* 68: 95-105
- Burkhard DJM (1991) Temperature and redox path of biotite-bearing intrusives: a method of estimation applied to S- and I-type granites from Australia. *Earth Planet Sci Lett* 104: 89-98. [https://doi.org/10.1016/0012-821X\(91\)90240-I](https://doi.org/10.1016/0012-821X(91)90240-I)
- Burnham DJM, Holloway JR, Davis NF (1969) Thermodynamic properties of water to 1000°C and 10,000 bars. *Geol Soc Am Spec Pap* 132: 96.
- Casetta F, Coltorti M, Marrocchino E (2017) Petrological evolution of the Middle Triassic Predazzo Intrusive Complex, Italian Alps. *Int Geol Rev* 60(8): 977-997. <https://doi.org/10.1080/00206814.2017.1363676>
- Cassinis G, Cortesogno L, Gaggero L, Perotti CR, Buzzi L (2008) Permian to Triassic geodynamic and magmatic evolution of the Brescian Prealps (eastern Lombardy, Italy). *B Soc Geol Ital* 127(3): 501-518.

- Castellarin A, Lucchini F, Rossi PL, Sartori L, Simboli G, Sommavilla E (1982) Note geologiche sulle intrusioni di Predazzo e dei M. Monzoni. Guida alla geologia del Sudalpino centro-orientale: Guide geologiche regionali SGI: 211-219.
- Castellarin A, Lucchini F, Rossi PL, Simboli G, Bosellini A, Sommavilla E (1980) Middle Triassic magmatism in Southern Alps II: A geodynamic model. Riv Ital Paleontol S 85(3-4): 1111-1124.
- Chappell BW, White AJR (2001) Two contrasting granite types: 25 years later. Aust J Earth Sci 48(4): 489-499. 10.1046/j.1440-0952.2001.00882.x
- Cherniak DJ, Liang Y (2012) Ti diffusion in natural pyroxene. Geochim Cosmochim Acta 98: 31-47. <https://doi.org/10.1016/j.gca.2012.09.021>
- Coltorti M, Siena F, Visonà D (1996) Aspetti petrologici del magmatismo Triassico dell'area di Predazzo. 78° Riunione estiva Soc. Geol. It: Geologia delle Dolomiti. San Cassiano (1996), Conference Abstract.
- Dallai L, Cioni R, Boschi C, D'Oriano C (2011) Carbonate-derived CO<sub>2</sub> purging magma at depth: influence on the eruptive activity of Somma-Vesuvius, Italy. Earth Planet Sci Lett 310(1): 84-95. <https://doi.org/10.1016/j.epsl.2011.07.013>
- Dal Piaz G, Bistacchi A, Gianotti F et al. (2015) Carta Geologica d'Italia-Foglio 070 Monte Cervino. Carta Geologica d'Italia, 1:50.000 scale: 70.
- De Vecchi G, De Zanche V, Sedeà R (1974) Osservazioni preliminari sulle manifestazioni magmatiche triassiche nelle Prealpi Vicentine (area di Recoaro-Schio-Posina). B Soc Geol Ital 93(2): 397-409.
- Della Lucia A (1997) Aspetti vulcanologici e petrologici del complesso vulcano-plutonico Triassico di Cima Pape (Pale di San Lucano, BL). Unpublished master thesis, University of Ferrara.

- Dimanov A, Jaoul O, Sautter V. (1996) Calcium self-diffusion in natural diopside single crystals. *Geochim Cosmochim Acta* 60(21): 4095-4106. [https://doi.org/10.1016/S0016-7037\(96\)00250-5](https://doi.org/10.1016/S0016-7037(96)00250-5)
- Di Matteo V, Carroll MR, Behrens H, Vetere F, Brooker RA (2004) Water solubility in trachytic melts. *Chem Geol* 213(1-3): 187-196. <https://doi.org/10.1016/j.chemgeo.2004.08.042>
- Doglioni C (1987) Tectonics of the Dolomites (Southern Alps, Northern Italy). *J Struct Geol* 9: 181-193. [https://doi.org/10.1016/0191-8141\(87\)90024-1](https://doi.org/10.1016/0191-8141(87)90024-1)
- Doglioni C (2007) Tectonics of the Dolomites. *Bull Angew Geol* 12(2): 11-15.
- Dymek FR (1983) Titanium, aluminium and interlayer cation substitution in biotite from high-grade gneisses, West Greenland. *Am Mineral* 68: 880-899.
- Eppelbaum L, Kutasov I, Pilchin A (2014) Thermal properties of rocks and density of fluids. In: *Applied geothermics*. Springer Berlin Heidelberg, pp. 99-149.
- Ferry JM, Wing BA, Penniston-Dorland SC, Rumble D (2002) The direction of fluid flow during contact metamorphism of siliceous carbonate rocks: new data for the Monzoni and Predazzo aureoles, northern Italy, and a global review. *Contrib Mineral Petrol* 142(6): 679-699. <https://doi.org/10.1007/s00410-001-0316-7>
- Gallien F, Abart R, Wyhlidal S (2007) Contact metamorphism and selective metasomatism of the layered Bellerophon Formation in the eastern Monzoni contact aureole, northern Italy. *Mineral Petrol* 91(1): 25-53. <https://doi.org/10.1007/s00710-007-0184-6>
- Gasparotto G, Simboli G (1991) Mineralogia, petrografia e schemi evolutivi delle magmatiti triassiche del complesso di Cima Pape (Dolomiti Orientali). *Mineral Petrogr Acta* 34: 205-234.
- Giacomoni PP, Ferlito C, Coltorti M, Bonadiman C, Lanzafame G (2014) Plagioclase as archive of magma ascent dynamics on “open conduit” volcanoes: The 2001–2006 eruptive period at Mt. Etna. *Earth Sci Rev* 138: 371-393. <https://doi.org/10.1016/j.earscirev.2014.06.009>

- Gianolla P (1992) Evoluzione mediotriassica del vulcanismo di Rio Freddo (Api Giulie, Italia). Mem Sci Geol 44: 193-209.
- Gianolla P, Avanzini M, Breda A et al. (2010) Dolomites, 7th International Triassic Field Workshop, Field trip to the World Heritage Site of the Tethyan Triassic. September 5-10 2010, Dolomites, Southern Alps, Italy. With the adesion of Fondazione Dolomiti-Dolomiten-Dolomites-Dolomitis Unesco.
- Grove TL, Baker MB, Kinzler RJ (1984) Coupled CaAl-NaSi diffusion in plagioclase feldspar: Experiments and applications to cooling rate speedometry. Geochim Cosmochim Acta 48: 2113-2121.
- Gualda GAR, Ghiorso MS, Lemons RV, Carley TL (2012) Rhyolite-MELTS: a Modified Calibration of MELTS Optimized for Silica-rich, Fluid-bearing Magmatic Systems. J Petrol 53: 875-890. <https://doi.org/10.1093/petrology/egr080>
- Henry DJ, Guidotti CV, Thomson JA (2005) The Ti-saturation surface for low-to-medium pressure metapelitic biotites: Implications for geothermometry and Ti-substitution mechanisms. Am Mineral 90(2-3): 316-328. <https://doi.org/10.2138/am.2005.1498>
- Holland T, Blundy J (1994) Non-ideal interactions in calcic amphiboles and their bearing on amphibole-plagioclase thermometry. Contrib Mineral Petrol 116(4): 433-447. <https://doi.org/10.1007/BF00310910>
- Huebner JS, Sato M (1970) The oxygen fugacity-temperature relationships of manganese oxide and nickel oxide buffers. Am Mineral 55: 934-952.
- Ickert RB (2013) Algorithms for estimating uncertainties in initial radiogenic isotope ratios and model ages. Chem Geol 340: 131-138. <https://doi.org/10.1016/j.chemgeo.2013.01.001>
- Kohn SC (2000) The dissolution mechanisms of water in silicate melts; a synthesis of recent data. Mineral Mag 64(3): 389-408. <https://doi.org/10.1180/002646100549463>
- Kress VC, Carmichael IS (1988) Stoichiometry of the iron oxidation reactions in silicate melts. Am Mineral 73: 1267-1274.

- Kress VC, Carmichael IS (1991) The compressibility of silicate liquids containing  $\text{Fe}_2\text{O}_3$  and the effect of composition, temperature, oxygen fugacity and pressure on their redox states. *Contrib Mineral Petrol* 108(1-2): 82-92. 10.1007/BF00307328
- Lange RA, Frey HM, Hektor J (2009) A thermodynamic model for the plagioclase-liquid hygrometer/thermometer. *Am Mineral* 94(4): 494-506. <https://doi.org/10.2138/am.2009.3011>
- Laurenzi MA, Visonà D, (1996)  $^{40}\text{Ar}/^{39}\text{Ar}$  Chronology of Predazzo magmatic complex (Southern Alps, Italy). 78° Riunione estiva Soc. Geol. It: Geologia delle Dolomiti. San Cassiano (1996): 16-18.
- Le Maitre RW (2002) A classification of igneous rocks and glossary of terms. Cambridge University Press.
- Leake BE, Arps CES, Birch WD (1997) Nomenclature of amphiboles: Report of the Subcommittee on Amphiboles of the International Mineralogical Association, Commission on New Minerals and Mineral Names. *Am Mineral* 82: 1019-1037. <https://doi.org/10.1180/minmag.1997.061.405.13>
- Lippolt H, Pidgeon R (1974) Isotopic mineral ages of a diorite from the Eisenkappel intrusion, Austria. *Zeitschrift für Naturforschung* 29a.
- Liu Y, Zhang Y, Behrens H (2005) Solubility of  $\text{H}_2\text{O}$  in rhyolitic melts at low pressures and a new empirical model for mixed  $\text{H}_2\text{O}$ - $\text{CO}_2$  solubility in rhyolitic melts. *J Volcanol Geotherm Res* 143(1-3): 219-235. <https://doi.org/10.1016/j.jvolgeores.2004.09.019>
- Lucchini F, Rossi PL, Simboli G (1982) Il magmatismo triassico dell'area di Predazzo (Alpi Meridionali, Italia). In Castellarin A, Vai GB (eds) Guida alla Geologia del Sudalpino centro-orientale: Guide Geologiche Regionali Società Geologica Italiana: pp. 221-230.
- Lugmair GW, Marti K (1978) Lunar initial  $^{143}\text{Nd}/^{144}\text{Nd}$ : differential evolution of Lunar crust and mantle. *Earth Planet Sci Lett* 39: 349-357. [https://doi.org/10.1016/0012-821X\(78\)90021-3](https://doi.org/10.1016/0012-821X(78)90021-3)

- Manzotti P, Ballèvre M, Dal Piaz GV (2017) Continental gabbros in the Dent Blanche Tectonic System (Western Alps): from the pre-Alpine crustal structure of the Adriatic palaeo-margin to the geometry of an alleged subduction interface. *J Geol Soc* 174(3): 541-556.
- Marocchi M, Morelli C, Mair V, Klötzli U, Bargossi GM (2008) Evolution of large silicic magma systems: new U–Pb zircon data on the NW Permian Athesian Volcanic Group (Southern Alps, Italy). *J Geol* 116: 480-498.
- Marrocchino E, Coltorti M, Visonà D, Thirwall, MF (2002) Petrology of Predazzo magmatic complex (Trento, Italy). *Geochim Cosmochim Acta* 66(15°): A486-A486.
- Martin EE, Macdougall JD (1995) Sr and Nd isotopes at the permian/triassic boundary: A record of climate change. *Chem Geol* 125(1-2): 73-99. [https://doi.org/10.1016/0009-2541\(95\)00081-V](https://doi.org/10.1016/0009-2541(95)00081-V)
- Marzocchi C (1987) Petrologia e metallogenesi del complesso eruttivo di Predazzo (TN): con particolare riguardo al settore meridionale. University of Ferrara, unpublished master thesis.
- Masotta M, Mollo S, Freda C, Gaeta M, Moore G (2013) Clinopyroxene–liquid thermometers and barometers specific to alkaline differentiated magmas. *Contrib Mineral Petrol* 166(6): 1545-1561. <https://doi.org/10.1007/s00410-013-0927-9>
- Menegazzo Vitturi L, Visonà D, Zantedeschi C (1995) Amphibole composition in rocks from Predazzo volcano-plutonic complex (Southern Alps, Italy). *Mem Sci Geol* 47: 87-94.
- Mietto P, Manfrin S, Preto N et al. (2012) The Global Boundary Stratotype Section and Point (GSSP) of the Carnian Stage (Late Triassic) at Prati di Stuores/ Stuores Wiesen Section (Southern Alps, NE Italy). *Episodes* 35(3): 414-430.
- Mollo S, Masotta M, Forni F, Bachmann O, De Astis G, Moore G, Scarlato P (2015) A K-feldspar–liquid hygrometer specific to alkaline differentiated magmas. *Chem Geol* 392: 1-8. <https://doi.org/10.1016/j.chemgeo.2014.11.010>

- Mollo S, Putirka K, Iezzi G, Del Gaudio P, Scarlato P (2011) Plagioclase–melt (dis) equilibrium due to cooling dynamics: implications for thermometry, barometry and hygrometry. *Lithos* 125(1): 221-235. <https://doi.org/10.1016/j.lithos.2011.02.008>
- Monjoie P, Bussy F, Schaltegger U, Mulch A, Lapierre H, Pfeifer HR (2007) Contrasting magma types and timing of intrusion in the Permian layered mafic complex of Mont Collon (Western Alps, Valais, Switzerland): evidence from U/Pb zircon and  $^{40}\text{Ar}/^{39}\text{Ar}$  amphibole dating. *Swiss J Geosci* 100(1): 125-135. <https://doi.org/10.1007/s00015-007-1210-8>
- Morimoto N (1988) Nomenclature of pyroxenes. *Mineral Petrol* 39(1): 55-76. <https://doi.org/10.1007/BF01226262>
- Morse SA, Brady JB (2017) Thermal History of the Upper Zone of the Kiglapait Intrusion. *J Petrol* 58(7): 1319-1332. [10.1093/petrology/egx055](https://doi.org/10.1093/petrology/egx055)
- Müller T, Dohmen R, Becker HW, Ter Heege JH, Chakraborty S (2013) Fe-Mg interdiffusion rates in clinopyroxene: experimental data and implications for Fe–Mg exchange geothermometers. *Contrib Mineral Petrol* 166(6): 1563-1576. [10.1007/s00410-013-0941-y](https://doi.org/10.1007/s00410-013-0941-y)
- Mundil R, Brack P, Laurenzi MA (1996) High resolution U/Pb single zircon age determinations: new constraints on the timing of Middle Triassic magmatism in the Southern Alps. 78° Riunione estiva Soc. Geol. It: Geologia delle Dolomiti. San Cassiano (1996), Conference Abstract.
- Myers JT, Eugster HP (1983) The system Fe-Si-O: Oxygen buffer calibrations to 1500 K. *Contrib Mineral Petrol* 82(1): 75-90. <https://doi.org/10.1007/BF00371177>
- Namur O, Humphreys MCS (2018) Trace Element Constraints on the Differentiation and Crystal Mush Solidification in the Skaergaard Intrusion, Greenland. *J Petrol* 1-31. doi: [10.1093/petrology/egy032](https://doi.org/10.1093/petrology/egy032)
- Nielsen TFD (2004) The Shape and Volume of the Skaergaard Intrusion, Greenland: Implications for Mass Balance and Bulk Composition. *J Petrol* 45(3): 507-530. [10.1093/petrology/egg092](https://doi.org/10.1093/petrology/egg092)



- Petersen JS, Morten L, Simboli G, Lucchini F (1980) REE abundances in the Predazzo-Monzoni intrusive complex, Dolomites, North Italy. *Riv Ital Paleontol* 85: 1065-1080.
- Pin C, Sills JD (1986) Petrogenesis of layered gabbros and ultramafic rocks from Val Sesia, the Ivrea Zone, NW Italy: trace element and isotope geochemistry. *Geol Soc Spec Publ* 24: 231-249. <https://doi.org/10.1144/GSL.SP.1986.024.01.21>
- Pouchou JL, Pichoir F (1991) Quantitative analysis of homogeneous or stratified microvolumes applying the model "PAP". In *Electron probe quantitation*. Springer US, pp. 31-75. [https://doi.org/10.1007/978-1-4899-2617-3\\_4](https://doi.org/10.1007/978-1-4899-2617-3_4)
- Povoden E, Horacek M, Abart R (2002) Contact metamorphism of siliceous dolomite and impure limestones from the Werfen formation in the eastern Monzoni contact aureole. *Mineral Petrol* 76(1): 99-120. <https://doi.org/10.1007/s007100200034>
- Princivalle F, Della Giusta A, De Min A, Piccirillo EM (1999) Crystal chemistry and significance of cation ordering in Mg-Al rich spinels from high-grade hornfels (Predazzo-Monzoni, NE Italy). *Mineral Mag* 63(2): 257-257. <https://doi.org/10.1180/002646199548367>
- Putirka KD (2008) Thermometers and barometers for volcanic systems. *Rev Mineral Geochem* 69(1): 61-120. <https://doi.org/10.2138/rmg.2008.69.3>
- Putirka K, Johnson M, Kinzler R, Longhi J, Walker D (1996) Thermobarometry of mafic igneous rocks based on clinopyroxene-liquid equilibria, 0–30 kbar. *Contrib Mineral Petrol* 123(1): 92-108. <https://doi.org/10.1007/s004100050145>
- Putirka K, Mikaelian H, Ryerson F, Shaw H (2003) New clinopyroxene-liquid thermobarometers for mafic, evolved, and volatile-bearing lava compositions, with applications to lavas from Tibet and the Snake River Plain, Idaho. *Am Mineral* 88: 1542-1554. <https://doi.org/10.2138/am-2003-1017>

- Quick JE, Sinigoi S, Peressini G, Demarchi G, Wooden JL, Sbisà A (2009) Magmatic plumbing of a large Permian caldera exposed to a depth of 25 km. *Geology* 37: 603-606. <https://doi.org/10.1130/G30003A.1>
- Ridolfi F, Renzulli A (2012) Calcic amphiboles in calc-alkaline and alkaline magmas: thermobarometric and chemometric empirical equations valid up to 1,130° C and 2.2 GPa. *Contrib Mineral Petrol* 163(5): 877-895. <https://doi.org/10.1007/s00410-011-0704-6>
- Ridolfi F, Renzulli A, Puerini M (2010) Stability and chemical equilibrium of amphibole in calc-alkaline magmas: an overview, new thermobarometric formulations and application to subduction-related volcanoes. *Contrib Mineral Petrol* 160(1): 45-66. <https://doi.org/10.1007/s00410-009-0465-7>
- Rotenberg E, Davis DW, Amelin Y, Ghosh S, Bergquist BA (2012) Determination of the decay-constant of  $^{87}\text{Rb}$  by laboratory accumulation of  $^{87}\text{Sr}$ . *Geochim Cosmochim Acta* 85: 41-57. <https://doi.org/10.1016/j.gca.2012.01.016>
- Rottura A, Bargossi GM, Caggianelli A, Del Moro A, Visonà D, Tranne CA (1998) Origin and significance of the Permian high-K calc-alkaline magmatism in the central-eastern Southern Alps, Italy. *Lithos* 45: 329-348. [https://doi.org/10.1016/S0024-4937\(98\)00038-3](https://doi.org/10.1016/S0024-4937(98)00038-3)
- Rottura A, Del Moro A, Caggianelli A, Bargossi GM, Gasparotto G (1997) Petrogenesis of the Monte Croce granitoids in the context of Permian magmatism in the Southern Alps, Italy. *Eur J Mineral* 9(6): 1293-1310. [10.1127/ejm/9/6/1293](https://doi.org/10.1127/ejm/9/6/1293)
- Sarti M, Ardizzoni F (1984) Tettonica Triassica nel gruppo di Cima Pape-Pale di Sanson (Dolomiti Bellunesi). *Mem Sci Geol* 36: 353-370.
- Schaltegger U, Brack P (2007) Crustal-scale magmatic systems during intracontinental strike-slip tectonics: U, Pb and Hf isotopic constraints from Permian magmatic rocks of the Southern Alps. *Int J Earth Sci* 96(6): 1131-1151. <https://doi.org/10.1007/s00531-006-0165-8>

- Schmid SM, Bernoulli D, Fügenschuh B et al. (2008) The Alpine-Carpathian-Dinaridic orogenic system: correlation and evolution of tectonic units. *Swiss J Geosci* 101(1): 139-183. <https://doi.org/10.1007/s00015-008-1247-3>
- Silver L, Stolper E (1985) A thermodynamic model for hydrous silicate melts. *J Geol* 93(2): 161-177.
- Sinigoi S, Quick JE, Demarchi G, Klotzli U (2016) Production of hybrid granitic magma at the advancing front of basaltic underplating: Inferences from the Sesia Magmatic System (south - western Alps, Italy). *Lithos* 252-253: 109-122. <https://doi.org/10.1016/j.lithos.2016.02.018>
- Sloman LE (1989) Triassic shoshonites from the dolomites, northern Italy: Alkaline arc rocks in a strike-slip setting. *J Geophys Res: Solid Earth* 94(B4): 4655-4666. [10.1029/JB094iB04p04655](https://doi.org/10.1029/JB094iB04p04655)
- Spera FJ (1980) Thermal evolution of plutons: a parameterized approach. *Science* 207: 299-301. [10.1126/science.207.4428.299](https://doi.org/10.1126/science.207.4428.299)
- Spera FJ (2000) Physical properties of magmas. In Sigurdsson H (ed.) *Encyclopedia of Volcanoes*. New York: Academic Press, pp. 171-190.
- Spera FJ, Bohron WA (2001) Energy-constrained open-system magmatic processes I: General model and energy-constrained assimilation and fractional crystallization (EC-AFC) formulation. *J Petrol* 42(5): 999-1018. <https://doi.org/10.1093/petrology/42.5.999>
- Stahle V, Frenzel G, Hess JC, Saupé F, Schmidt ST, Schneider W (2001) Permian metabasalt and Triassic alkaline dykes in the northern Ivrea zone: clues to the post-Variscan geodynamic evolution of the Southern Alps. *Schweiz Mineral Petrogr Mitt* 81(1): 1-21.
- Stampfli GM, Borel GD (2002) A plate tectonic model for the Paleozoic and Mesozoic constrained by dynamic plate boundaries and restored synthetic oceanic isochrones. *Earth Planet Sci Lett* 196(1): 17-33. [https://doi.org/10.1016/S0012-821X\(01\)00588-X](https://doi.org/10.1016/S0012-821X(01)00588-X)
- Stampfli GM, Borel GD (2004) The TRANSMED transects in space and time: constraints on the paleotectonic evolution of the Mediterranean domain. In *The TRANSMED Atlas: The*

- Mediterranean region from crust to mantle, pp. 53-80. [https://doi.org/10.1007/978-3-642-18919-7\\_3](https://doi.org/10.1007/978-3-642-18919-7_3)
- Stolper E (1982) The speciation of water in silicate melts. *Geochim Cosmochim Acta* 46(12): 2609-2620. [https://doi.org/10.1016/0016-7037\(82\)90381-7](https://doi.org/10.1016/0016-7037(82)90381-7)
- Trill RJ, Lachance GR (1966) A practical solution to the matrix problem in X-ray analysis. II. Application to a multicomponent alloy system. *Can Spectrosc* 11(3): 63-71.
- Vardabasso S (1929) Rapporti tra attività magmatica e vicende tettoniche nella provincia petrografica di Predazzo: *Studi Trentini di Scienze Naturali* 11.
- Vardabasso S (1930) Carta geologica del territorio eruttivo di Predazzo e Monzoni. Ufficio Idrografico del Magistrato alle Acque di Venezia, 1:25000 scale.
- Visonà D (1997) The Predazzo multipulse intrusive body (Western Dolomites, Italy). Field and mineralogical studies. *Mem Sci Geol* 49: 117-125.
- Visonà D, Zanferrari A (2000) Some constraints on geochemical features in the Triassic mantle of the easternmost Austroalpine–Southalpine domain: evidence from the Karawanken pluton (Carinthia, Austria). *Int J Earth Sci* 89(1): 40-51. <https://doi.org/10.1007/s005310050316>
- Voshage H, Hofmann AW, Mazzucchelli M, Rivalenti G, Sinigoi S, Raczek I, Demarchi G (1990) Isotopic evidence from the Ivrea Zone for a hybrid lower crust formed by magmatic underplating. *Nature* 347(6295): 731-736. [10.1038/347731a0](https://doi.org/10.1038/347731a0)
- Waldbaum DR, Thompson JB (1969) Mixing properties of sanidine crystalline solutions: IV. Phase diagrams from equations of state. *Am Mineral* 54: 1274-1298.
- Willcock MAW, Bargossi GM, Weinberg RF, Gasparotto G, Cas RAF, Giordano G, Marocchi M (2015) A complex magma reservoir system for a large volume intra-to extra-caldera ignimbrite: Mineralogical and chemical architecture of the VEI8, Permian Ora ignimbrite (Italy). *J Volcanol Geotherm Res* 306: 17-40. <https://doi.org/10.1016/j.jvolgeores.2015.09.015>

Zanetti A, Mazzucchelli M, Sinigoi S, Giovanardi T, Peressini G, Fanning M (2013) SHRIMP U–Pb Zircon Triassic intrusion age of the Finero mafic complex (Ivrea–Verbano zone, Western Alps) and its geodynamic implications. *J Petrol* 54(11): 2235-2265. <https://doi.org/10.1093/petrology/egt046>

Ziegler PA, Stampfli GM (2001) Late Palaeozoic-Early Mesozoic plate boundary reorganization: collapse of the Variscan orogen and opening of Neotethys. *Nat Brescia* 25: 17-34.

Zindler A, Hart SR (1986) Chemical geodynamics. *Annu Rev Earth Planet Sci* 14: 493-571.

## Figure Captions

### Fig. 1 (colour online)

Simplified geological map of the Predazzo Intrusive Complex (PIC). On the left bottom corner, the study area location with respect to the NE sector of Italy is shown

### Fig. 2 (colour online)

(a) Total Alkali vs. Silica and (b) K<sub>2</sub>O vs. Na<sub>2</sub>O diagrams for Predazzo Intrusive Complex rocks (Le Maitre 2002). SS = Shoshonitic Silica Saturated; SU = Shoshonitic Silica Undersaturated; GU = Granitic Unit

### Fig. 3 (colour online)

Textural sketches of Predazzo Intrusive Complex rocks and corresponding photomicrographs showing the crystallization relationships between biotite and amphibole in the intercumulus assemblage of (a, b) Shoshonitic Silica Saturated monzodiorites and (c, d) Shoshonitic Silica Undersaturated monzogabbros. Each labelled mineral phase in the right photomicrographs is contraddistinct by a different colour in the left sketches. Amph = amphibole; Ap = apatite; Bt

= biotite; Cpx = clinopyroxene; K-Feld = K-feldspar; Ox = Fe-Ti oxide; Plag = plagioclase; Qz = quartz; Ser = sericite

#### Fig. 4 (colour online)

Mg# vs.  $Kd_{Fe-Mg}^{Cpx-Liq}$  of clinopyroxene from the (a) Shoshonitic Silica Saturated and (b) Shoshonitic Silica Undersaturated rocks. The white symbols represent the disequilibrium between crystals and their host rock composition, whose whole rock Mg# (wr Mg#) is also reported. The filled symbols represent the attained equilibrium conditions after the calculation of melt composition in equilibrium. “Liq” indicates both the composition of the crystals host rocks (white symbols, prior to equilibration process) and that of the calculated “melt” (filled symbols, after equilibration process). The length of the dashed arrows is directly function of the amount of disequilibrium between the crystals and their host rock. The equilibrium range of  $Kd_{Fe-Mg}^{Cpx-Liq} = 0.24-0.30$  (black lines) is from Putirka et al. (2003)

#### Fig. 5 (colour online)

Anorthite ( $X_{An}$ ) vs.  $Kd_{An-Ab}^{Plag-Liq}$  of plagioclase from the (a) Shoshonitic Silica Saturated and (b) Shoshonitic Silica Undersaturated rocks. As in Fig. 4, white symbols represent the disequilibrium between crystals and their host rock composition (whose Mg# is reported as “wr Mg#”), whereas filled symbols represent the attained equilibrium conditions after the equilibration processes. “Liq” indicates both the composition of the crystals host rocks (white symbols, prior to equilibration process) and that of the calculated “melt” (filled symbols, after equilibration process). The length of the dashed arrows is directly function of the amount of disequilibrium between the crystals and their host rock. The chosen equilibrium range of  $Kd_{An-Ab}^{Plag-Liq} = 0.27 \pm 0.11$  (black lines) is from Putirka (2008)

#### Fig. 6 (colour online)

Flow chart representing the rationality of our models for clinopyroxene (Cpx) and plagioclase (Plag) thermobarometry and hygrometry, from the starting mineral compositions (black squares) to the final  $P$ - $T$ - $H_2O$  triplets. (a) Model for clinopyroxenes in the less differentiated Shoshonitic Silica Saturated rocks; (b) Model for clinopyroxenes in the evolved Shoshonitic Silica Saturated and in the Shoshonitic Silica Undersaturated rocks; (c) Model for plagioclases in both Shoshonitic Silica Saturated and Shoshonitic Silica Undersaturated rocks

**Fig. 7 (colour online)**

(a) Temperature vs. pressure and (b) temperature vs. water content diagrams for Predazzo Intrusive Complex rocks. SS = Shoshonitic Silica Saturated; SU = Shoshonitic Silica Undersaturated. The reported values were obtained from the several thermobarometric approaches explained in text. Cpx = clinopyroxene; Amph = amphibole; Plag = plagioclase; K-Feld = K-feldspar. Dashed interval in (a) represent the best-fit pressure range between the various estimates, whereas the shaded field represents the temperature interval resulted from biotite thermometry. Depth was calculated by considering a  $\Delta P/\Delta z$  of 0.29 kbar/km

**Fig. 8 (colour online)**

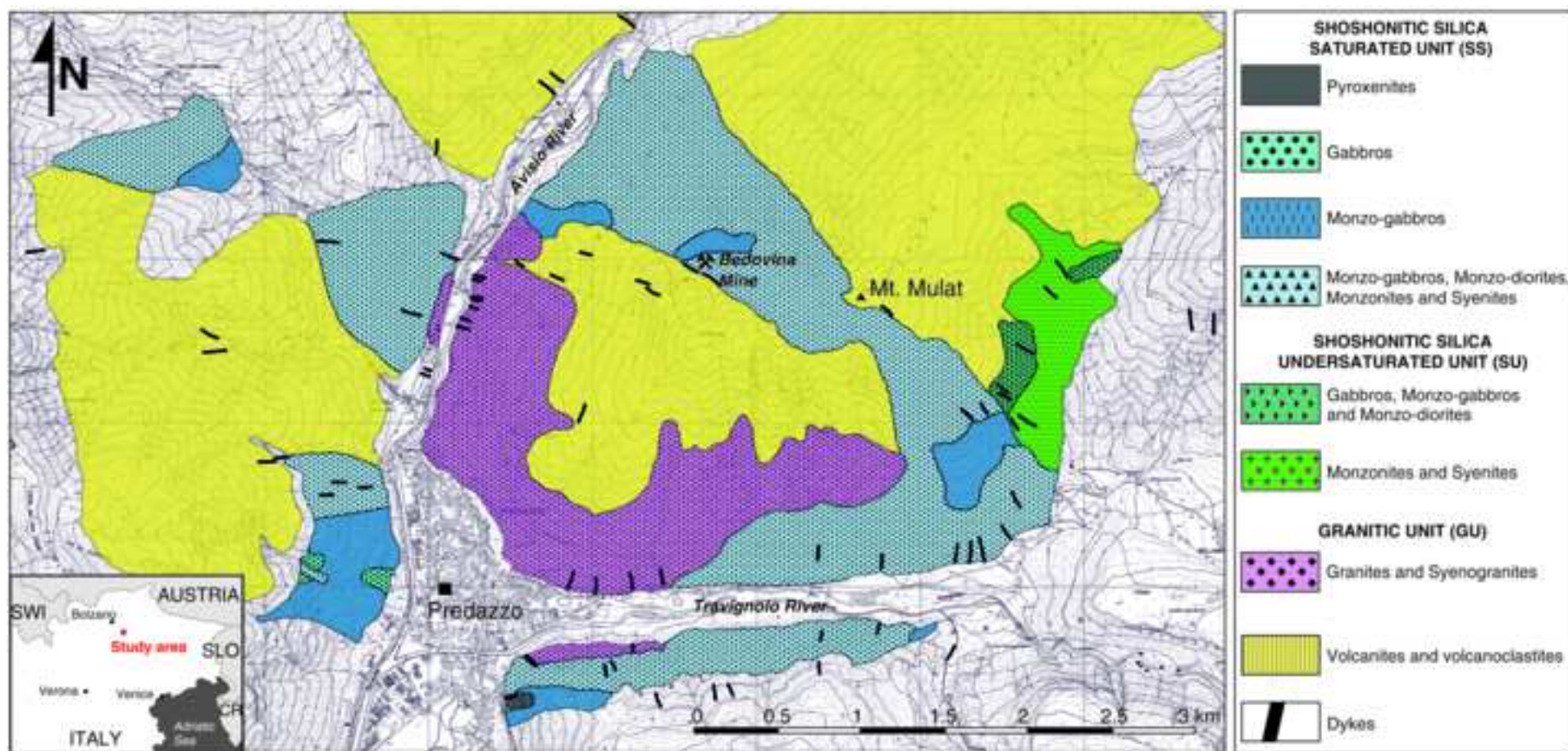
Temperature vs. oxygen fugacity (expressed in  $\log fO_2$ ) diagram for Predazzo Intrusive Complex rocks. SS = Shoshonitic Silica Saturated; SU = Shoshonitic Silica Undersaturated. FMQ and NNO buffers are from Myers and Eugster (1983) and Huebner and Sato (1970), respectively. Up on the right, insert with the same oxygen fugacity data expressed in terms of  $\Delta FMQ$  to facilitate the comparison between the various magmatic suites

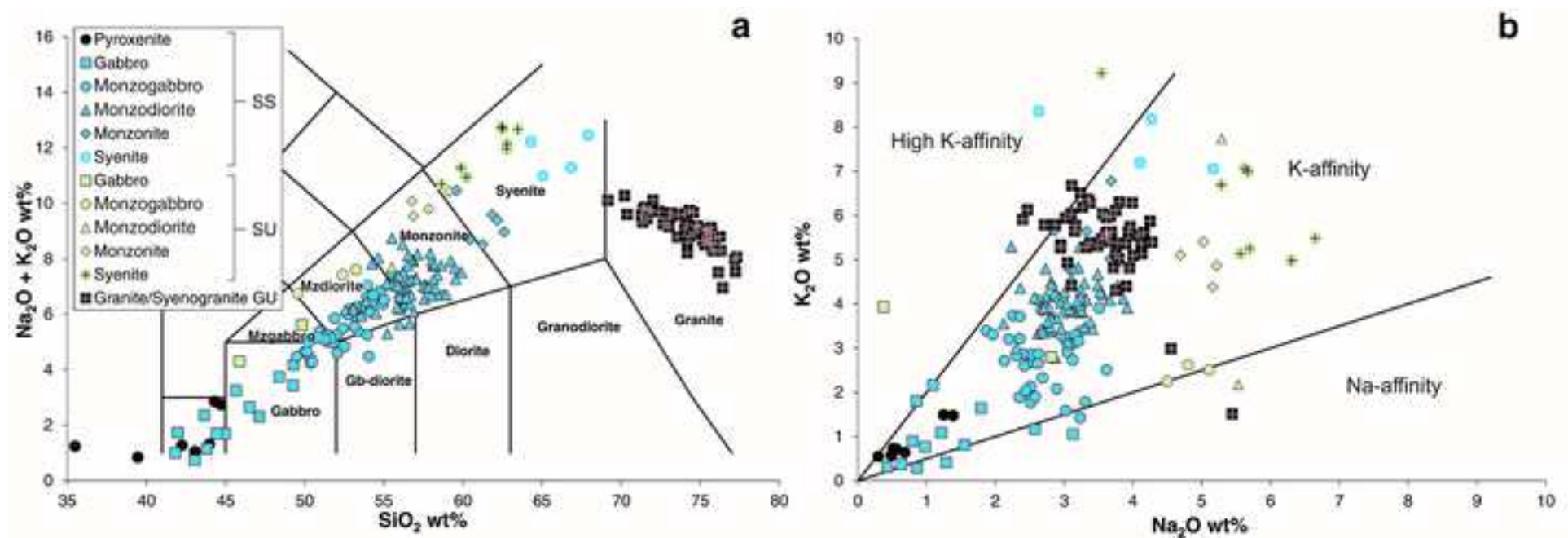
**Fig. 9 (Colour online)**

Diagrams showing the  $^{87}Sr/^{86}Sr$  vs.  $^{143}Nd/^{144}Nd$  isotopic ratios of Predazzo Intrusive Complex rocks compared to those of Permo-Triassic crustal components (all values corrected to 234 Ma).

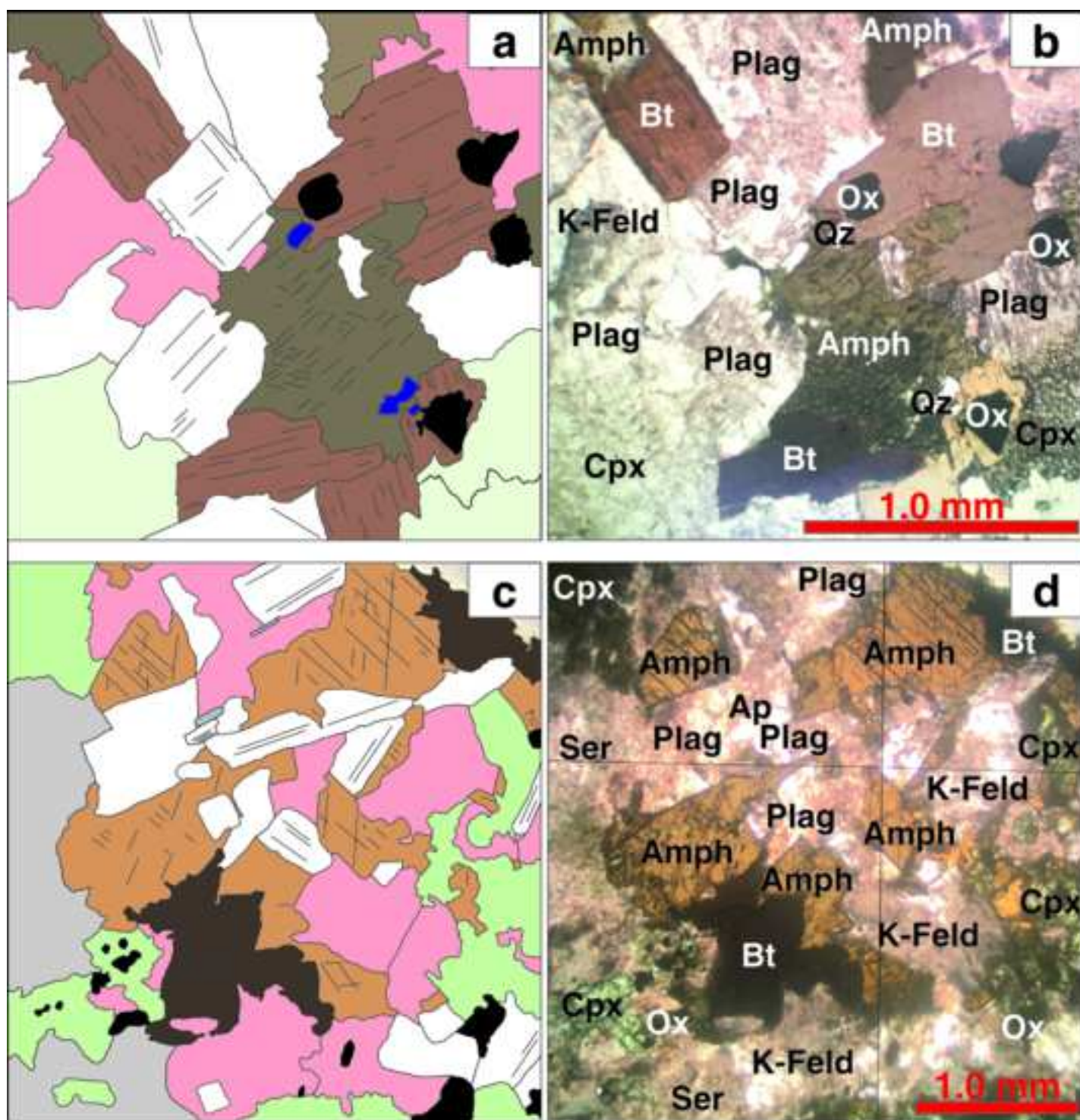
SS = Shoshonitic Silica Saturated; SU = Shoshonitic Silica Undersaturated. Triassic carbonates field from Martin and Macdougall (1995) and Blendiger et al. (2015); Permian intrusives (Mt. Croce and Serie dei Laghi) field from Rottura et al. (1997) and Sinigoi et al. (2016, and references therein); Athesina Volcanic District (AVD) Permian ignimbrites field from Barth et al. (1993); Val Sesia Permian mafic rocks field from Voshage et al. (1990), Pin and Sills (1996) and Sinigoi et al. (2016); Kinzigite formation field from Voshage et al. (1990). (a) Sr-Nd isotopic ratios of Predazzo Intrusive Complex rocks plotted against those of the Permo-Triassic crustal components, the enriched 1 (EMI), high- $\mu$  (HIMU, where  $\mu = {}^{238}\text{U}/{}^{204}\text{Pb}$ ) and depleted (DMM) mantle end-members (Zindler and Hart 1986); the insert corresponds to the area reported in diagram (b). (b) EC-AFC trends (Bohrson and Spera 2001; Spera and Bohrson 2001) for the Shoshonitic Silica Saturated suite by considering variable crustal assimilants. 1 = assimilation of Triassic carbonates; 2 = assimilation of AVD ignimbrites; 3 = assimilation of Mt. Croce granodiorites; 4 = assimilation of Serie dei Laghi granites; 5 = assimilation of Kinzigite formation amphibolites

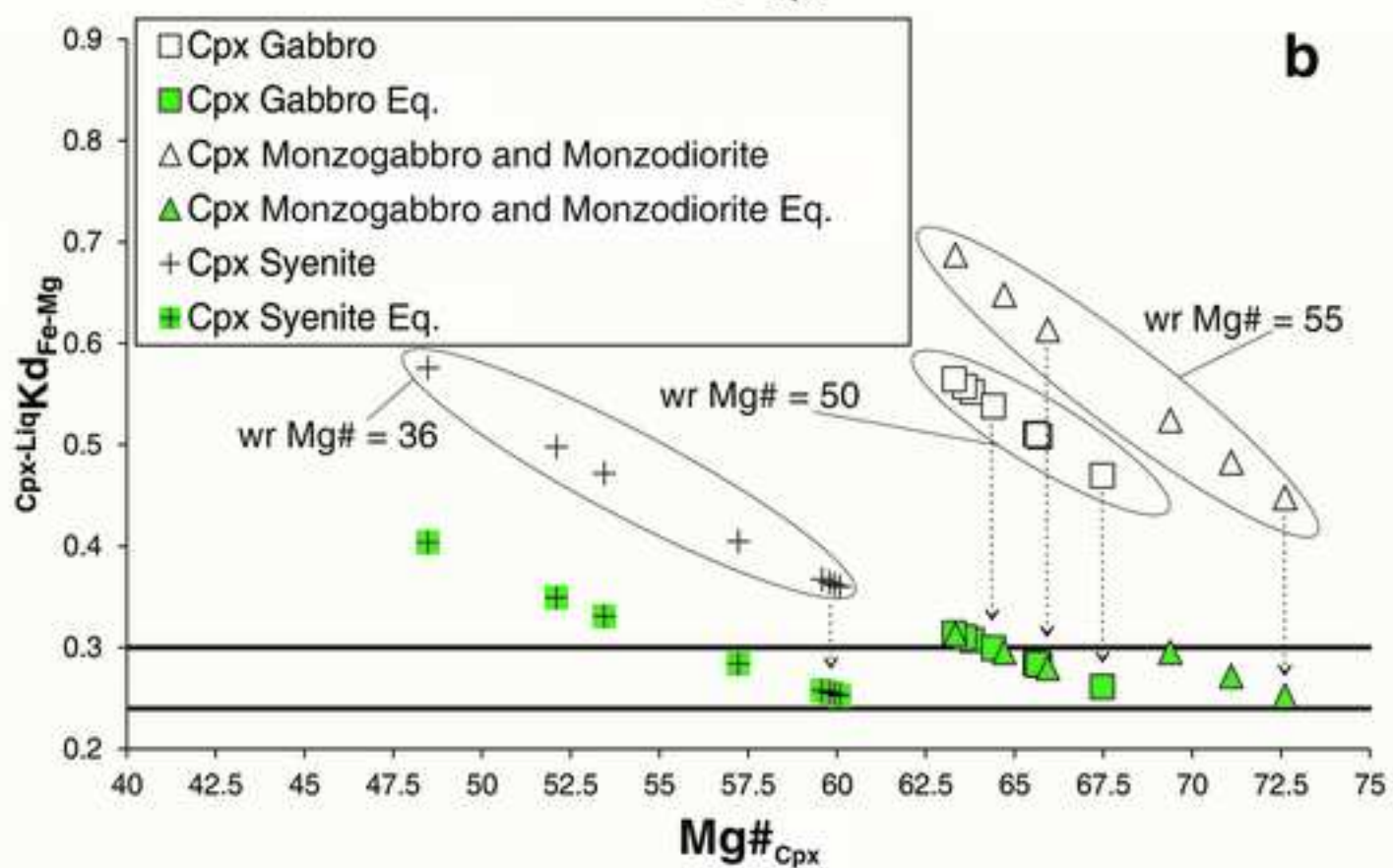
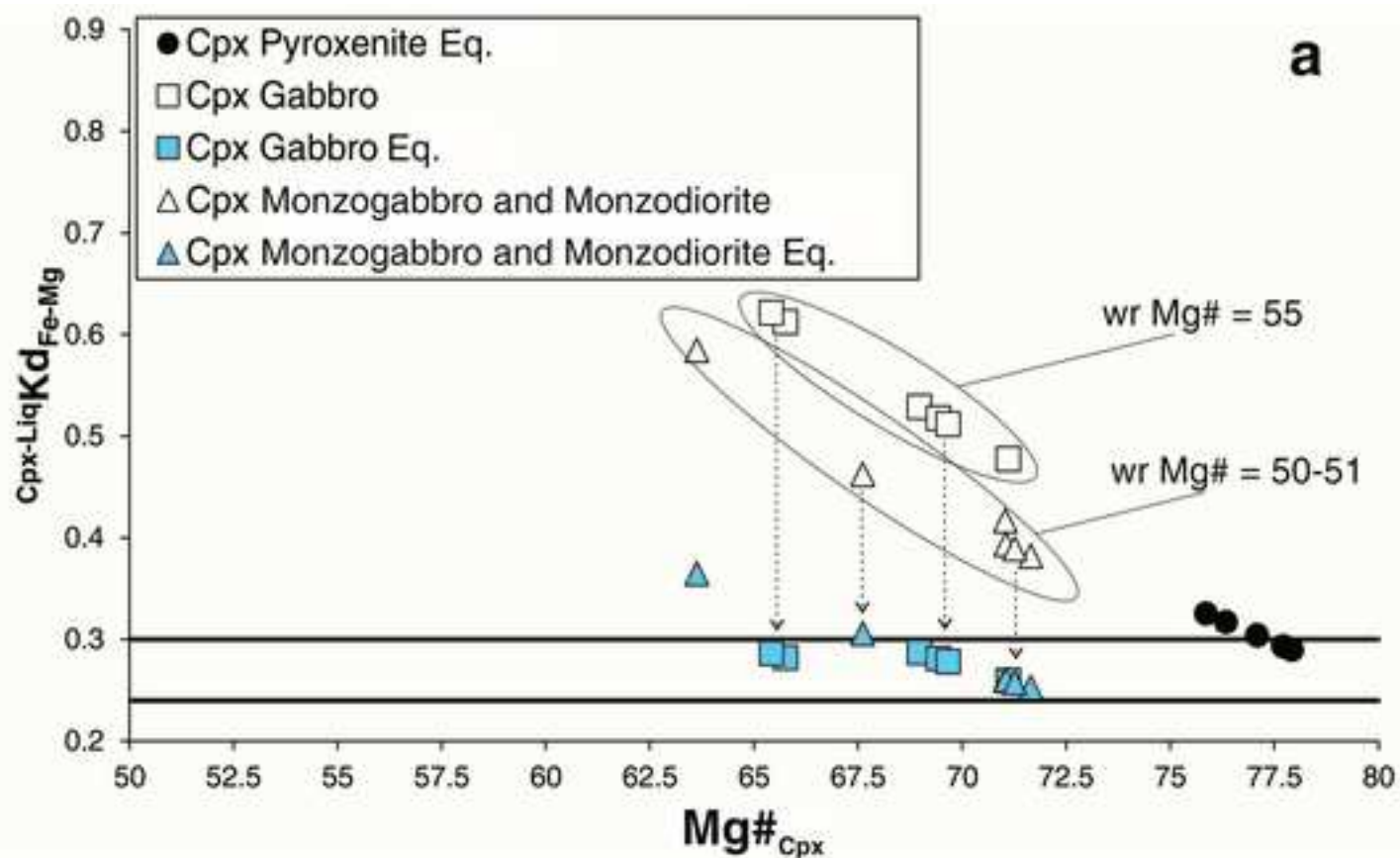




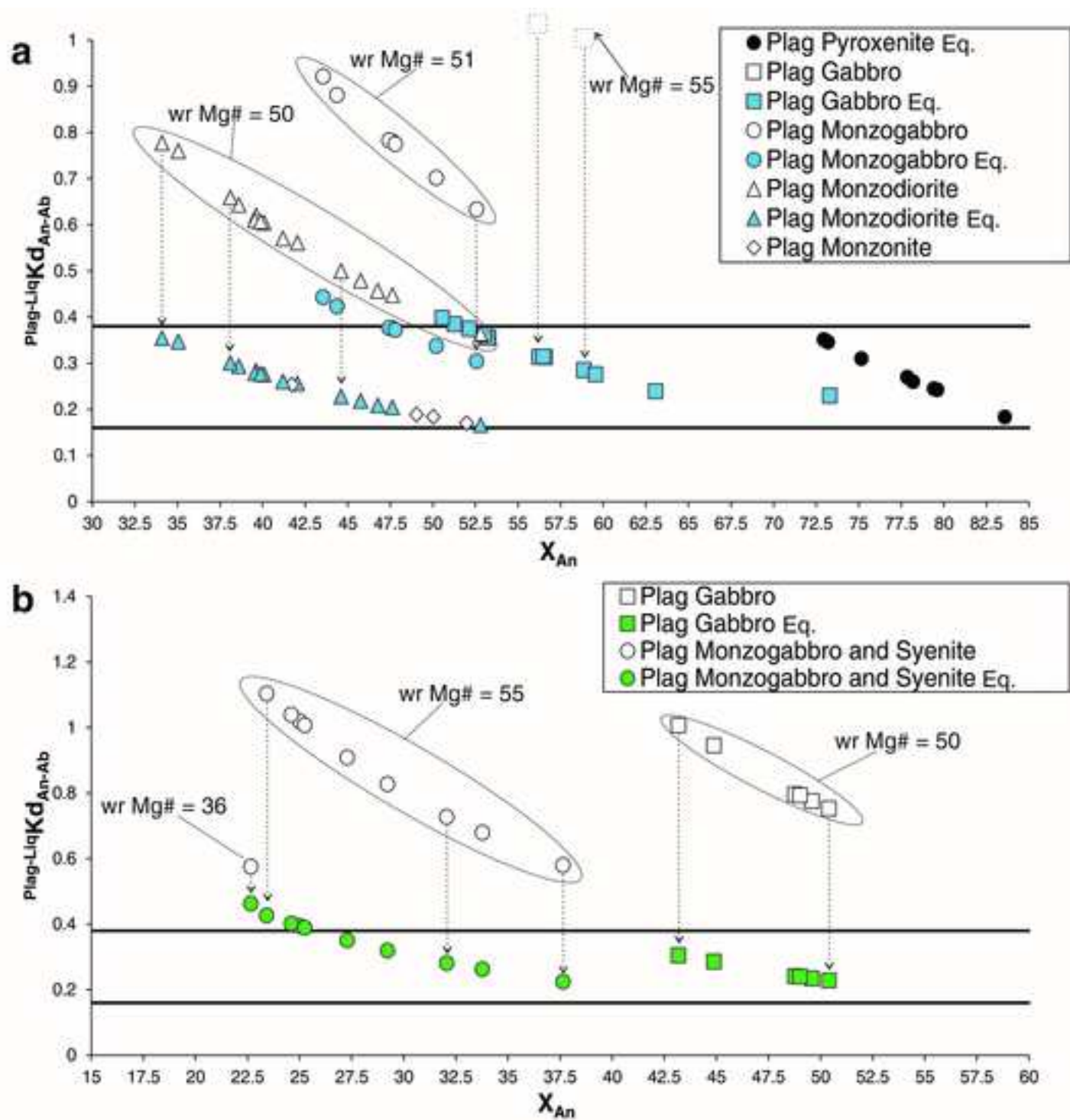


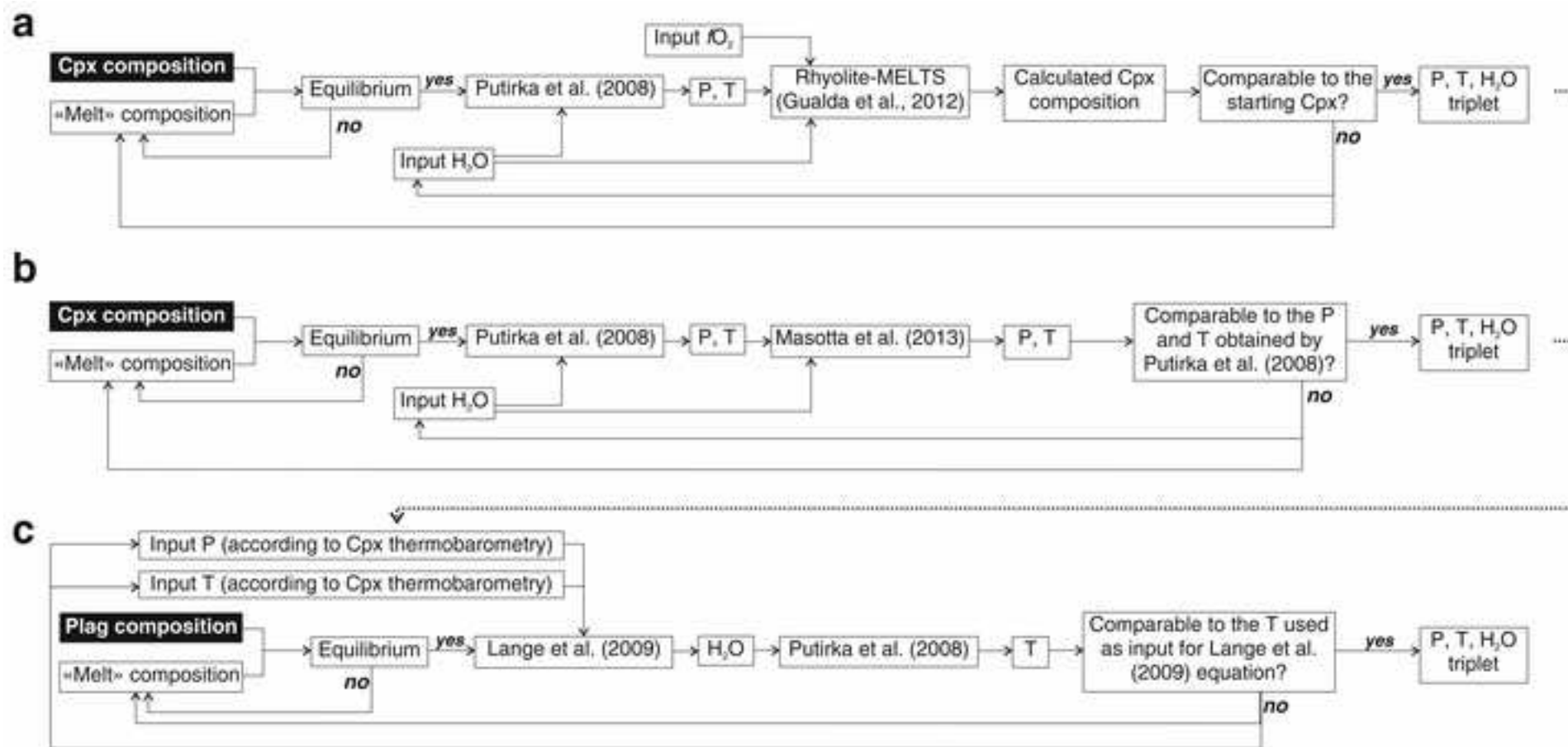


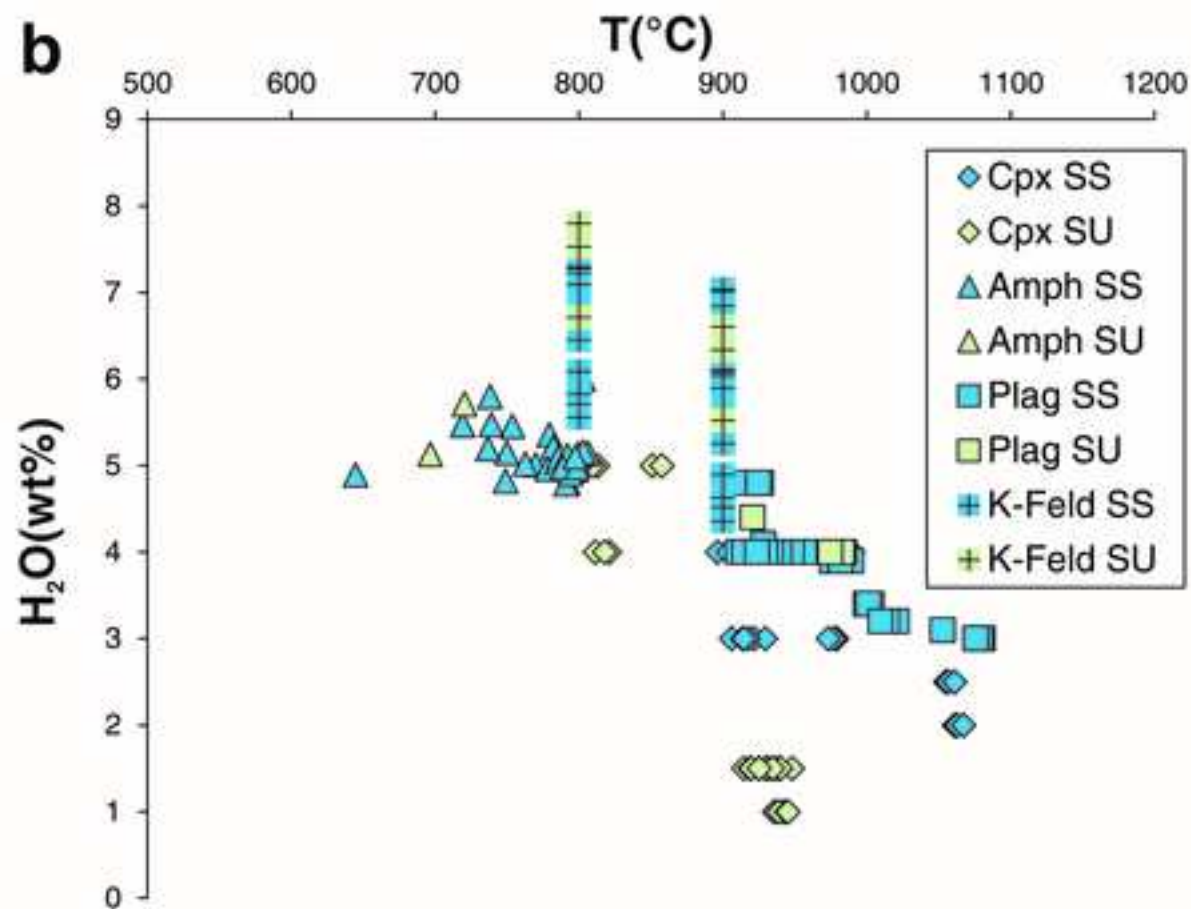
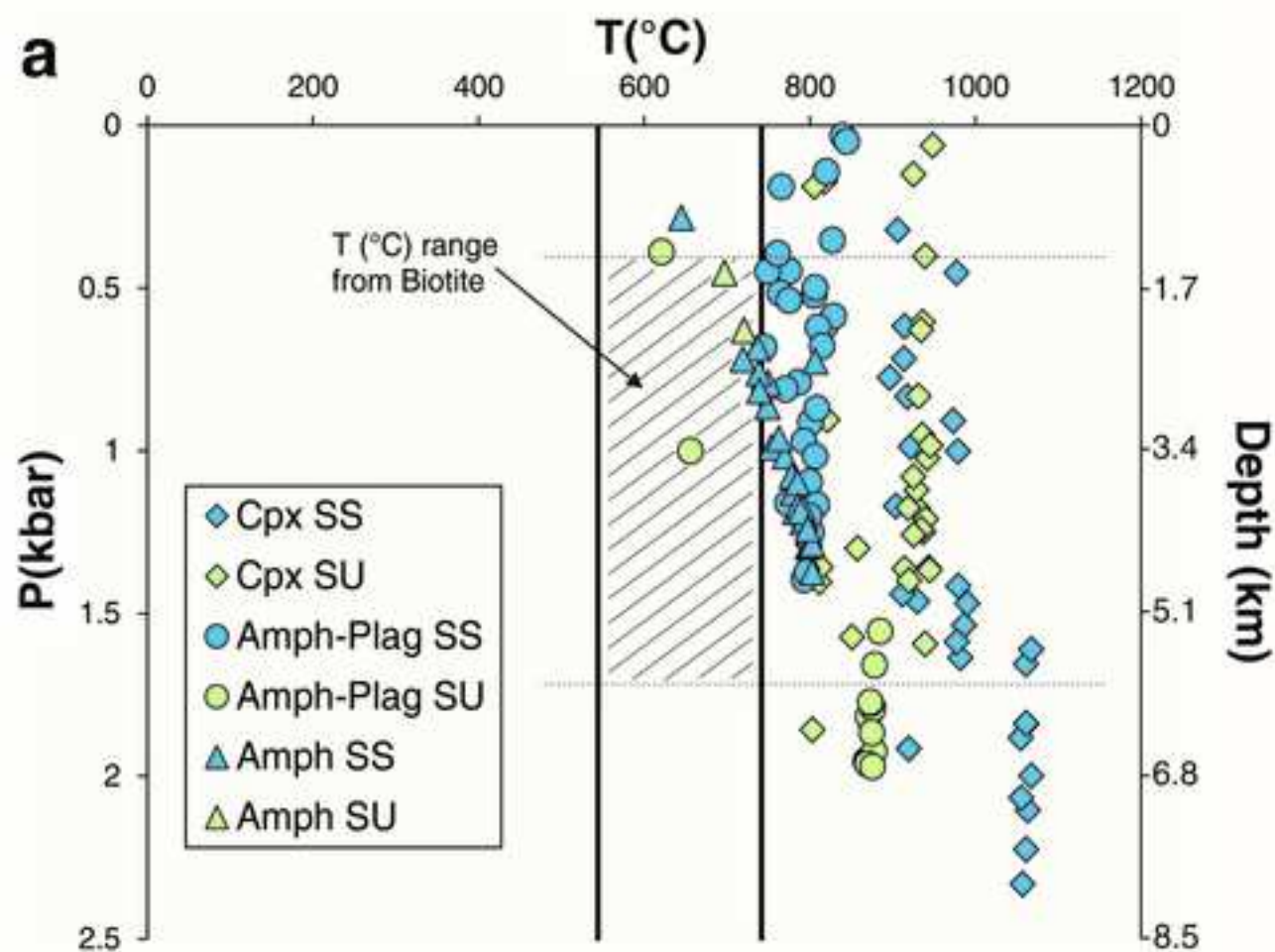


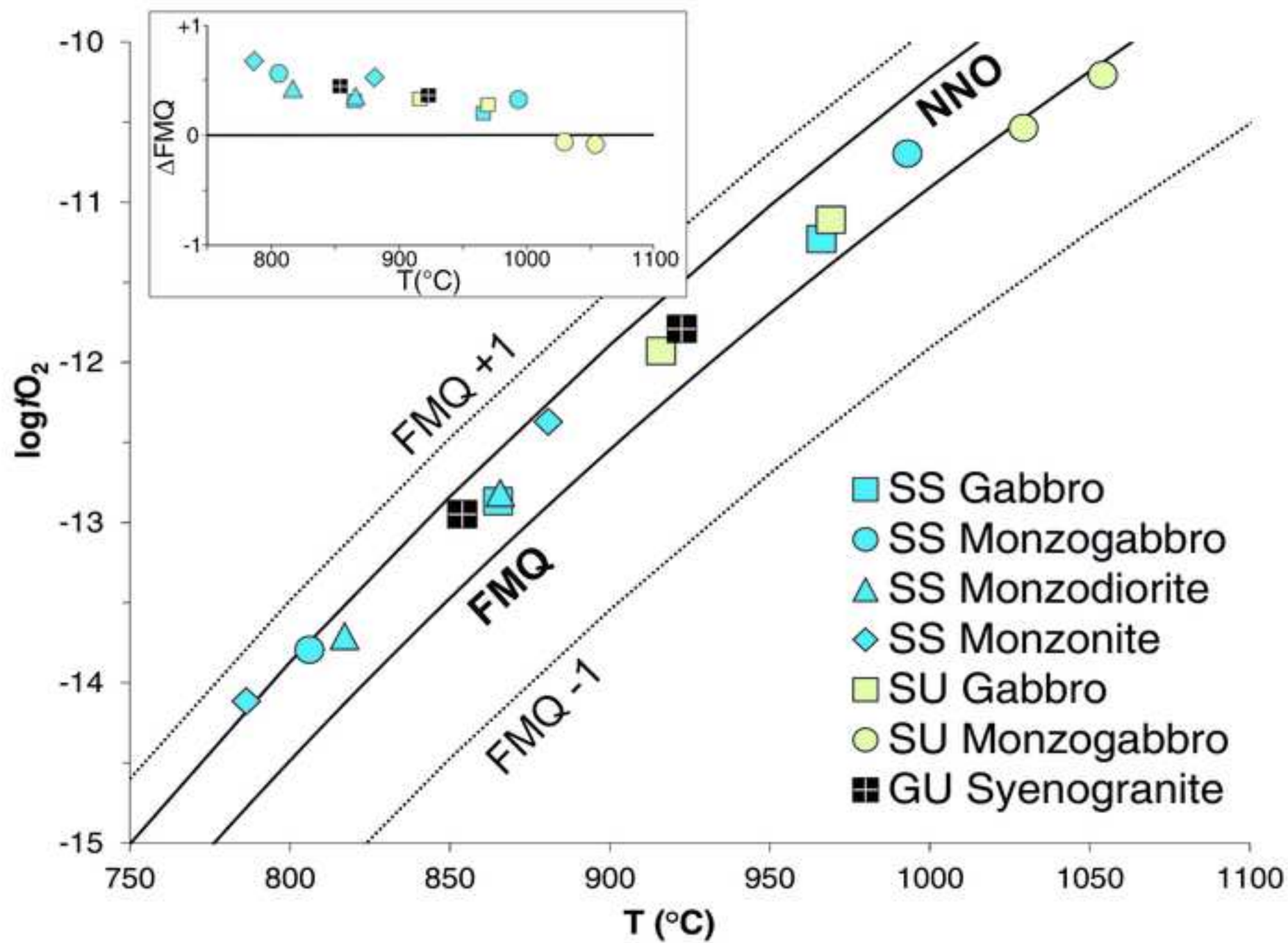














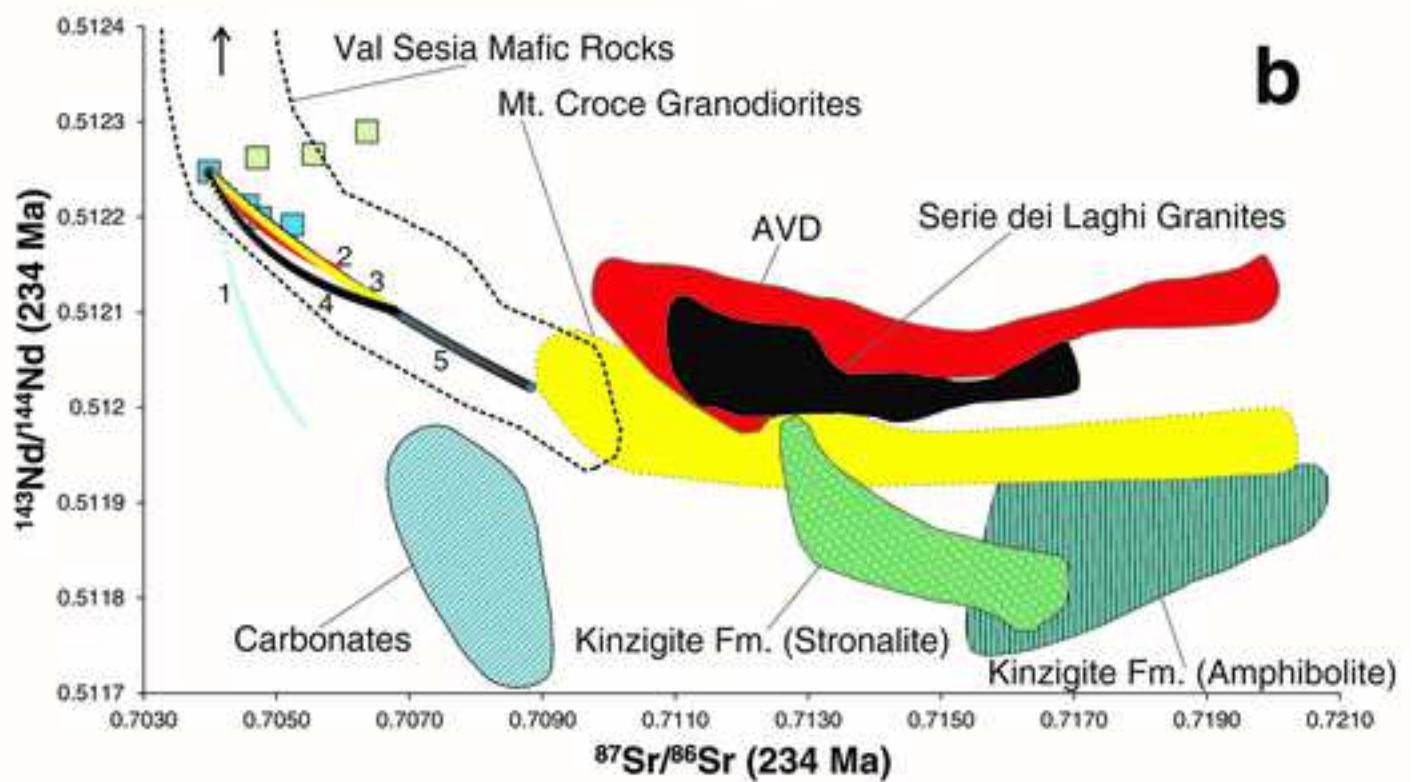
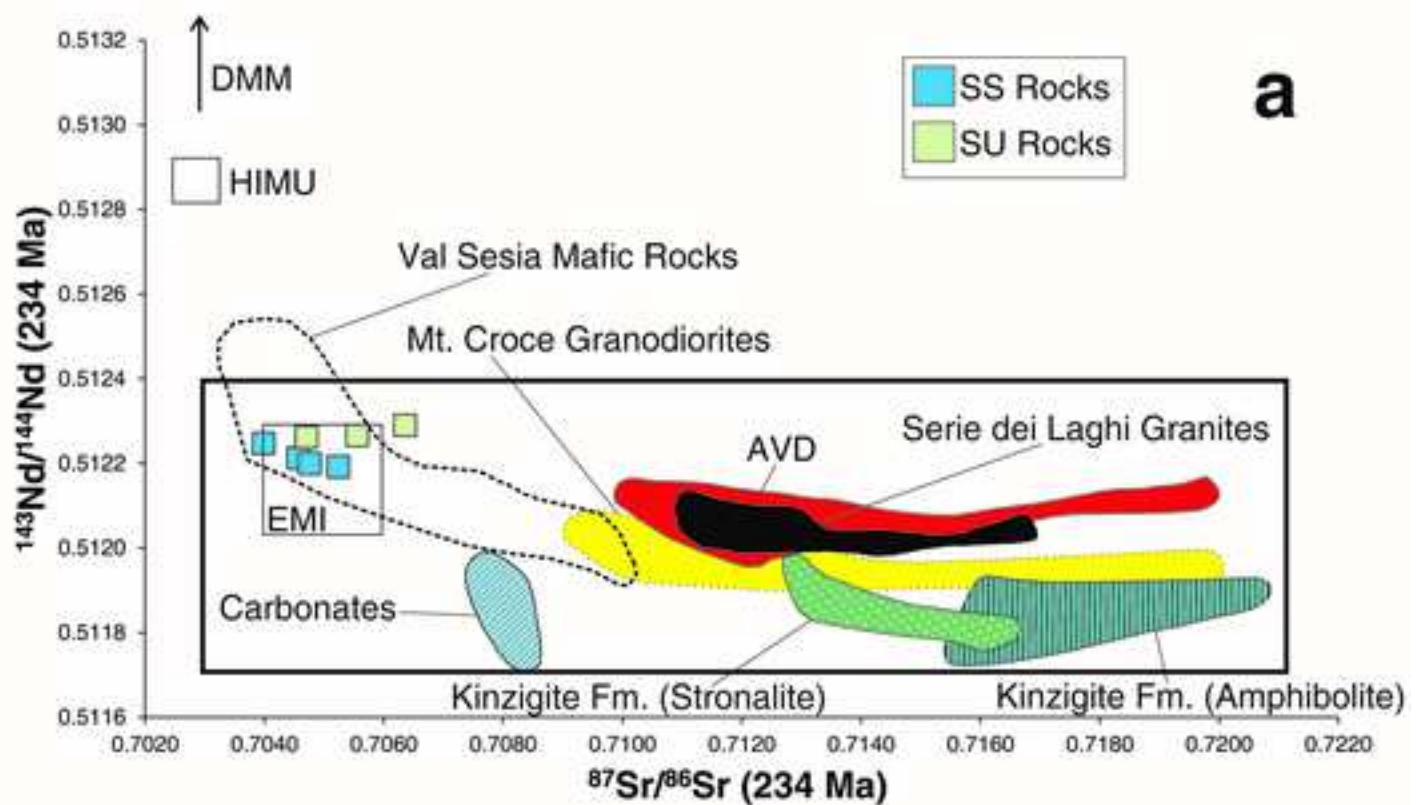


**Table 1. Major and trace element whole rock composition of selected Shoshonitic Silica Saturated (SS), Shoshonitic Silica Undersaturated (SU) and Granitic Unit (GU) rocks. Px: pyroxenite; Gb: gabbro; Mzgb: monzogabbro; Mzdr: monzodiorite; Mz: monzonite; Sy: syenite; Gr: granite; Sygr: syenogranite. Fe<sub>2</sub>O<sub>3</sub> and FeO were calculated by considering a Fe<sub>2</sub>O<sub>3</sub>/ FeO ratio of 0.15, in agreement with a fO<sub>2</sub> around FMQ buffer (Kress and Carmichael, 1991). Mg# = Mg/[Mg Fe<sup>2+</sup>] mol%; n.d. = not detected. All trace element (ppm) were analysed by ICP-MS except Pb, Zn, Ni, Co, Cr, V, Cu and Ba (XRF).**

Suite	SS	SS	SS	SS	SS	SS	SU	SU	SU	SU	SU	SU	GU	GU
Lithology	Px	Gb	Mzgb	Mzdr	Mz	Sy	Gb	Mzgb	Mzdr	Mz	Sy	Sy	Gr	Sygr
Sample	FC31E	FC30C	FC43D	FC37B	EM79	EM64	EM15	FC2B	EM9	EM6	EM5	EM107	EM90B	EM31
<b>Oxide (wt%)</b>														
SiO <sub>2</sub>	35.48	45.64	52.56	55.43	61.84	67.91	49.83	52.39	55.48	56.86	60.22	62.44	76.41	70.21
TiO <sub>2</sub>	2.07	1.08	0.85	0.80	0.43	0.17	0.93	1.13	0.24	0.58	0.46	0.28	0.04	0.26
Al <sub>2</sub> O <sub>3</sub>	6.20	16.78	18.92	17.30	19.82	16.54	17.91	17.08	23.80	21.71	19.58	18.68	13.79	15.58
Fe <sub>2</sub> O <sub>3</sub>	3.74	1.55	1.03	1.01	0.47	0.22	1.34	1.06	0.37	0.59	0.49	0.21	0.11	0.31
FeO	24.90	10.34	6.88	6.74	3.11	1.51	8.91	7.05	2.44	3.94	3.31	1.44	0.74	2.07
MnO	0.25	0.18	0.19	0.20	0.07	0.07	0.18	0.41	0.18	0.19	0.16	0.11	0.02	0.03
MgO	12.54	6.97	4.03	3.73	1.14	0.22	4.97	4.80	0.51	1.50	0.84	0.45	0.28	0.24
CaO	13.57	14.16	8.68	6.71	3.34	0.90	9.56	8.28	3.94	4.81	3.80	3.20	1.65	1.01
Na <sub>2</sub> O	0.51	1.09	2.79	3.24	3.62	4.27	2.81	4.80	5.29	5.16	5.70	3.54	5.44	3.99
K <sub>2</sub> O	0.73	2.16	3.37	4.30	5.96	8.18	2.80	2.62	7.73	4.38	5.25	9.22	1.51	6.29
P <sub>2</sub> O <sub>5</sub>	0.02	0.05	0.68	0.54	0.20	0.00	0.76	0.38	0.02	0.28	0.18	0.43	0.00	0.00
Tot.	100	100	100	100	100	100	100	100	100	100	100	100	100	100
LOI	0.00	2.57	1.33	1.09	1.72	0.99	1.21	1.57	4.33	1.13	0.60	1.20	1.53	1.23
Mg#	<b>47.29</b>	<b>54.56</b>	<b>51.08</b>	<b>49.65</b>	<b>39.48</b>	<b>20.72</b>	<b>49.86</b>	<b>54.81</b>	<b>27.26</b>	<b>40.34</b>	<b>31.01</b>	<b>35.57</b>	<b>40.60</b>	<b>17.33</b>
<b>Trace element (ppm)</b>														
Pb	14.8	14.2	17.8	27.5	21.0	23.0	13.0	44.1	45.0	37.0	28.0	27.0	n.d.	13.0
Zn	148	72.3	103	107	51.0	54.0	115	202	147	148	86.0	50.0	8.00	30.0
Ni	69.3	32.0	5.90	5.90	6.00	5.00	15.0	5.90	11.0	5.00	8.00	6.00	4.00	7.00
Co	62.9	52.7	27.2	24.4	9.00	6.00	40.0	29.5	4.00	9.00	7.00	3.00	n.d.	2.00
Cr	61.7	68.6	6.9	11.2	9.00	5.00	23.0	58.9	9.00	3.00	5.00	1.00	5.00	3.00
V	1600	565	153	144	32.0	15.0	239	165	36.0	80.0	67.0	29.0	13.0	9.00
Cu	13.0	17.3	85.7	79.4	n.d.	n.d.	n.d.	35.3	n.d.	n.d.	n.d.	n.d.	n.d.	n.d.
Rb	16.2	42.3	52.7	81.4	221	187	42.5	89.1	326	184	97.9	318	112	284
Ba	178	223	479	546	772	553	782	482	506	1129	498	616	121	190
Sr	95.4	440	676	556	755	284	849	621	818	1351	254	569	83.4	28.2
Nb	3.83	3.68	10.5	13.4	18.0	24.0	7.22	44.4	60.0	18.0	35.3	52.0	64.7	48.7
Zr	47.0	39.0	38.0	34.5	208	323	35.1	359	499	262	206	623	153	211
Hf	1.60	1.48	1.54	1.67	1.71	5.31	1.51	7.48	4.54	n.d.	5.66	6.95	5.05	5.81
U	0.22	0.48	0.93	1.59	2.46	3.89	1.08	2.92	11.8	7.39	5.26	11.6	11.0	2.55
Th	0.66	1.67	3.68	6.56	12.5	27.0	3.60	9.57	46.7	27.8	33.7	112	44.3	14.4
Y	14.1	11.1	11.9	13.7	21.9	24.5	13.6	23.8	13.7	26.0	14.8	49.9	27.1	5.0
Ta	0.26	0.30	0.52	0.68	n.d.	n.d.	0.51	1.57	n.d.	n.d.	1.34	n.d.	1.51	1.06
La	4.49	7.16	15.9	18.5	26.6	24.3	17.7	95.6	63.9	45.9	38.4	117	2.12	9.75
Ce	12.4	15.5	37.2	49.6	59.5	56.8	44.5	195	99.5	85.1	125	237	6.44	33.6
Pr	2.01	2.47	4.34	4.96	7.10	6.96	4.80	13.6	8.99	8.95	8.04	24.9	1.24	2.51
Nd	10.5	11.9	18.6	20.8	27.2	27.1	20.8	47.3	24.3	30.1	28.9	81.8	7.46	9.21
Sm	2.92	2.87	3.63	4.11	5.60	5.34	4.11	7.18	3.24	4.94	4.49	12.9	3.46	1.55
Eu	0.65	0.77	0.89	0.96	1.70	1.07	1.16	1.33	0.89	1.68	0.93	1.75	0.21	0.09
Gd	2.67	2.50	3.19	3.66	5.20	4.74	3.71	6.86	4.18	5.46	4.03	12.2	3.57	1.44
Tb	0.46	0.43	0.47	0.55	0.78	0.76	0.54	0.88	0.41	0.60	0.56	1.55	0.82	0.21
Dy	2.41	2.12	2.17	2.58	4.16	4.35	2.47	3.93	2.24	3.18	2.55	8.67	4.95	1.08
Ho	0.47	0.42	0.43	0.52	0.89	0.92	0.49	0.80	0.52	0.75	0.54	1.72	1.06	0.23
Er	1.22	1.08	1.12	1.38	2.25	2.57	1.27	2.22	1.59	2.09	1.53	5.34	3.04	0.73
Tm	0.18	0.17	0.18	0.22	0.38	0.44	0.20	0.37	0.26	0.35	0.27	0.84	0.52	0.13
Yb	1.06	0.96	0.95	1.25	2.51	3.08	1.08	2.16	1.78	2.30	1.61	5.78	3.17	0.89
Lu	0.15	0.14	0.15	0.19	0.35	0.47	0.17	0.34	0.27	0.35	0.25	0.83	0.45	0.14

**Table 2. Whole rock  $^{87}\text{Sr}/^{86}\text{Sr}$  and  $^{143}\text{Nd}/^{144}\text{Nd}$  isotopes of Shoshonitic Silica Saturated (SS), Shoshonitic Silica Undersaturated (SU) and Granitic Unit (GU) rocks. Samples were corrected for 234 Ma (Laurenzi and Visonà 1996; Mundil et al. 1996) of radiogenic ingrowth using the trace element abundances determined by ICP-MS, the decay rates of Rotenberg et al. (2012) and Lugmair and Marti (1978). Initial ratios (i) and uncertainties ( $2\sigma$ ) were propagated according to Ickert (2013).**

Sample	Lithology	Suite	Age (Ma)	Rb (ppm)	Sr (ppm)	$^{87}\text{Sr}/^{86}\text{Sr}$	$^{87}\text{Rb}/^{86}\text{Sr}$	$^{87}\text{Sr}/^{86}\text{Sr}(\text{i})$	$2\sigma$	Sm (ppm)	Nd (ppm)	$^{143}\text{Nd}/^{144}\text{Nd}$	$^{147}\text{Sm}/^{144}\text{Nd}$	$^{143}\text{Nd}/^{144}\text{Nd}(\text{i})$	$2\sigma$	Distance to edge (m)
FC31E	Pyroxenite	SS	234	16.19	95.45	0.706630	0.4907	0.705024	0.000025	2.92	10.46	-	0.1483	-	-	170
FC30C	Gabbro	SS	234	42.27	440.27	0.706149	0.2777	0.705240	0.000020	2.87	11.86	0.512415	0.1463	0.512191	0.000007	420
FC43D	Monzogabbro	SS	234	52.73	675.82	0.705304	0.2257	0.704565	0.000022	3.63	18.60	0.512392	0.1180	0.512211	0.000007	565
EM79	Monzonite	SS	234	220.50	754.80	0.707524	0.8452	0.704757	0.000032	5.60	27.16	0.512389	0.1246	0.512198	-	740
EM64	Syenite	SS	234	186.70	284.10	0.710211	1.9018	0.703985	0.000065	5.34	27.12	0.512429	0.1189	0.512247	0.000006	1000
EM15	Gabbro	SU	234	42.55	849.41	0.705182	0.1449	0.704707	0.000018	4.11	20.83	0.512444	0.1192	0.512261	0.000008	385
FC2B	Monzogabbro	SU	234	89.14	620.85	0.707719	0.4154	0.706359	0.000028	7.18	47.25	0.512430	0.0918	0.512289	0.000005	135
EM107	Syenite	SU	234	318.30	569.10	0.710856	1.6187	0.705556	0.000055	12.94	81.78	0.512412	0.0956	0.512266	0.000006	300
EM5	Syenite	SU	234	97.87	253.65	0.709851	1.1166	0.706196	0.000042	4.49	28.87	-	0.0826	-	-	158
EM31	Syenogranite	GU	234	324.50	148.19	-	-	-	-	9.69	62.08	0.512350	0.0942	0.512206	0.000007	376
EM88	Syenogranite	GU	234	371.86	15.99	-	-	-	-	8.43	39.41	0.512502	0.1291	0.512304	0.000016	735

**Table 3. Major element composition of the calculated melts used to retrieve the equilibrium conditions for clinopyroxene and plagioclase thermobarometry and for K-feldspar hygrometry (see text for explanation). SS = Shoshonitic Silica Saturated; SU = Shoshonitic Silica Undersaturated; Mg# =  $Mg/[Mg\ Fe^{2+}]$  mol%.**

Method	Suite	Crystal host rock	Estimated melt composition to attain equilibrium												Mg#	
			SiO <sub>2</sub> (wt%)	TiO <sub>2</sub>	Al <sub>2</sub> O <sub>3</sub>	Fe <sub>2</sub> O <sub>3</sub>	FeO	MnO	MgO	CaO	Na <sub>2</sub> O	K <sub>2</sub> O	P <sub>2</sub> O <sub>5</sub>			
Clinopyroxene-melt thermobarometer	SS	Pyroxenite	50.9	1.2	20.7	1.0	7.0	0.1	4.0	9.3	2.9	2.3	0.6	50.8	Trachybasalt	
	SS	Gabbro	54.9	0.6	21.0	0.8	5.4	0.1	2.1	8.2	3.2	3.2	0.4	41.4	Basaltic trachyandesite	
	SS	Gabbro	64.1	0.6	17.3	0.7	4.5	0.2	1.5	2.7	3.1	5.2	0.2	36.6	Trachyandesite	
	SS	Monzogabbro/monzodiorite	62.6	0.6	17.2	0.6	3.9	0.1	1.5	4.3	3.3	5.6	0.3	40.2	Trachyandesite	
	SU	Gabbro/monzogabbro	62.2	0.3	18.5	0.3	1.7	0.1	0.5	3.1	3.9	9.0	0.6	36.4	Trachyandesite	
	SU	Syenite	63.5	0.3	19.7	0.3	1.8	0.1	0.4	1.4	5.7	7.0	0.0	28.0	Trachyte	
Plagioclase-melt thermobarometer	SS	Pyroxenite	50.0	1.1	17.1	1.3	8.8	0.2	5.1	10.9	2.5	2.1	0.7	50.7	Trachybasalt	
	SS	Gabbro	53.6	0.8	17.4	1.1	7.6	0.2	4.1	8.4	2.8	3.4	0.5	49.3	Basaltic trachyandesite	
	SS	Monzogabbro	57.9	0.6	17.8	0.8	5.1	0.1	2.7	6.6	3.8	4.4	0.1	48.5	Basaltic trachyandesite	
	SS	Monzodiorite/monzonite	62.6	0.6	17.2	0.6	3.9	0.1	1.5	4.3	3.3	5.6	0.3	40.2	Trachyandesite	
	SU	Gabbro	57.8	0.7	20.2	0.6	4.0	0.2	1.5	4.9	4.7	5.1	0.4	39.3	Trachyandesite	
	SU	Monzogabbro to syenite	62.7	0.4	18.4	0.4	2.5	0.1	0.5	3.0	5.3	6.7	0.0	24.1	Trachyte	
K-Feldspar-melt hygrometer	SS	Gabbro/monzogabbro	62.6	0.6	17.2	0.6	3.9	0.1	1.5	4.3	3.3	5.6	0.3	40.2	Trachyandesite	
	SS	Monzodiorite to syenite	64.3	0.3	19.5	0.3	1.8	0.1	0.3	1.4	5.2	7.1	0.0	20.3	Trachyte	
	SU	Monzogabbro/monzodiorite	63.5	0.3	19.7	0.3	1.8	0.1	0.4	1.4	5.7	7.0	0.0	28.0	Trachyte	

**Table 4. Pressure, temperature,  $fO_2$  and  $H_2O$  parameters obtained by mineral pairs, mineral-melt and single mineral calculations on Shoshonitic Silica Saturated (SS), Shoshonitic Silica Undersaturated (SU) and Granitic Unit (GU) rocks. For each applied method, the corresponding reference, target and error on the single parameters are reported. Values used as input for each calculation are marked with (\*); n.r. indicates a parameter that was not required as input by the chosen equation. Cpx = clinopyroxene; Amph = amphibole; Plag = plagioclase; Bt = biotite; K-Feld = K-feldspar; Mt = magnetite.**

Suite and sample	Method	Target	Reference	T(°C)	Error (°C)	P (kbar)	Error (kbar)	H <sub>2</sub> O (wt%)	Error (wt%)	log $fO_2$	Error (log $fO_2$ )
SS Pyroxenite	Cpx-melt	P,T	Putirka (2008), eq. 32b, 33	1050-1070	±10-20	1.6-2.3	±2.6	2-2.5 (*)	-	n.r.	-
SS Pyroxenite	Cpx-melt	Cpx comp.	Rhyolite-MELTS (Gualda et al. 2012)	1060 (*)	-	1.5 (*)	-	2.5 (*)	-	-9.3 (*)	-
SS Gabbro	Cpx-melt	P,T	Putirka (2008), eq. 32b, 33	910-930°C	±10-20	1.0-1.9	±2.6	3-4 (*)	-	n.r.	-
SS Gabbro	Cpx-melt	P,T	Masotta et al. (2013), eq. Talk and Palk2012	910-980	±18	0.5-1.4	±1.2	3-4 (*)	-	n.r.	-
SS Monzogabbro/monzodiorite	Cpx-melt	P,T	Masotta et al. (2013), eq. Talk and Palk2012	940-990	±18	1.4-1.6	±1.2	3-4 (*)	-	n.r.	-
SU Gabbro/monzogabbro	Cpx-melt	P,T	Putirka (2008), eq. 32b, 33	930-940	±10-20	0.4-1.6	±2.6	1-1.5 (*)	-	n.r.	-
SU Gabbro/monzogabbro	Cpx-melt	P,T	Masotta et al. (2013), eq. Talk and Palk2012	920-940	±18	0.2-1.4	±1.2	1.5 (*)	-	n.r.	-
SU Syenite	Cpx-melt	P,T	Putirka (2008), eq. 32b, 33	810-820	±10-20	0.2-1.4	±2.6	4-5 (*)	-	n.r.	-
SU Syenite	Cpx-melt	P, T	Masotta et al. (2013), eq. Talk and Palk2012	850-860	±18	1.3-1.6	±1.2	4-5 (*)	-	n.r.	-
SS Gabbro to monzodiorite	Amph-Plag	T	Holland and Blundy (1994)	750-845	±40	n.r.	-	n.r.	-	n.r.	-
SS Gabbro to monzodiorite	Amph-Plag	P	Anderson and Smith (1995); Anderson (1996)	n.r.	-	0.1-1.2	±0.6	n.r.	-	n.r.	-
SS Gabbro to monzodiorite	Amph	P,T,H <sub>2</sub> O	Ridolfi et al. (2010); Ridolfi and Renzulli (2012)	720-810	±23-24	0.7-1.4	±0.05-0.15	4.8-6.0	±0.8	-	-
SU Gabbro/monzogabbro	Amph-Plag	T	Holland and Blundy (1994)	620-880	±40	n.r.	-	n.r.	-	n.r.	-
SU Gabbro/monzogabbro	Amph-Plag	P	Anderson and Smith (1995); Anderson (1996)	n.r.	-	0.4-1.9	±0.6	n.r.	-	n.r.	-
SU Gabbro	Amph	P,T,H <sub>2</sub> O	Ridolfi et al. (2010); Ridolfi and Renzulli (2012)	700-720	±23-24	0.5-0.6	±0.05-0.15	5.1-5.7	±0.8	-	-
SS Pyroxenite	Bt	T	Henry et al. (2005)	690-740	±12-24	n.r.	-	n.r.	-	n.r.	-
SS Gabbro to monzonite	Bt	T	Henry et al. (2005)	540-660	±12-24	n.r.	-	n.r.	-	n.r.	-
SU Gabbro/monzogabbro	Bt	T	Henry et al. (2005)	640-660	±12-24	n.r.	-	n.r.	-	n.r.	-
SS Pyroxenite	Plag-melt	H <sub>2</sub> O	Lange et al. (2009)	1060 (*)	-	1.5 (*)	-	3.0	±0.7	n.r.	-
SS Pyroxenite	Plag-melt	P,T	Putirka (2008), eq. 24a	1076-1081	±36	1.5 (*)	-	3.0 (*)	-	n.r.	-
SS Gabbro	Plag-melt	H <sub>2</sub> O	Lange et al. (2009)	920-1016 (*)	-	1.2-1.5 (*)	-	3.1-3.4	±0.7	n.r.	-
SS Gabbro	Plag-melt	P,T	Putirka (2008), eq. 24a	999-1053	±36	1.2-1.5 (*)	-	3.1-3.4 (*)	-	n.r.	-
SS Monzogabbro/monzodiorite	Plag-melt	H <sub>2</sub> O	Lange et al. (2009)	920 (*)	-	1.2 (*)	-	3.9-4.8	±0.7	n.r.	-
SS Monzogabbro/monzodiorite	Plag-melt	P,T	Putirka (2008), eq. 24a	917-989	±36	1.2 (*)	-	3.9-4.8 (*)	-	n.r.	-

**Table 3. (continued)**

Suite and sample	Method	Target	Reference	T(°C)	Error (°C)	P (kbar)	Error (kbar)	H <sub>2</sub> O (wt%)	Error (wt%)	logfO <sub>2</sub>	Error (log fO <sub>2</sub> )
SU Gabbro	Plag-melt	H <sub>2</sub> O	Lange et al. (2009)	990 (*)	-	1.5 (*)	-	4.1	±0.7	n.r.	-
SU Gabbro	Plag-melt	P,T	Putirka (2008), eq. 24a	975-990	±36	1.5 (*)	-	4.1 (*)	-	n.r.	-
SU Monzogabbro	Plag-melt	H <sub>2</sub> O	Lange et al. (2009)	920 (*)	-	1.2 (*)	-	4.4	±1.0	n.r.	-
SU Monzogabbro	Plag-melt	P,T	Putirka (2008), eq. 24a	936	±36	1.2 (*)	-	4.4 (*)	-	n.r.	-
SS Gabbro to monzogabbro	K-Feld-melt	H <sub>2</sub> O	Mollo et al. (2015)	800-900 (*)	-	n.r.	-	4.4-6.5	±0.94	n.r.	-
SS Monzodiorite to syenite	K-Feld-melt	H <sub>2</sub> O	Mollo et al. (2015)	800-900 (*)	-	n.r.	-	4.6-7.3	±0.94	n.r.	-
SU Monzogabbro to monzonite	K-Feld-melt	H <sub>2</sub> O	Mollo et al. (2015)	800-900 (*)	-	n.r.	-	5.5-7.8	±0.94	n.r.	-
SS Gabbro	Bt/K-Feld/Mt	fO <sub>2</sub>	Burkhard (1991)	865-966	±7	1.5 (*)	-	n.r.	-	-11.2/-12.9	±0.3
SS Monzogabbro/monzodiorite	Bt/K-Feld/Mt	fO <sub>2</sub>	Burkhard (1991)	806-993	±7	1.5 (*)	-	n.r.	-	-10.7-13.8	±0.3
SS Monzonite	Bt/K-Feld/Mt	fO <sub>2</sub>	Burkhard (1991)	786-881	±7	1.5 (*)	-	n.r.	-	-12.4/-14.1	±0.3
SU Gabbro/monzogabbro	Bt/K-Feld/Mt	fO <sub>2</sub>	Burkhard (1991)	916-1054	±7	1.5 (*)	-	n.r.	-	-10.2/-11.9	±0.3
GU Syenogranite	Bt/K-Feld/Mt	fO <sub>3</sub>	Burkhard (1991)	853-922	±7	1.5 (*)	-	n.r.	-	-11.8/-12.9	±0.3

**Table 5. Starting Shoshonitic Silica Saturated (SS) and Shoshonitic Silica Undersaturated (SU) magmas, assimilant end-members and input thermodynamic data used in the EC-AFC model. Calculated and absolute values are from Bohrsen and Spera (2001) and Spera and Bohrsen (2001) upper crustal case. Specific heat and liquidus T of carbonate assimilant were calculated according to Dallai et al. (2011) and Eppelbaum et al. (2014) respectively. References are also reported for all chosen assimilants compositions.**

Starting magma	Liquidus T(°C)	Initial T (°C)	Solidus T(°C)	Specific Heat [J/(KgK)]	Heat of Crystallization (J/Kg)	Heat of Fusion (J/Kg)
SS monzogabbro	1212	1100	600	1567	396000	270000
SU monzogabbro	1251.65	1100	600	1515	396000	270000

Assimilant	Liquidus T(°C)	Initial T (°C)	Specific Heat [J/(KgK)]	Reference for isotopic <sup>87</sup> Sr/ <sup>86</sup> Sr and <sup>143</sup> Nd/ <sup>144</sup> Nd composition
Carbonate	650	300	1170	Martin and Macdougall (1995); Blendiger et al. (2015)
Rhyolitic Ignimbrite (AVD)	1077	300	1376	Barth et al. (1993)
Mt. Croce Granodiorites	1111	300	1398	Rottura et al. (1997)
Serie dei Laghi Granites	1026	300	1379	Sinigoi et al. (2016) and references therein
Kinzigite Amphibolite	1196	300	1447	Voshage et al. (1990)